NUREG/CR-3316
SAND83-1154

Verification and Field Comparison of the Sandia Waste-Isolation Flow and Transport Model (SWIFT)

Prepared by D. S. Ward, M. Reeves, L. E. Duda

Sandia National Laboratories

Prepared for
U.S. Nuclear Regulatory Commission

GPO Printed copy price: $6.50

NUREG/CR-3316
SAND83-1154

Verification and Field Comparison of the Sandia Waste-Isolation Flow and Transport Model (SWIFT)

Manuscript Completed: February 1984
Date Published: April 1984

Prepared by
D. S. Ward*, M. Reeves*, L. E. Duda

Sandia National Laboratories
Albuquerque, NM 87185

Prepared for
Division of Waste Management
Office of Nuclear Material Safety and Safeguards
U.S. Nuclear Regulatory Commission
Washington, D.C. 20555
NRC FIN A1166

*Presently with Geo Trans, Inc.

ABSTRACT

The SWIFT Model has been developed and maintained by Sandia National Laboratories. The Nuclear Regulatory Commission has sponsored this work under its high-level nuclear waste program. SWIFT is a fully-coupled, transient, three-dimensional model. It is implemented by a finite-difference code which solves the equations for flow and transport in geologic media and is used to evaluate repository-site performance. This document represents an important part of the quality-assurance records for the code. Here the process simulators for flow, heat and radionuclide transport are examined using two different types of tests. The analytical verifications test SWIFT calculations against analytical solutions, and the field comparisons test SWIFT calculations against field data. Both types of tests yield good agreement between the SWIFT computations and the comparative data.

TABLE OF CONTENTS

TABLE OF CONTENTS

(continued)

LIST OF FIGURES

LIST OF FIGURES

(Continued)

LIST OF FIGURES

(Continued)

LIST OF FIGURES

(Continued)

LIST OF TABLES

LIST OF TABLES

(Continued)

ACKNOWLEDGEMENTS

The authors would like to thank Ms. Lynette S. Knippa for her seemingly tireless efforts and for her demonstrated expertise in typing both equations and text. This document would not have been possible without her help.

1 INTRODUCTION

The SWIFT Model (Sandia Waste-Isolation Flow and Transport Model) has been developed for the evaluation of repository-site performance. It is a fully-coupled, transient, three-dimensional model, and it is implemented by a finite-difference code* which solves the equations for flow and transport in geologic media. Having evolved from the U.S. Geological Survey Code, SWIP (Survey Waste Injection Program) this code has experienced continuous improvements and maintenance since 1977. As such, it has become a very comprehensive and effective tool containing most of the processes envisioned for a fluid-saturated repository of high-level nuclear waste.

1.1 QUALITY ASSURANCE

In order to assure the scientific quality of model and code, a quality-assurance program was initiated in 1980. Under this program, two different types of documentation are called for. One is an internal record of the code's evolution. An important part of this record is the code baseline. This document describes a particular version of the code which has been placed in permanent storage. It identifies the version with a unique number, and it identifies the storage location. It also lists the code modifications which have occurred since the last baseline. Such a baseline was, of course, issued for the version of the SWIFT code used in this report.

The other type of documentation is the external record, which, of course, is available for external distribution. Here the requirements are consistent with those stated in the NUREG report by Silling [1983]. The documents by Reeves and Cranwell [1981], Reeves et al [1984a] and Reeves et al [1984b] form

---

* The term "model", as used herein, denotes the representation of a process, or, in this case of SWIFT, representations of coupled processes. As such, this term may include both mathematical and numerical characterizations of a particular process. When applied to a particular site or system, the terms "site model" or "system model" will be used. The term "code", as used herein, denotes simply a set of computer instructions for performing the operations specified by the numerical model. This usage is consistent with the NRC technical position [Silling, 1983].

an important part of the SWIFT external record. They describe the theoretical and numerical aspects of the model and the code, and they provide a guide to the data input.

1.2 CODE ASSESSMENT

There is another part of the external record, however, which is the focus of this report. It is an assessment of code adequacy. Basically there are two different types of tests to be performed, namely verification and validation. The object of the first type of test is to show that the code accurately performs the operations specified by the model [Silling, 1983]. Here analytic-to-code comparisons are performed, although code-to-code comparisons and perhaps other less stringent procedures might be used.

The object of the second type of test, i.e., that of validation, is to show that the computer code is a correct representation of the physical process or system [Silling, 1983]. Obviously, a comparison to field data is required. However, such a comparison may take one of two different forms. One is that of calibration. This is the weaker form of validation in that it tests the ability of the code (and the model) to fit the field data with adjustments of the physical parameters. It is assumed, of course, that the parameter values so obtained are reasonable in that they are consistent with similar media. All of the field comparisons performed for this report would properly be classified as calibrations. As was noted from the review of this document, some researchers prefer to classify calibration as a form of verification rather than a form of validation. With such a definition, this document would be viewed, in its entirety as verification.

The other form of validation is that of prediction. This is usually the stronger form in that it tests the ability of the code to fit the field data with no adjustments of the physical parameters. Typically, a portion of the field data is designated as calibration data, and a calibrated site model is obtained through reasonable adjustments of parameter values. Yet another portion of the data is designated as prediction data, and the calibrated site model is used to simulate similar data for comparison. The quality of such a test is therefore determined by the extent to which the site model is "stressed beyond" the calibration data on which it is based. This, of course, is a matter of judgement.

1.3 TESTING PROCEDURE

The objective of the work reported in this document is to assess the adequacy of the SWIFT code in an independently verifiable manner. For this document a set of 11 problems was selected. Insofar as possible, standardized benchmark* problems were chosen in order to facilitate later code-to-code comparisons. Many of the problems (four of the eleven) came from Benchmarking Problems for Repository Siting Models by Ross et al [1982]. Another came from the INTRACOIN [1983] code-comparison study. In each case test specifications and test results are provided in the main text. Then in the microfiche, which appears inside the back cover, complete listings of input and output are given. A number, identifying the version of the code, is printed in the header for each output. Thus each output is traceable to the permanently stored version of the code which was actually used for the test. This means that every result given in this report may be independently checked.

1.4 SCOPE AND ORGANIZATION

Process simulators for flow, heat and radionuclide transport in porous media are the focus of this document. Various submodels, such as the well submodel, the aquifer-influence conditions and the waste-leach (radionuclide-source) submodel are included, but only insofar as they arise in assessment of the process simulators. Accordingly, the main body of the text is organized by process simulator as well as by type of test (analytic verification or field comparison). For convenience, all of the notation is placed in a single symbol lexicon.

---

* The term "benchmark" denotes simply a reference problem to be used as a basis for comparison.

2 VERIFICATION OF THE FLOW

2.1 FULLY PENETRATING WELL WITH CONSTANT DISCHARGE [THEIS, 1935][1]

2.1.1 Objectives

The purposes for simulating this problem are to test the following aspects of the SWIFT Code:

- pressure solutions,
- rate-controlled well,
- aquifer-influence function,
- radial and Cartesian coordinates,
- SI and English Engineering units.

2.1.2 Description of Problem[2]

A well fully penetrates an infinite confined aquifer and is pumped at a constant rate, as shown in Figure 2-1. There is assumed to be no leakage. The object is to determine drawdown as a function of position and time. The equation to be solved is:

$$T \frac{1}{r} \frac{\partial}{\partial r} \left(r \frac{\partial s}{\partial r} \right) = S \frac{\partial s}{\partial t} \qquad (2\text{-}1)$$

where the boundary/initial conditions are on drawdown s and flow rate Q are:

$$s(r,t=0) = 0 , \qquad r > 0 \qquad (2\text{-}2)$$

$$s(r = \infty,t) = 0 , \qquad t > 0 \qquad (2\text{-}3)$$

---

1 Benchmark Problem 3.1 [Ross et al, 1982].
2 All symbols are defined in Section 8.

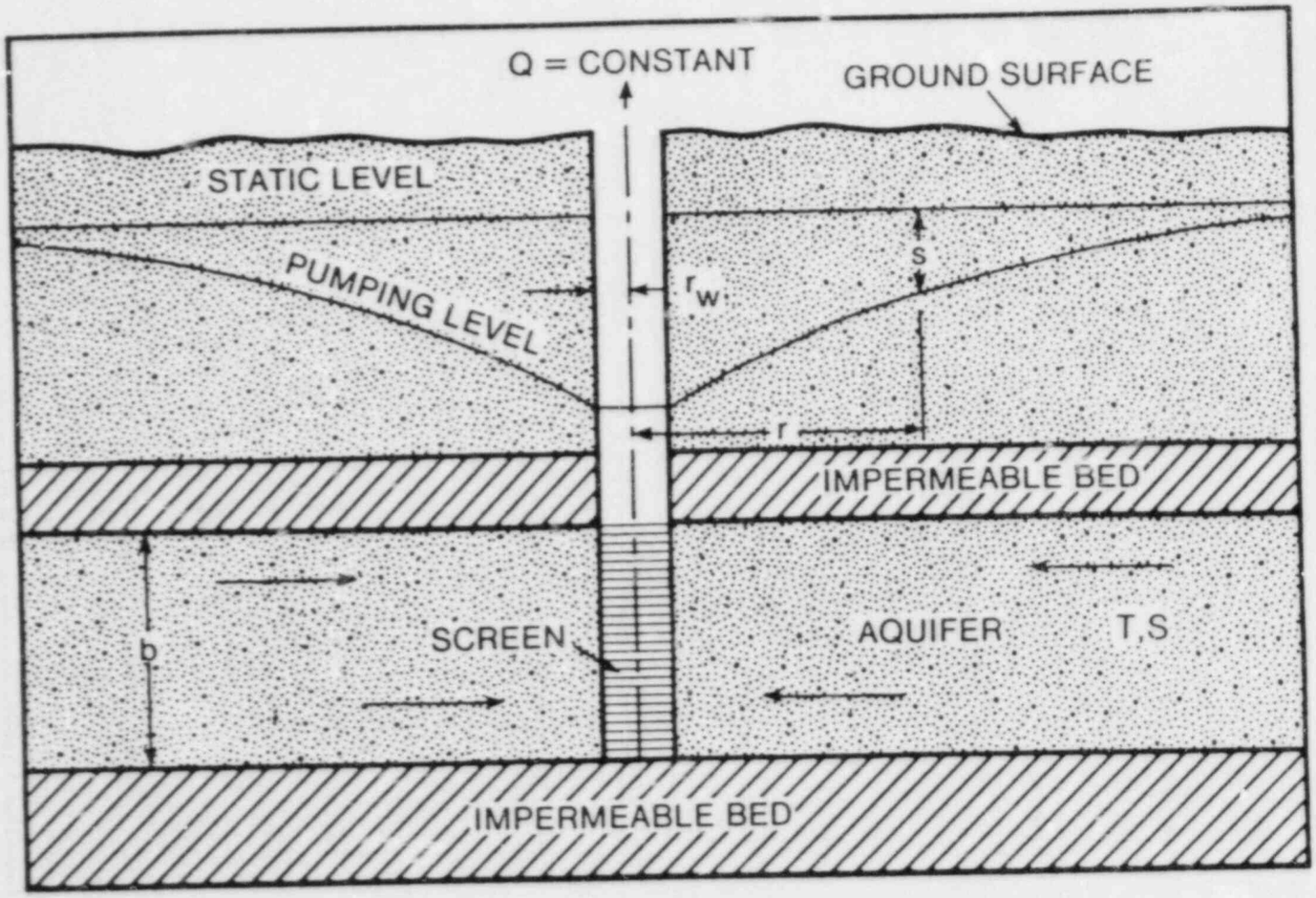

Figure 2-1. Schematic Diagram of a Fully Penetrating Well in a Confined Aquifer, Problem 2.1.

$$Q = \begin{cases} 0, & t = 0 \\ \text{constant} > 0, & t > 0 \end{cases} \qquad (2\text{-}4)$$

2.1.3 Assumptions

The assumptions involved in the above analysis are the following:

- The aquifer has infinite areal extent.
- The aquifer is confined with no leakage.
- The aquifer is homogeneous, horizontal, isotropic and of uniform thickness over the area influenced by the pumping test.
- Prior to pumping, the potentiometric surface is horizontal for the aquifer.
- Pumping is performed at a constant rate.
- The pumped well penetrates the entire aquifer and thus receives water from the entire thickness of the aquifer by horizontal flow.
- The diameter of the pumped well is sufficiently small that its internal storage may be neglected.
- The water removed from storage is discharged instantaneously with decline of head.
- Darcy's law applies throughout the system, and non-laminar flow near the well may be neglected.

2.1.4 Analytical Solution

For the analytical solution, the inner boundary condition of Equation (2-4) is taken to be that of a point source:

$$\lim_{r \to 0} r \frac{\partial s}{\partial r} = -\frac{Q}{2\pi T}, \qquad t > 0 \qquad (2\text{-}5)$$

The solution of Equation (2-1), subject to the conditions of Equations (2-2), (2-3) and (2-5), is the Theis relation:

$$s = (Q/4\pi T)W(u) \qquad (2\text{-}6a)$$

where the dimensionless variable u is given by

$$u = r^2 S/4Tt \qquad (2\text{-}6b)$$

and W(u) is the familar well function. (See Reed [1980] for numerical generation of this function.)

$$W(u) = \int_u^\infty e^{-y}/y \, dy \qquad (2\text{-}6c)$$

2.1.5 Input Specifications

The input parameters for this problem are taken directly from Ross et al [1982], p. 11. They are presented here, for a standard hydrological notation, in Table 2.1. They are presented in SWIFT notation in Table 2.2. The values of the first six parameters shown in Table 2.2 are consistent with those of the storage and transmissivity parameters shown in Table 2.1, as may be verified from the following relations:

$$S = \rho(g/g_c)\phi cb \qquad \text{[dimensionless]}$$

and

$$T = \rho gkb/\mu = Kb \qquad [L^2/T]$$

A complete listing of the input data is given in the microfiche at the end of this document. The data format is described in the documentation listed in Section 2.1.2. However, the researcher may find it more convenient to examine an echo of the input data as given with the calculated results. These are included in the output listings, which are also given in the microfiche.

Table 2-1. Parameter Specifications for Problem 2.1.

Parameter	Symbol	Value	
		SI	English
Storativity	S	10^{-3}	10^{-3}
Transmissivity	T	10^{-3} m^2/s	930 ft^2/d
Pumping rate	Q	3.0×10^{-3} m^3/s	9153 ft^3/d

Table 2-2. SWIFT Parameters for Problem 2.1.

Parameter	Symbol	Value	
		SI	English
Porosity	ϕ	0.20	0.20
Hydraulic conductivity	K	3.28×10^{-4} m/s	93 ft/d
Viscosity	μ	0.001 Pa-s	1 cp
Density	ρ	999.5 kg/m^3	62.4 lb/ft^3
Compressibility	c	1.67×10^{-7} 1/Pa	1.15×10^{-3} 1/psi
Aquifer thickness	b	3.05 m	10 ft
Wellbore radius	r_w	0.1143 m	0.375 ft
Aquifer radius	r_e	6096 m	20000 ft
Pumping rate	Q	3.0×10^{-3} m^3/s	9153 ft^3/d

2.1.6 Output Specifications

The output for this problem consists of drawdowns versus time and distance. As specified by Ross et al [1982], the drawdown should be given as a function of time at 100 m and as a function of distance at 100 days.

2.1.7 Numerical Solution

Program SWIFT solves the same flow equation as that given in Equation (2-1), although it is restated in terms of pressure as the dependent variable. However, there are differences at the inner and outer boundaries. At the inner boundary a finite wellbore of radius r_w is considered by the program. Nevertheless, this effect should be confined to a region of several wellbore radii surrounding the origin. The value used for the well radius is given in Table 2.2.

With respect to the outer boundary condition, a gridded mesh, of course, can not be extended to $r = \infty$. However, the code does match onto an analytic solution at the extremity, r_e, of the mesh. This matching is done through the approximate Carter-Tracy method [Reeves et al, 1984a and Carter and Tracy, 1960] in order to minimize computation. In effect, then, the gridded mesh is imbedded within an infinite aquifer with the effects of the latter determining the boundary condition. This is the origin of the term "aquifer-influence function". Although, to some extent, this procedure is subject to direct verification by this test, the chosen matching radius, r_e, (see Table 2-2) is sufficiently distant from the cone of depression that the adverse effects of this approximate condition should be negligible.

As an additional test of the code, both SI and English Engineering units were used with both radial and Cartesian grids. Thus, in all, there are four distinct input data sets. For the radial grid (see Figure 2-2a) there were 50 blocks ranging in size from 0.4097 m near the wellbore to 877 m near the outer reservoir boundary. For the Cartesian grid, a quarter system was used (see Figure 2-2b). Here a 15 x 15 grid was used with block dimensions ranging in size from 1 m at the well to 4096 m at the outer extremity of the grid. No-flow symmetry conditions were applied along the coordinate axes, and a Carter-Tracy condition was again used at the outer extremity of the system.

(a) Radial Grid

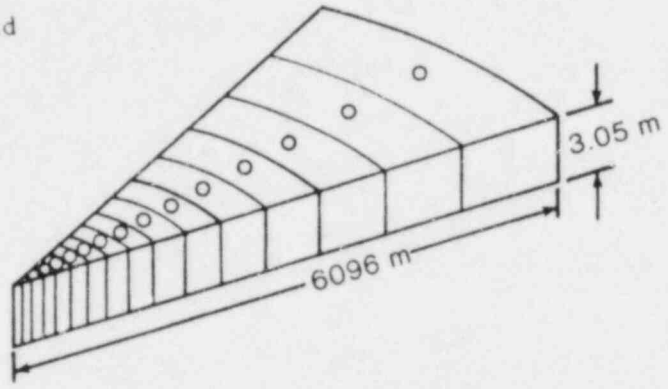

(b) Cartesian Grid

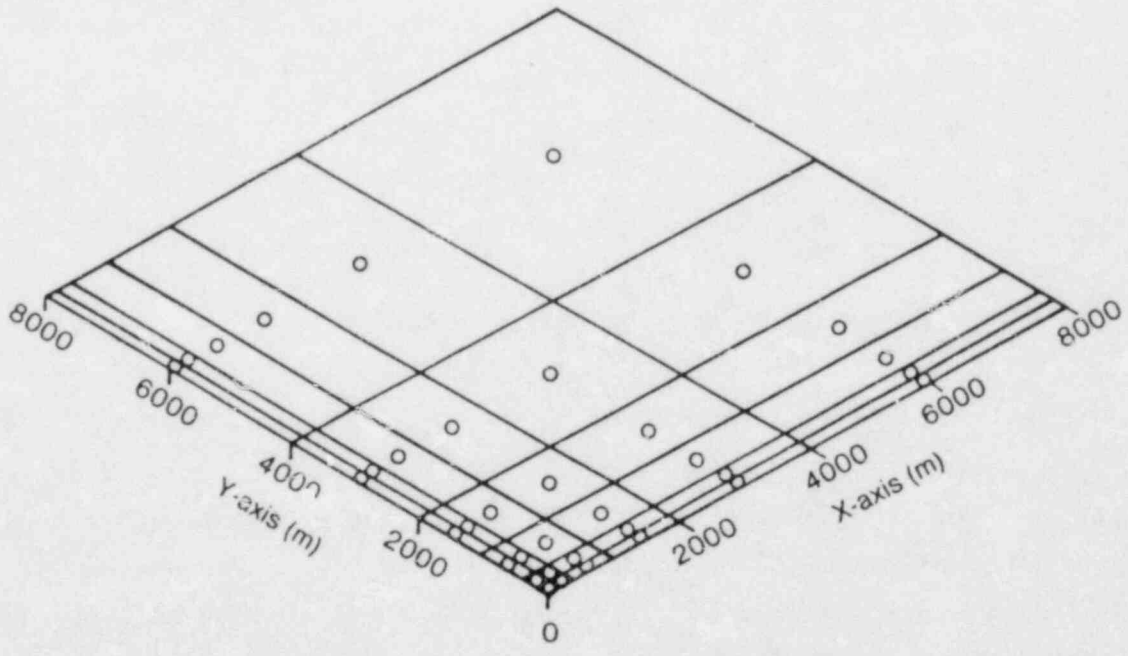

Figure 2-2. Grids Used in the Well-Test Analyses.

A quarter section was used for the Cartesian system in order to minimize the required computer resources. However, a close comparison of Figure 2-2b with Figure 2-2a shows that the Cartesian system is not exactly a symmetric quarter section of the radial system. This is due to the fact that, in the former, the well is block centered rather than being located at the adjacent corner of the grid. Nevertheless, due to the relative distances and areas involved, the effect of these discrepancies is expected to be small except possibly in the near vicinity of the well.

2.1.8 Results

The results are shown in Figures 2-3 and 2-4, where numerically and analytically determined pressure drops may be compared. Pressure is the dependent variable for the SWIFT calculation. However, drawdown is obtained very simply from the drop in pressure, Δp, from the initial pressure by the relation:

$$s = \Delta p/\rho(g/g_c)$$

As shown in these two figures, the agreement between numerical and analytical results is quite satisfactory with the Cartesian grid yielding the greater error. Most likely, this arises from the relative coarseness of the mesh used in the Cartesian grid. Simulations were performed in both SI and English systems of units, and the results were virtually identical.

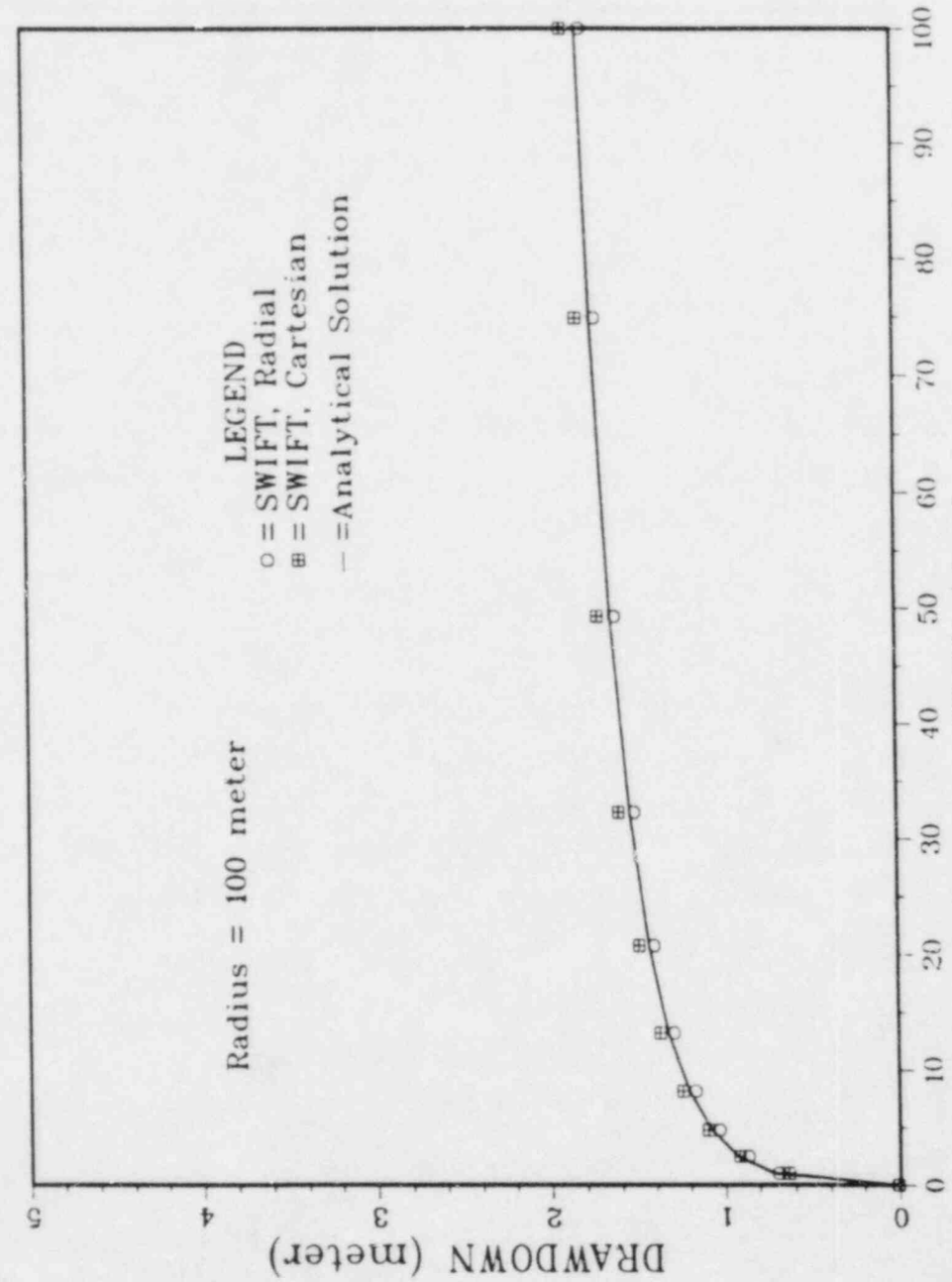

Figure 2-3. Drawdown as a Function of Time for a Constant-Discharge Well.

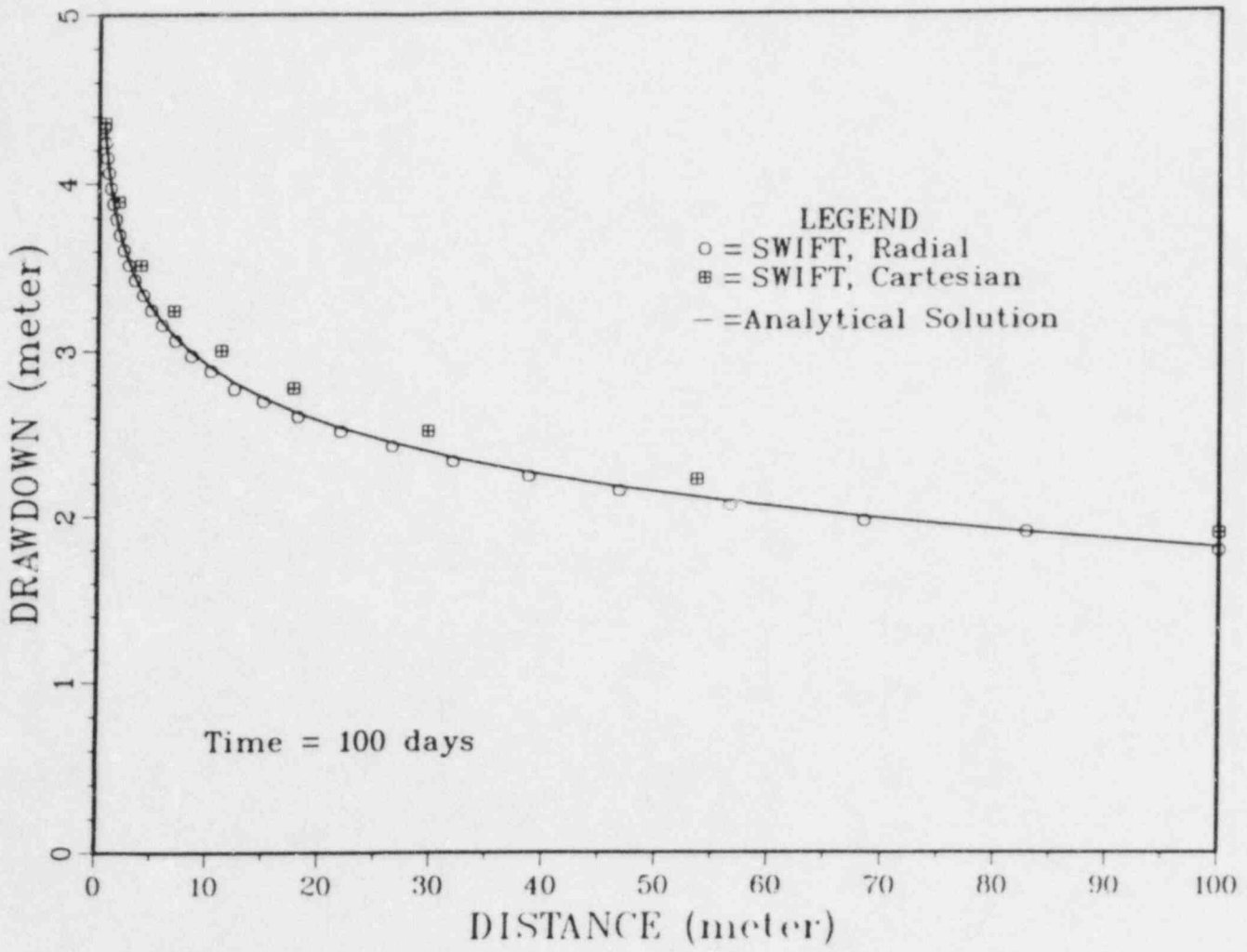

Figure 2-4. Drawdown as a Function of Distance for a Constant-Discharge Well.

2.2 FULLY PENETRATING WELL WITH CONSTANT DRAWDOWN [JACOB AND LOHMAN, 1952]

2.2.1 Objectives

The purposes for simulating this problem are to test the following aspects of the SWIFT Code:

- pressure solution,
- constant-pressure well,
- aquifer-influence function,
- radial coordinates,
- SI and English Engineering units.

2.2.2 Description of Problem

A well fully penetrates an infinite confined aquifer (see Figure 2-5). Fluid production is performed by maintaining a constant head, or drawdown, within the wellbore. The object is to determine the pumping rate as a function of time and the drawdown as a function of space and time. The equation to be solved is:

$$\frac{1}{r}\frac{\partial}{\partial r}\left(r\,\frac{\partial s}{\partial r}\right) = \frac{S}{T}\frac{\partial s}{\partial t} \qquad (2\text{-}7)$$

and the boundary/initial conditions are:

$$s(r,t=0) = 0\,, \qquad r \geq r_w \qquad (2\text{-}8a)$$

$$s(r=r_w,t) = \begin{cases} 0\,, & t = 0 \\ s_w = \text{constant}\,, & t > 0 \end{cases} \qquad (2\text{-}8b)$$

$$s(r=\infty,t) = 0\,, \qquad t \geq 0 \qquad (2\text{-}8c)$$

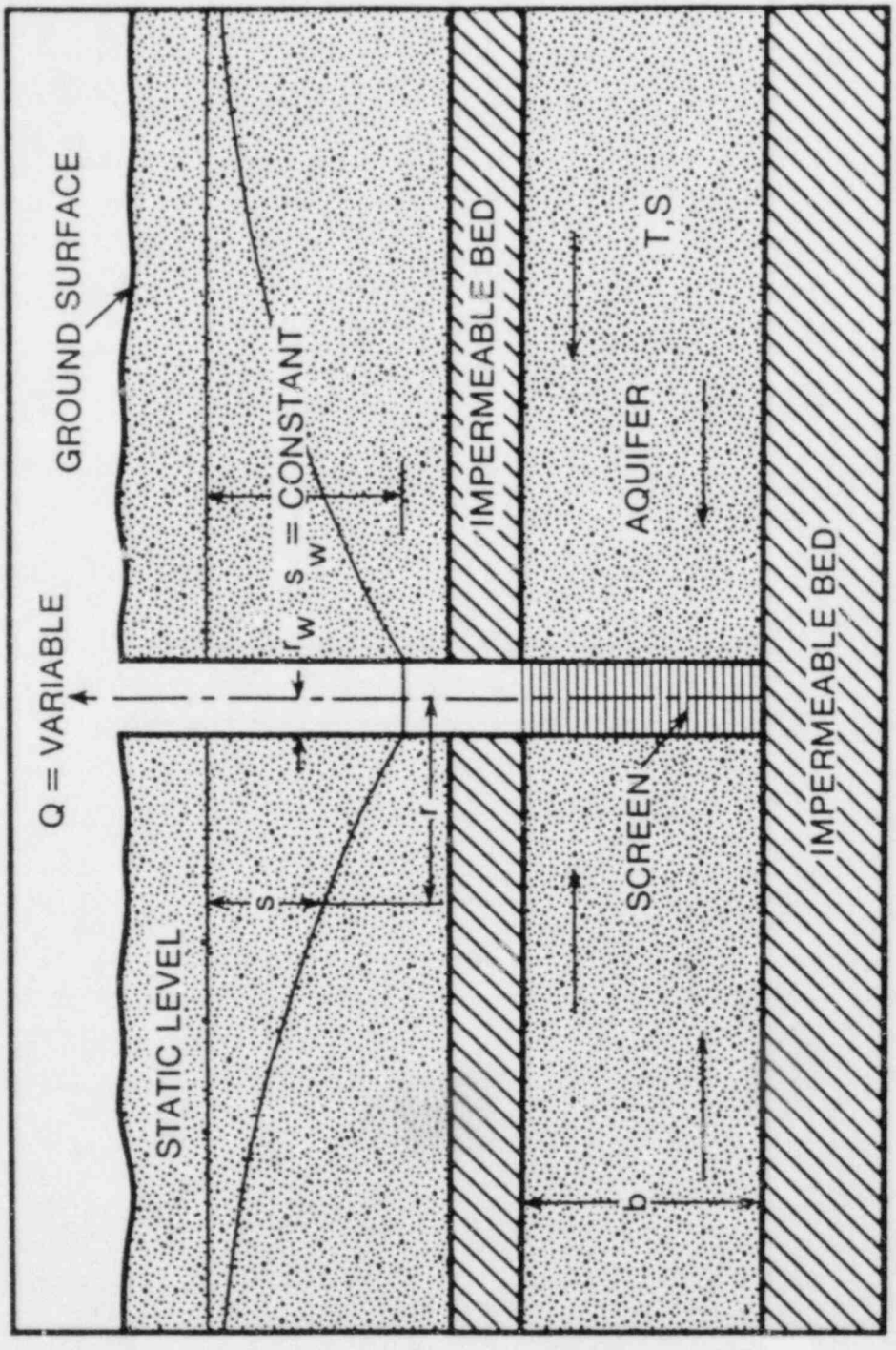

Figure 2-5. Schematic Diagram of a Fully Penetrating Constant-Drawdown Well in a Confined Aquifer, Problem 2.2.

2.2.3 Assumptions

The assumptions invoked in the above analysis are essentially the same as for the Theis solution in Section 2.1. The only difference is the prescription here of the constant drawdown, s_w, in the wellbore rather than the constant flow rate, Q, used there.

2.2.4 Analytical Solution

The solution of Equation (2-7) subject to Equations (2-8) is:

$$s = s_w A(\tau,\rho) \tag{2-9}$$

where the dimensionless arguments are given by:

$$\tau = Tt/Sr_w^2 \tag{2-10a}$$

and

$$\rho = r/r_w \tag{2-10b}$$

The constant-drawdown function $A(\tau,\rho)$ is obtained by Hantush [1964] and is tabulated by Reed [1980].

The well discharge rate may be obtained from Equation (2-9). It is:

$$Q = 2\pi Ts_w G(\tau) \tag{2-11}$$

The dimensionless flow rate $G(\tau)$ is tabulated by Jacob and Lohman [1952] and is generated herein using the algorithm supplied by Reed [1980].

2.2.5 Input Specifications

With only two exceptions, the input parameters for this problem were chosen to be identical to those of Problem 2.1 (see Tables 2-1 and 2-2). Here, in place of a specified pumping rate, a constant drawdown:

$$s_w = 3.999 \text{ m} \tag{2-12a}$$

is used. This value corresponds to a differential pressure drop of:

$$\Delta p = 39{,}100 \text{ Pa} \qquad (5.67 \text{ psi}) \qquad (2\text{-}12b)$$

2.2.6 Output Specifications

The output for this problem consists of pumping rate and drawdown as functions of time.

2.2.7 Numerical Solution

Although SWIFT solves the same equation used with the analytic approach, there are differences at the inner and outer boundaries. These are the well skin which is assumed to surround the wellbore and the Carter-Tracy boundary condition [Reeves et al, 1984a and Carter and Tracy, 1960] at the outer extremity of the gridding.

The SWIFT formulation assumes that a skin surrounds the wellbore and that the pressure drop across this skin is proportional to the flow rate. The constant of proportionality is called the well index. This is a useful facility for a field problem. However, for this idealized problem, the effects of the skin must be minimized, and the well index is determined directly from the reservoir permeability. It is:

$$WI_o = 4.41 \times 10^{-3} \text{ m}^2/\text{s} \qquad (4.10 \times 10^{3} \text{ ft}^2/\text{d}) \qquad (2\text{-}13)$$

The latter (i.e., the Carter-Tracy condition) is an approximate method for matching onto an infinite-aquifer solution in order to include the effects of the aquifer surrounding the reservoir. Athough, to some extent, this procedure is subject to direct verification by this test, the chosen matching radius, r_e, is sufficiently distant from the cone of depression that the adverse effects of this approximate condition should be negligible.

2.2.8 Results

Figure 2-6 presents plots of pumping rate versus time, and Figure 2-7 presents plots of drawdown versus time. In each case the agreement between analytical and numerical results is quite satisfactory.

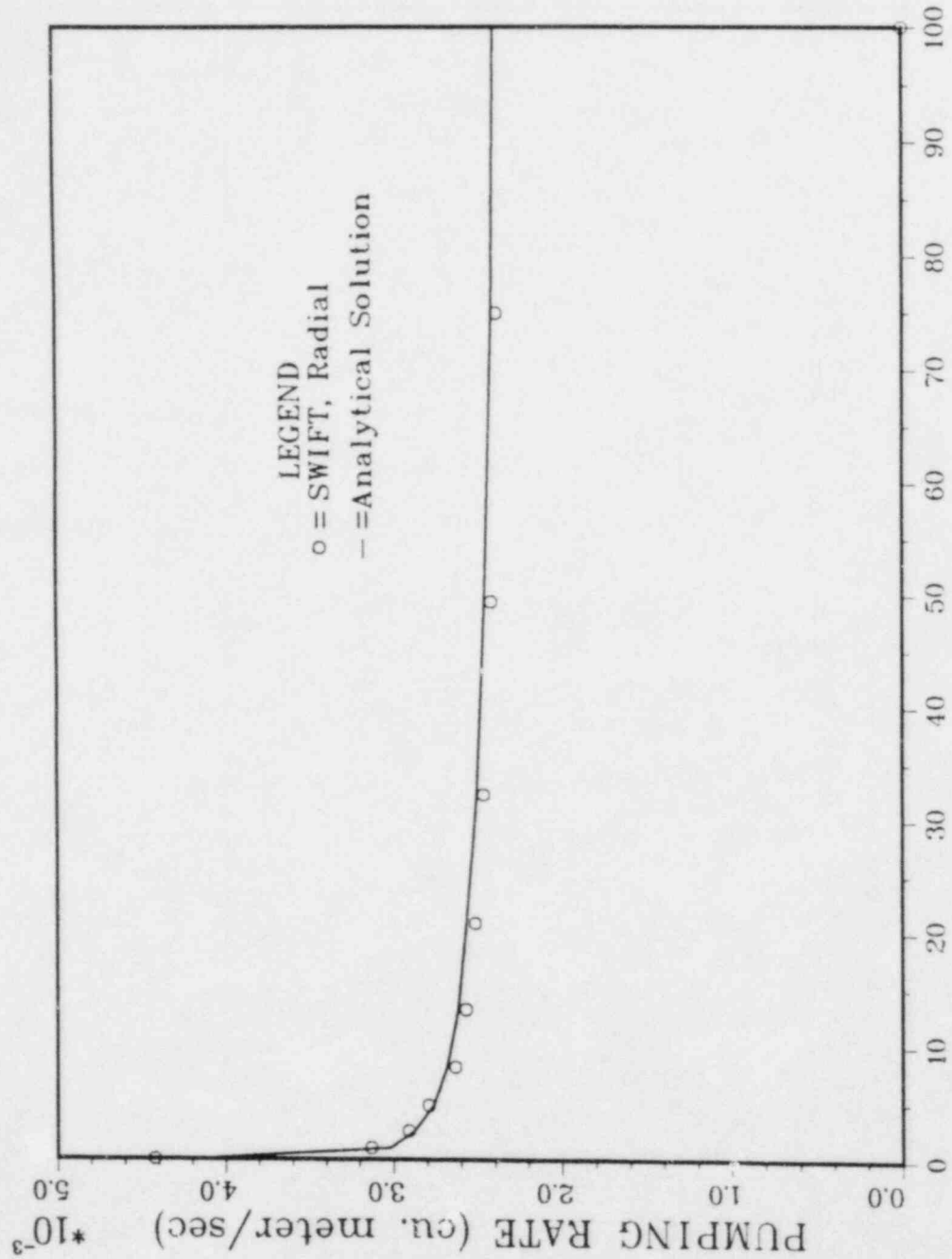

Figure 2-6. Pumping Rate as a Function of Time for a Constant-Drawdown Well.

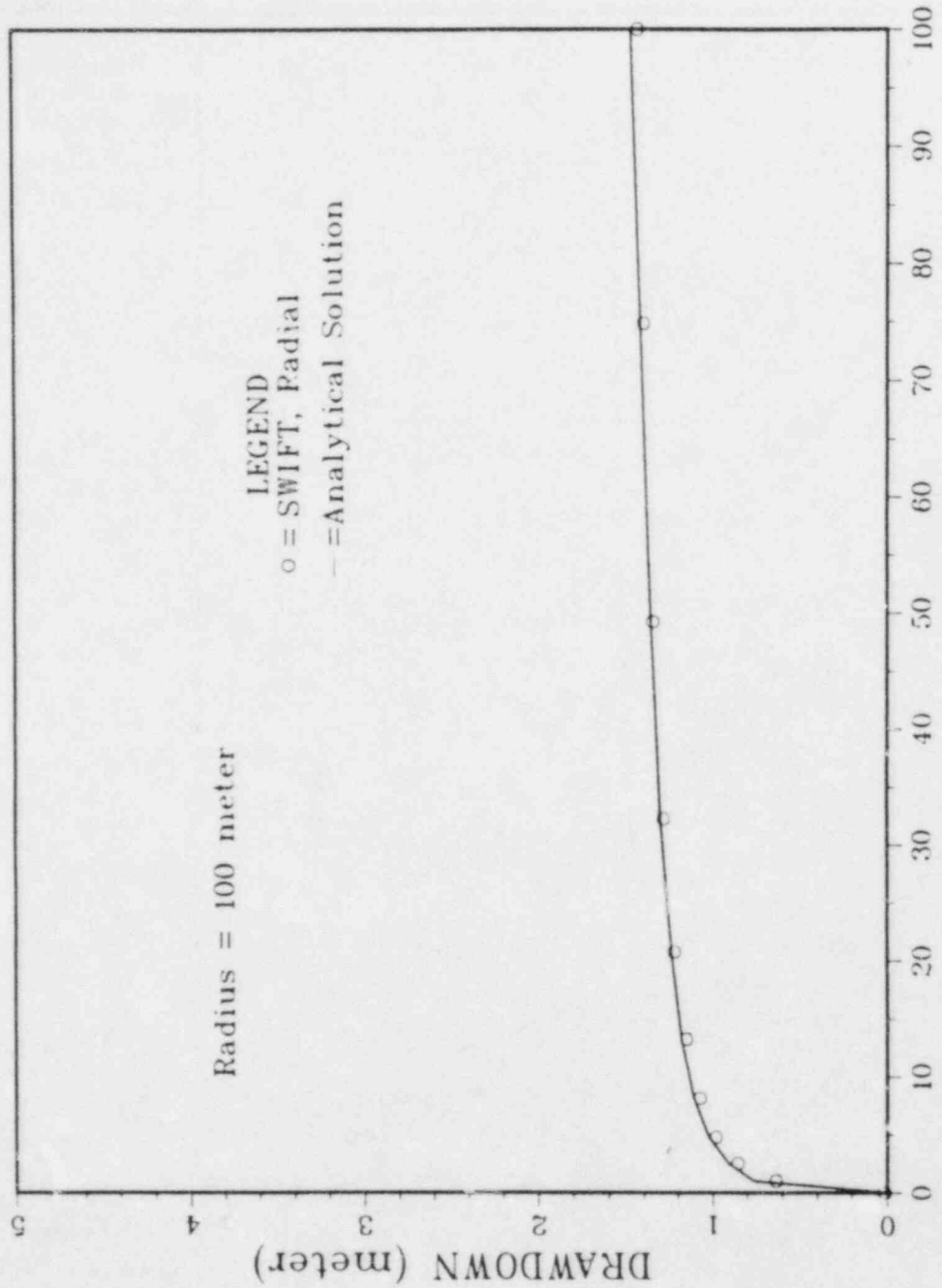

Figure 2-7. Drawdown as a Function of Time for a Constant-Drawdown Well.

2.3 FULLY PENETRATING WELL IN A HORIZONTAL ANISOTROPIC AQUIFER [PAPADOPULOS, 1965]*

2.3.1 Objectives

The purposes for simulating this problem are to test the following aspects of the SWIFT Code:

- pressure solution,
- anisotropic permeability tensor,
- rate-controlled well condition,
- two-dimensional Cartesian geometry,
- SI and English Engineering units.

2.3.2 Description of Problem

A well fully penetrates an infinite confined aquifer and is pumped at a constant rate, as shown schematically in Figure 2-1. The aquifer is taken to be anisotropic and parallel to the horizontal plane. If, further, the coordinate axes are aligned with the principal axes of the transmissivity tensor, the equation to be solved may be written as:

$$T_x \frac{\partial^2 s}{\partial x^2} + T_y \frac{\partial^2 s}{\partial y^2} + Q\,\delta(x)\,\delta(y) = S \frac{\partial s}{\partial t} \qquad (2\text{-}14)$$

where δ is a Dirac delta function.

Another coordinate transformation could be performed to facilitate the solution of this equation, namely:

$$\bar{x} = x \quad \text{and} \quad \bar{y} = (T_x/T_y)^{1/2} y \qquad (2\text{-}15)$$

---

* Benchmark Problem 3.3 [Ross et al, 1982].

This would, in effect, reduce the problem to the isotropic case, with the well-known Theis solution. This transformation is not considered further here, however, since one of the primary objectives of this problem is to test the anisotropic capabilities of the SWIFT code.

Boundary/initial conditions are:

$$s(x,y,t=0) = 0 \quad , \quad x \geq 0 \text{ and } y \geq 0 \tag{2-16a}$$

$$s(x = \pm \infty, y, t) = 0 \quad , \quad t > 0 \tag{2-16b}$$

and

$$s(x, y = \pm \infty, t) = 0 \quad , \quad t > 0 \tag{2-16c}$$

2.3.3 Assumptions

The assumptions invoked in the above analysis are essentially the same as for the Theis solution in Section 2.1. However, an anisotropic aquifer is permitted in this case.

2.3.4 Analytical Solution

As anticipated above in the transformation noted in Equation (2-15), the solution is closely related to the Theis solution (Equation (2-6)). It is:

$$s = (Q/4\pi \sqrt{T_x T_y}\,)\, W(u_{xy}) \tag{2-17a}$$

[Reed, 1980] where the dimensionless variable u is given by:

$$u_{xy} = (S/4t)\,(T_x y^2 + T_y x^2)/T_x T_y \tag{2-17b}$$

and W is the familar well function.

2.3.5 Input Specifications

Input parameters for this problem are taken directly from page 19 of Ross et al [1982]. With only two exceptions they are identical to those specified in Tables 2-1 and 2-2. Here, for the anisotropic case, the components of the transmissivity tensor are given by:

$$T_x = 10^{-3}\ m^2/s \quad \text{and} \quad T_y = 10^{-4}\ m^2/s \tag{2-18a}$$

The corresponding values of hydraulic conductivity, used in the SWIFT input are:

$$K_x = 3.28 \times 10^{-4}\ m/s \quad \text{and} \quad K_y = 3.28 \times 10^{-5}\ m/s \tag{2-18b}$$

2.3.6 Output Specifications

Output for this problem consists of drawdowns versus time and distance. As specified by Ross et al [1982], the drawdown as a function of time is to be determined at points (x,y) of (100 m, 0) and (0, 100 m). Further, the drawdown, as measured along both x and y axes is to be calculated at t = 100 d.

2.3.7 Numerical Solution

Two aspects of the numerical algorithm are not completely identical to the analytical statement of the problem. These aspects relate to the numerical grid and to the infinite boundary condition. Firstly, in order to minimize computer resources, a quarter-section grid similar to Figure 2-2b was used. (A radial grid is not appropriate since this problem does not have radial symmetry.) Relative to previous simulations (see Section 2.1.7) three additional rows of blocks were added in the x-direction, thus extending the system length from 8197.5 to 65,542 m. The cone of depression of an anisotropic aquifer is elliptical, thus requiring a larger domain in the

direction of the major axis, in this case, in the x-direction. This is not exactly a symmetric section of the areal plane surrounding the well. However, because of the small geometric discrepancy, the effects are expected to be negligible.

Secondly, the infinite boundary condition of Equations (2-16) are approximated by no-flow conditions at the outer periphery of the system. However, since

$$L_x >> (T_x \tau / S)^{1/2} \quad \text{and} \quad L_y >> (T_y \tau / S)^{1/2} \tag{2-19}$$

where τ = 100 d is the maximum simulation time, the cone of depression should not be disturbed appreciably by the finite boundaries. On purely physical grounds, the cone of depression should have the dimensions of the right-hand sides of the Inequalities (2-19). Thus, the cone of depression should be well contained in the 65 km x 8.2 km region.

2.3.8 Results

Figure 2-8 shows drawdown as a function of time for the points (100 m, 0) along the x-axis and (0, 100 m) along the y-axis. Figure 2-9 then gives the drawdown as a function of distance along the two axes at time t = 100 d. The comparison between analytical and numerical results is satisfactory throughout. However, as expected, the comparison is somewhat better in the space and time domains which correspond to the finer spatial grid.

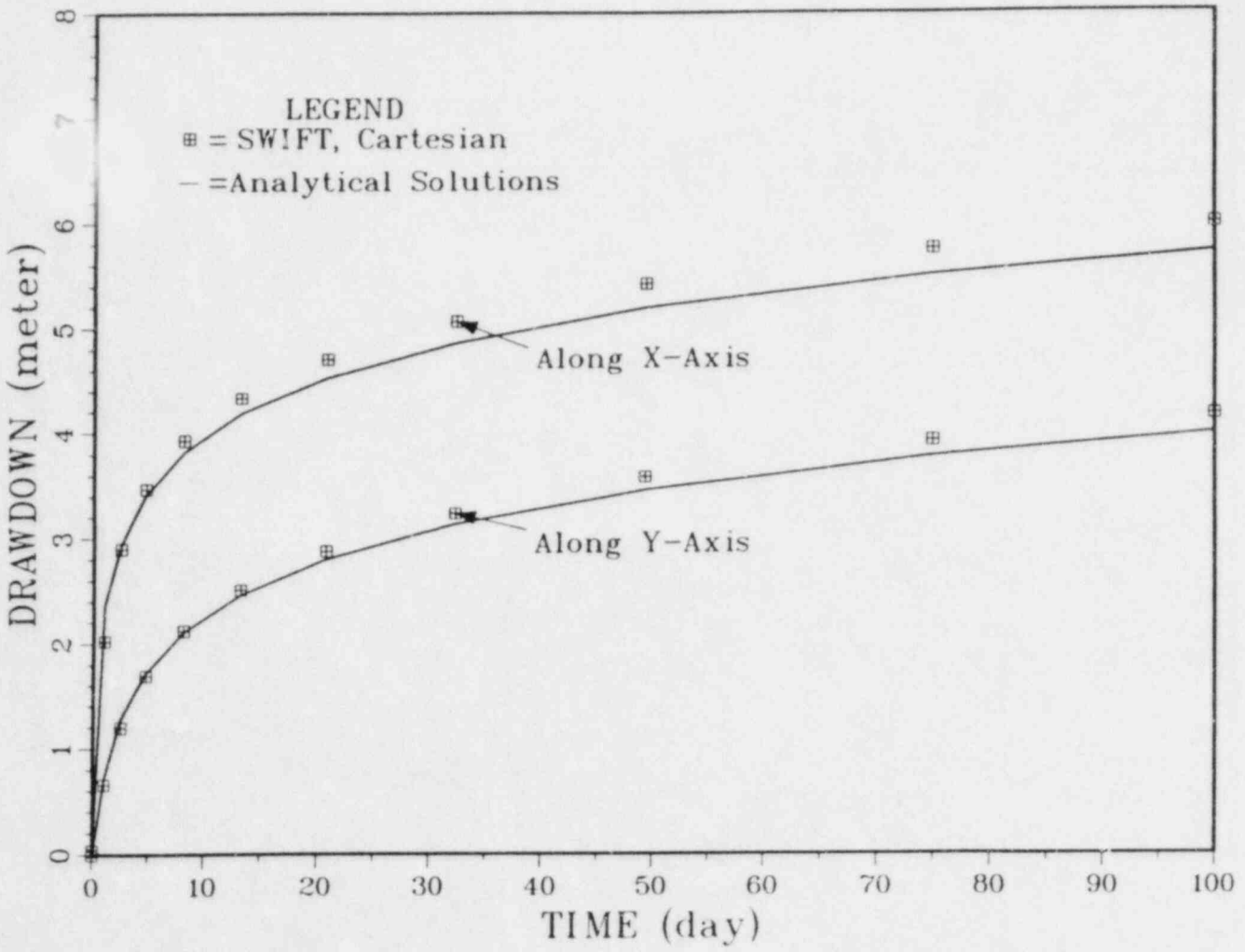

Figure 2-8. Drawdown as a Function of Time for a Constant-Discharge Well, Problem 2.3.

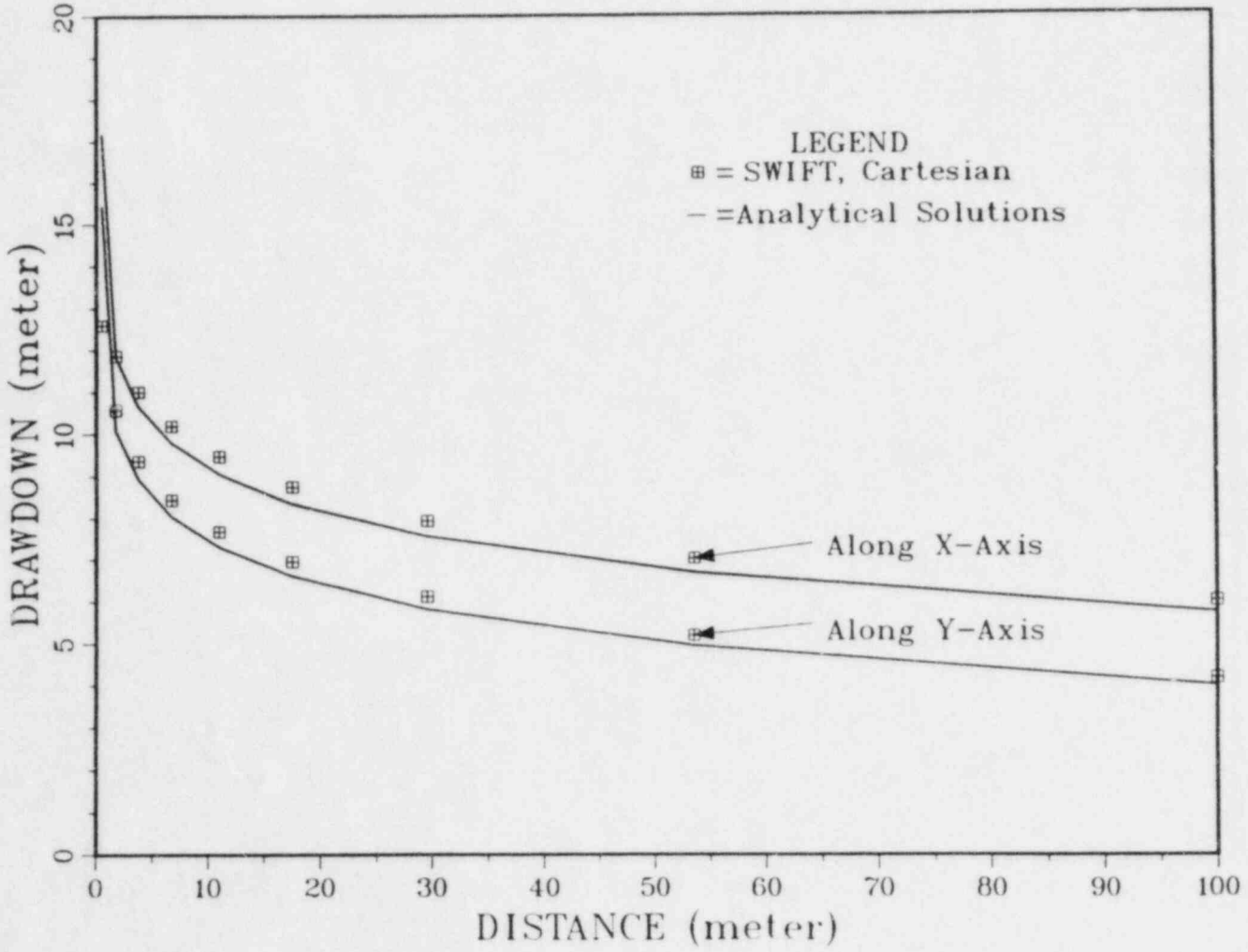

Figure 2-9. Drawdown as a Function of Distance for a Constant-Discharge Well.

2.4 FULLY PENETRATING WELL IN A LEAKY AQUIFER, SMALL VALUES OF TIME [HANTUSH, 1960]*

2.4.1 Objectives

The purposes for simulating this problem are to test the following aspects of the SWIFT Code:

- pressure solution,
- coupling of vertical flow in an aquitard with horizontal flow in an aquifer,
- rate-controlled well condition,
- aquifer-influence function,
- radial geometry,
- SI and English Engineering units.

2.4.2 Description of Problem

A well fully penetrates an infinite aquifer and is pumped at a constant rate. The aquifer is bounded from below by an impermeable bed and from above by a confining bed or aquitard. The latter influences the aquifer to a moderate degree since it is weakly conductive and contains some fluid storage. A schematic drawing is shown as Figure 2-10.

There are two flow equations here, one for the aquifer and one for the aquitard. The former is given by:

$$T \frac{1}{r} \frac{\partial}{\partial r} \left(r \frac{\partial s}{\partial r}\right) + K' \frac{\partial s'}{\partial z} = S \frac{\partial s}{\partial t} \qquad (2\text{-}20)$$

where the second term provides the coupling to the aquitard. It is subject to the following boundary/initial conditions:

$$s(r, t=0) = 0 \quad , \quad r > 0 \qquad (2\text{-}21a)$$

---

* Benchmark Problem 3.2, Ross et al [1982].

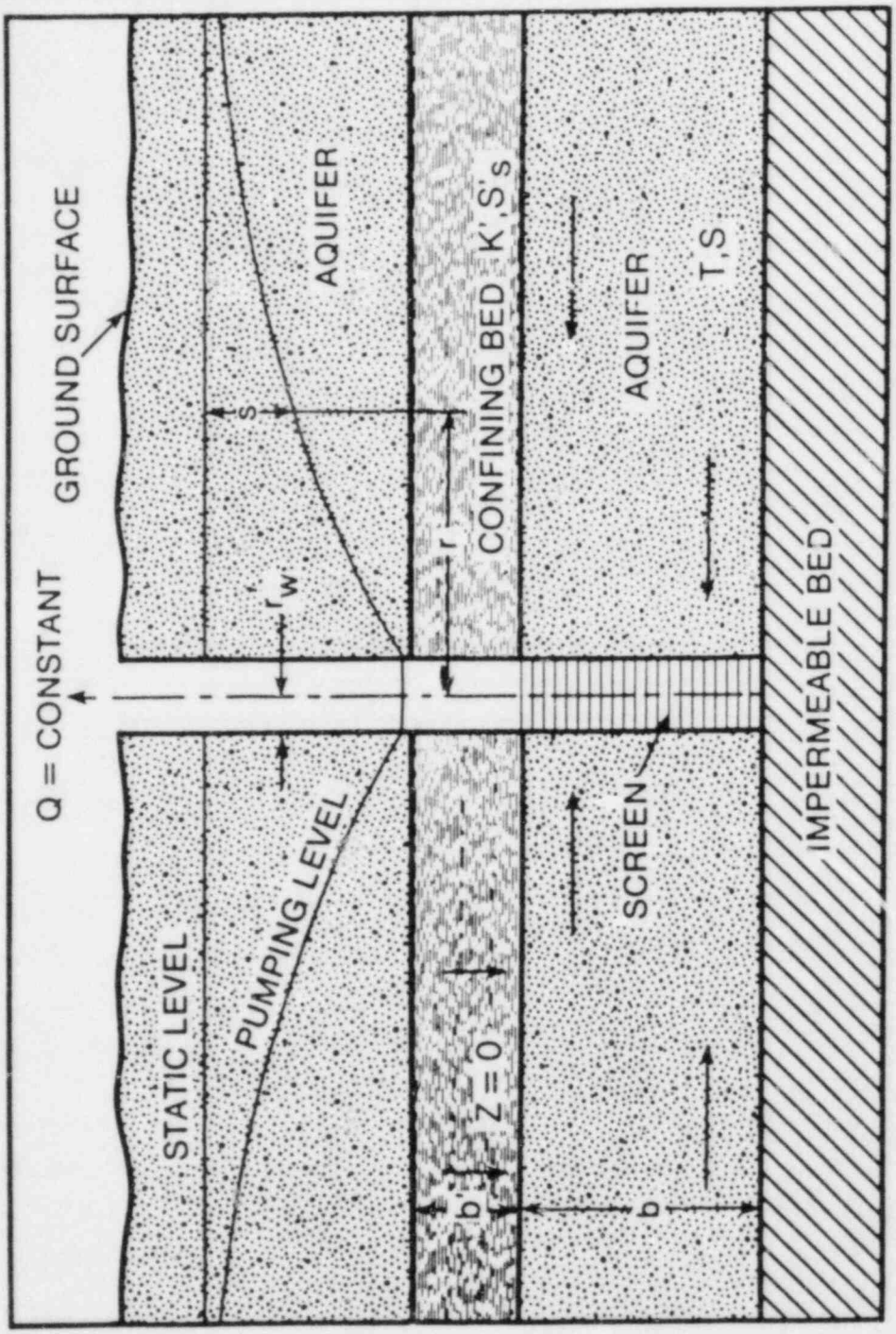

Figure 2-10. Schematic Diagram of a Fully Penetrating Constant-Discharge Well in a Leaky Aquifer, Problem 2.4.

$$s(r = \infty, t) = 0 \quad , \quad t > 0 \tag{2-21b}$$

and

$$\lim_{r \to 0} \left(r \frac{\partial s}{\partial r} \right) = - \frac{Q}{2\pi T} \quad , \quad t > 0 \tag{2-21c}$$

The equation for the aquitard is:

$$K' \frac{\partial^2 s'}{\partial z^2} = S'_s \frac{\partial s'}{\partial t} \tag{2-22}$$

The initial condition is:

$$s'(r, z, t=0) = 0 \quad , \quad r > 0, \quad -b' < z < 0 \tag{2-23a}$$

and the interface boundary condition is:

$$s'(r, z=0, t) = s \quad , \quad r > 0, \quad t > 0 \tag{2-23b}$$

where z is measured positive downward from the aquifer-aquitard interface.

For the upper boundary on the aquitard, however, two conditions may be considered, i.e., either:

Case 1: $$s'(r, z=-b', t) = 0 \quad , \quad r > 0, \quad t > 0 \tag{2-24}$$

or

Case 2: $$\frac{\partial s'}{\partial z} (r, z=-b', t) = 0 \quad , \quad r > 0, \quad t > 0 \tag{2-25}$$

In Case 1 there is assumed to be an aquifer overlying the confining bed from which leakage may occur. In Case 2 there is assumed to be an impermeable bed overlying the aquitard.

2.4.3 Assumptions

The assumptions invoked in the above analysis are the following:

- The aquifer has infinite areal extent.
- The aquifer is confined with leakage.
- This leakage is the result of flow through the confining beds and/or a reduction of storage in the confining beds.
- The head in the upper aquifer (see Figure 2-10) supplying the leakage is constant.
- The aquifer is homogeneous and horizontal and of uniform thickness over the area influenced by the pumping test.
- The confining bed is homogeneous, horizontal and uniform in thickness.
- The permeability contrast between aquifer and confining bed is sufficiently great that flow is horizontal in the aquifer and vertical in the aquitard.
- Prior to pumping, the potentiometric surfaces are horizontal for the aquifer, for the confining bed, and for the layer supplying the leakage.
- Pumping is performed at a constant rate.
- The pumped well penetrates the entire aquifer and thus receives water from the entire thickness of the aquifer by horizontal flow.
- The diameter of the pumped well is sufficiently small that its internal storage may be neglected.
- The water removed from storage is discharged instantaneously with decline of head.
- Darcy's law applies throughout the system, and non-Darcy velocities near the well may be neglected.

2.4.4 Analytical Solution

For small values of time, the solution [Hantush, 1960] for both cases is:

$$s = (Q/4\pi t)\, H(u,\beta) \quad , \quad t \lesssim [b'^2 S'_s/10K'] \tag{2-26}$$

where the dimensionless variables are:

$$u = r^2 S/4Tt \tag{2-27a}$$

and

$$\beta = (r/4)\,(K'S'_s/TS)^{1/2} \tag{2-27b}$$

Here H is obtained from the infinite integral:

$$H(u,\beta) = \int_u^\infty (e^{-y}/y)\,\mathrm{erfc}\,\{\beta[u/y(y-u)]^{1/2}\}\,dy \tag{2-27c}$$

This solution, originally reported by Hantush [1960], is also given in Reed [1980]. The latter reference also gives the large-time solutions for both Case 1 and Case 2 boundary conditions, as defined above.

2.4.5 Input Specifications

Input specifications for this problem are taken directly from Ross et al [1983] p. 17. They are presented here, for a standard hydrological notation, in Table 2-3. They are also presented in SWIFT notation in Table 2-4. Both SI and English Engineering units are used in order to further test the code.

2.4.6 Output Specifications

The output for this problem consists of drawdown versus time and distance. The analytic solution is valid only for values of time less than about 10^5 s (about 24 h), and all simulated times are to be kept substantially lower than this value. Drawdown as a function of time should be obtained at a radial distance of 20 m from the well, and drawdown as a function of radial distance should be obtained for a time of 30 min.

Table 2-3. Parameter Specifications for Problem 2.4.

Parameter	Symbol	Value	
		SI	English
Aquifer storativity	S	10^{-4}	10^{-4}
Aquifer transmissivity	T	10^{-3} m^2/s	930 ft^2/d
Aquitard specific storativity	S'_s	3.0×10^{-3} m^{-1}	9.0×10^{-4} ft^{-1}
Aquitard hydraulic conductivity	K'	3.0×10^{-10} m/s	8.5×10^{-5} ft/d
Aquitard thickness	b'	0.3 m	.984 ft
Pumping rate	Q	0.014 m^3/s	42717 ft^3/d

Table 2-4. SWIFT Parameters for Problem 2.4.

Parameter	Symbol	Value	
		SI	English
Aquifer porosity	ϕ	.004	.004
Aquifer hydraulic conductivity	K	3.28×10^{-4} m/s	93 ft/d
Aquifer thickness	b	3.05 m	10 ft
Aquitard porosity	ϕ'	0.4	0.4
Aquitard hydraulic conductivity	K'	3.0×10^{-10} m/s	8.5×10^{-5} ft/d
Aquitard thickness	b'	0.3 m	.984 ft
Pumping rate	Q	0.014 m^3/s	42717 ft^3/d
Fluid viscosity	μ	0.001 Pa-s	1 cp
Fluid density	ρ	1000 kg/m^3	62.4 lb/ft^3
Rock compressibility	c_R	7.67×10^{-7} Pa^{-1}	5.28×10^{-3} psi^{-1}
Wellbore radius	r_w	.1143 m	.375 ft
Aquifer radius	r_e	6096 m	20,000 ft

2.4.7 Numerical Solution

The radial grid used here was similar to that in Problem 2.1 (see Figure 2-2). The mesh, in this case, was modified slightly so that drawdown at $r = 20$ m could be observed. In Problem 2.1, the drawdown was observed at $r = 100$ m. In both tests equal log Δr's were employed (see Reeves et al [1984a]). In addition, boundary conditions at the well and at the aquifer radius were handled in the same manner as for the previous problem.

2.4.8 Results

The results are shown in Figures 2-11 and 2-12, where numerical and analytical results may be compared. Figure 2-11 does show some degrading of the numerical solution as the time step is increased. However, the agreement between numerical and analytical calculations is still quite acceptable.

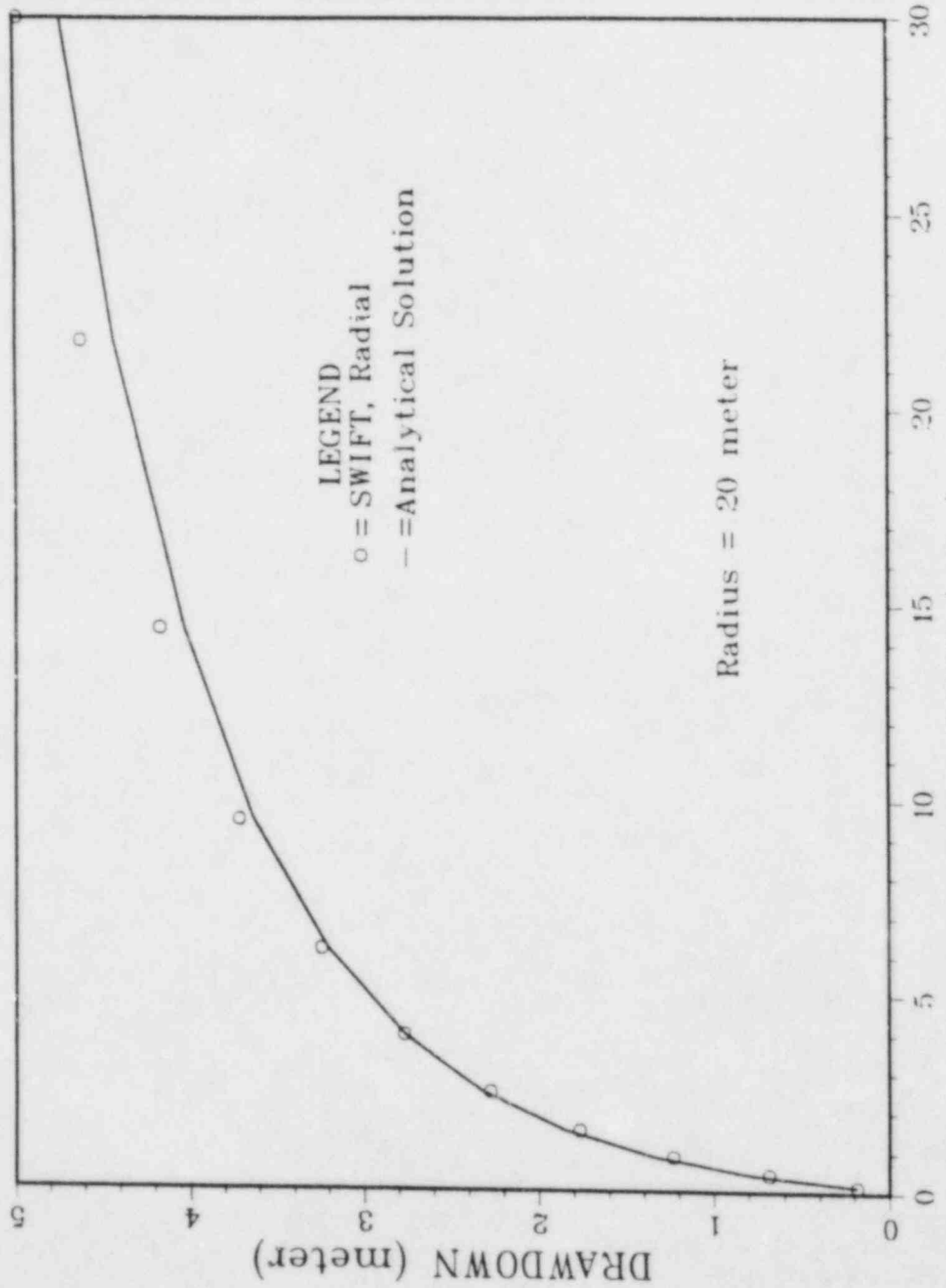

Figure 2-11. Drawdown as a Function of Time for a Leaky Aquifer.

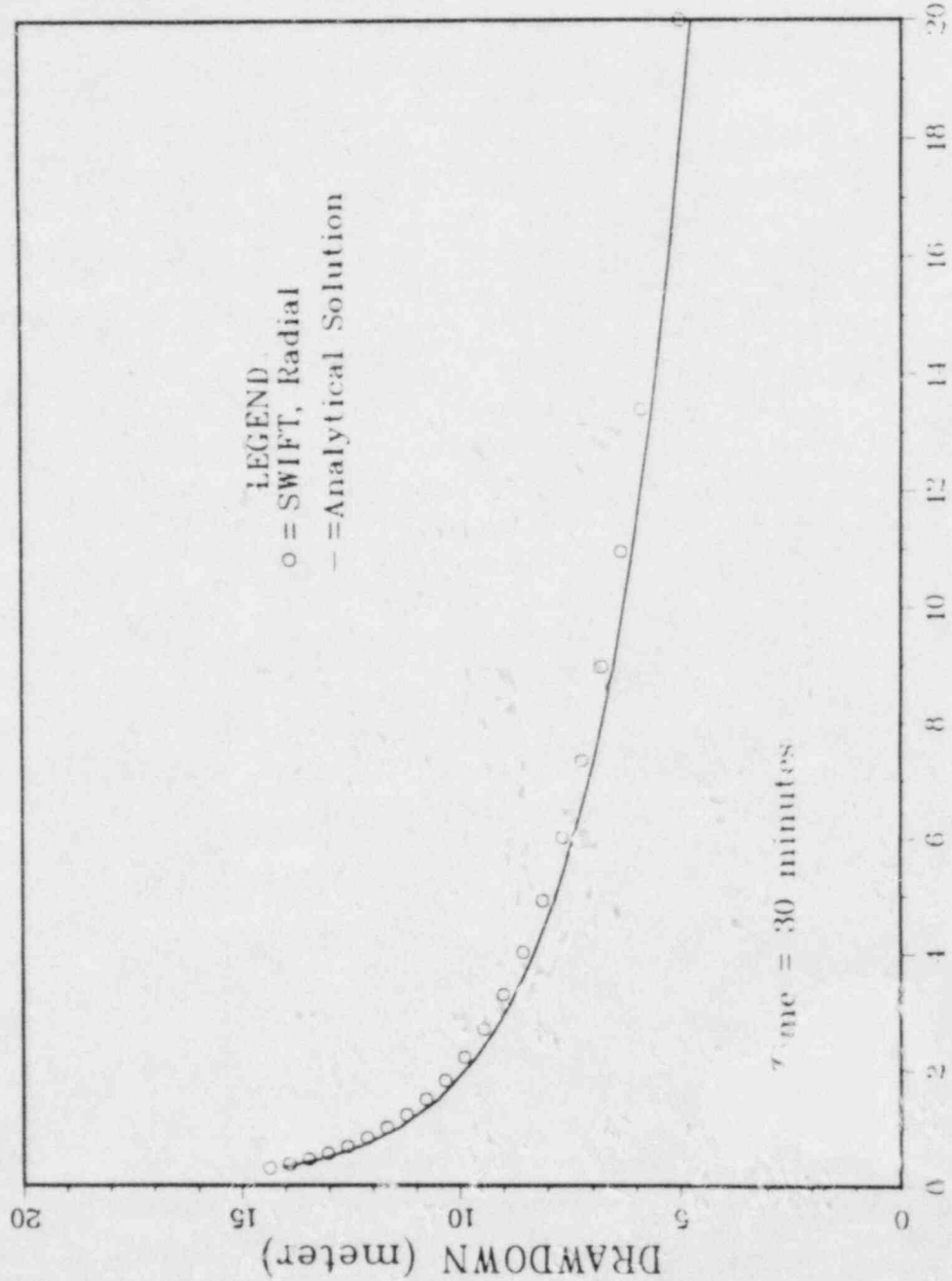

Figure 2-12. Drawdown as a Function of Distance for a Leaky Aquifer.

3 VERIFICATION OF THE HEAT TRANSPORT

3.1 ONE-DIMENSIONAL CONVECTIVE-DISPERSIVE TRANSPORT [COATS AND SMITH, 1964]

3.1.1 Objectives

The purposes for simulating this problem are to test the following aspects of the SWIFT Code:

- thermal convection,
- thermal dispersion,
- thermal conduction,
- thermal retardation,
- aquifer-influence function,
- heat injection via wells,
- SI and English Engineering units.

3.1.2 Description of Problem

A hot incompressible fluid is injected into a confined aquifer, where thermal convection, conduction and dispersion occur. There is no significant heat loss to the confining layers. Mathematically, the injection process may be treated by two different boundary conditions. One is a type-one condition in which a constant temperature, T_1, is imposed at the boundary. The other is a type-three condition deriving from a constant heat input, where the rate of heat input to the system is of sufficient magnitude that the boundary temperature converges asymptotically to the same temperature, T_1.

The equation to be solved is:

$$- v \frac{\partial T}{\partial x} + D \frac{\partial^2 T}{\partial x^2} = \frac{\partial T}{\partial t} \qquad (3\text{-}1)$$

Here D contains both fluid dispersion, $\alpha_L u$, and fluid/rock conduction, K_m.

$$D = (\alpha_L u \rho c_p + K_m)/K\phi\rho c_p \qquad (3\text{-}2a)$$

In addition, a retardation, K, arises from the heat capacity of the rock so that the retarded interstitial velocity is derived from the Darcy velocity, u, by:

$$v = u/K\phi \tag{3-2b}$$

where

$$K = 1 + (1-\phi)\rho_R c_{\rho R}/\phi\rho c_p \tag{3-2c}$$

Initial/boundary conditions are specified on a semi-infinite strip as:

$$T(x,t=0) = T_o, \qquad x \geq 0 \tag{3-3a}$$

$$T(x=\infty,t) = T_o, \qquad t \geq 0 \tag{3-3b}$$

and

$$T(x=0,t) = T_1, \qquad t > 0 \tag{3-4a}$$

for the type-one boundary. Equation (3-4a) is changed to a flux condition for the type-three boundary, i.e.,

$$vT_1 = vT - D\frac{\partial T}{\partial x} \tag{3-4b}$$

3.1.3 Assumptions

The assumptions involved in the above analysis are the following:

- Flow and transport are in one dimension.
- The domain is semi-infinite.
- Hydraulic and thermal parameters are constant.
- Buoyancy may be neglected within the aquifer.
- There is no heat transport within the confining layers.

3.1.4 Analytical Solution

For the type-one condition imposed at x=0, the solution is:

$$o^{(1)} = (1/2)\{\mathrm{erfc}[(x-vt)/2\sqrt{Dt}] + \exp(vx/D)\mathrm{erfc}[(x+vt)/2\sqrt{Dt}]\} \tag{3-5}$$

For the type-three conditions imposed at x=0, the solution is:

$$\Theta^{(3)} = (1/2)\{\mathrm{erfc}[(x-vt)/2\sqrt{Dt}] - \exp(vx/D)\mathrm{erfc}[(x+vt)/2\sqrt{Dt}]\}$$
$$- (v/2D)(x+vt)\exp(vx/D)\mathrm{erfc}[(x+vt)/2\sqrt{Dt}] \qquad (3\text{-}6)$$
$$+ \sqrt{v^2 t/\pi D}\,\exp[-(x-vt)^2/4Dt]$$

where Θ, the dimensionless temperature, is:

$$\Theta = (T-T_o)/(T_1-T_o) \qquad (3\text{-}7)$$

3.1.5 Input Specifications

Input parameters for this problem are given in Table 3-1. They may be used directly in both of the analytical solutions, Equations (3-5) and (3-6). They may also be used directly in the SWIFT input, a copy of which is presented in the microfiche accompanying this report.

3.1.6 Output Specifications

The output of this problem consists of temperature as a function of distance for two fixed times and for both boundary conditions. Those fixed times are taken to be 2148 d and 4262 d.

3.1.7 Numerical Solution

The input necessary for analytical solution must be supplemented with certain geometrical data. The numerical scheme is, of course, incapable of simulating a semi-infinite system. Thus, the system is chosen to be sufficiently long (2,000 ft) that the front will be affected in only a minor way even at its most advanced position (≈ 800 ft). In addition, gridding is required in both the space and time domains. Since a centered-in-time,

Table 3-1. Parameter Specifications for Problem 3.1.

Parameter	Symbol	Value	
		SI	English
Thermal conductivity of the medium	K_m	2.16 W/(m·°C)	30 Btu/(ft·d·°F)
Heat capacity of the rock	c_{pR}	2.01×10^6 J/(m^3·°C)	30 Btu/(ft^3·°F)
Porosity	ϕ	0.10	0.10
Density of the rock	ρ_R	1602 kg/m^3	100 lb/ft^3
Dispersivity	α_L	14.4 m	47.2 ft
Darcy velocity	u	3.53×10^{-7} m/s	0.1 ft/d
Heat capacity of the fluid	c_p	4185 J/(kg·°C)	1 Btu/(lb·°F)
Density of the fluid	ρ	1000 kg/m^3	62.4 lb/ft^3
Retardation factor	K	5.33	5.33
Retarded dispersion	D	1.15×10^{-5} m^2/s	10.7 ft^2/d
Retarded velocity	v	6.63×10^{-7} m/s	0.188 ft/d
Initial temperature	T_o	37.78 °C	100 °F
Boundary temperature	T_1	93.33 °C	200 °F

centered-in-space differencing is adopted, the incremental values must be chosen accordingly (see Reeves et al [1984a], Chapter 7). The additional information used in the SWIFT simulation is shown in Table 3-2.

A final point to be discussed here is the specification of the third-type boundary condition in the numerical solution. This is accomplished using a well in the first grid block. Since such a source acts on the cell as a whole, it may be considered as being located at the grid-block center. Thus, a correction of $\Delta x_1/2$ is called for. Such a correction has been made in the results.

3.1.8 Results

The results are presented in Figure 3-1. As shown, the agreement between numeric and analytic is quite satisfactory. Simulations were performed in both SI and English systems of units, and the results were virtually identical.

Table 3-2. Discretization Parameters for Problem 3.1.

Parameter	Symbol	Value	
		SI	English
Length	L	610 m	2000 ft
Space increment	Δx	30.5 m	100 ft
Time increment	Δt	4.84×10^5 s	5.6 d
Space differencing	CIS*	---	---
Time differencing	CIT*	---	---

* CIS means centered-in-space and CIT means centered-in-time.

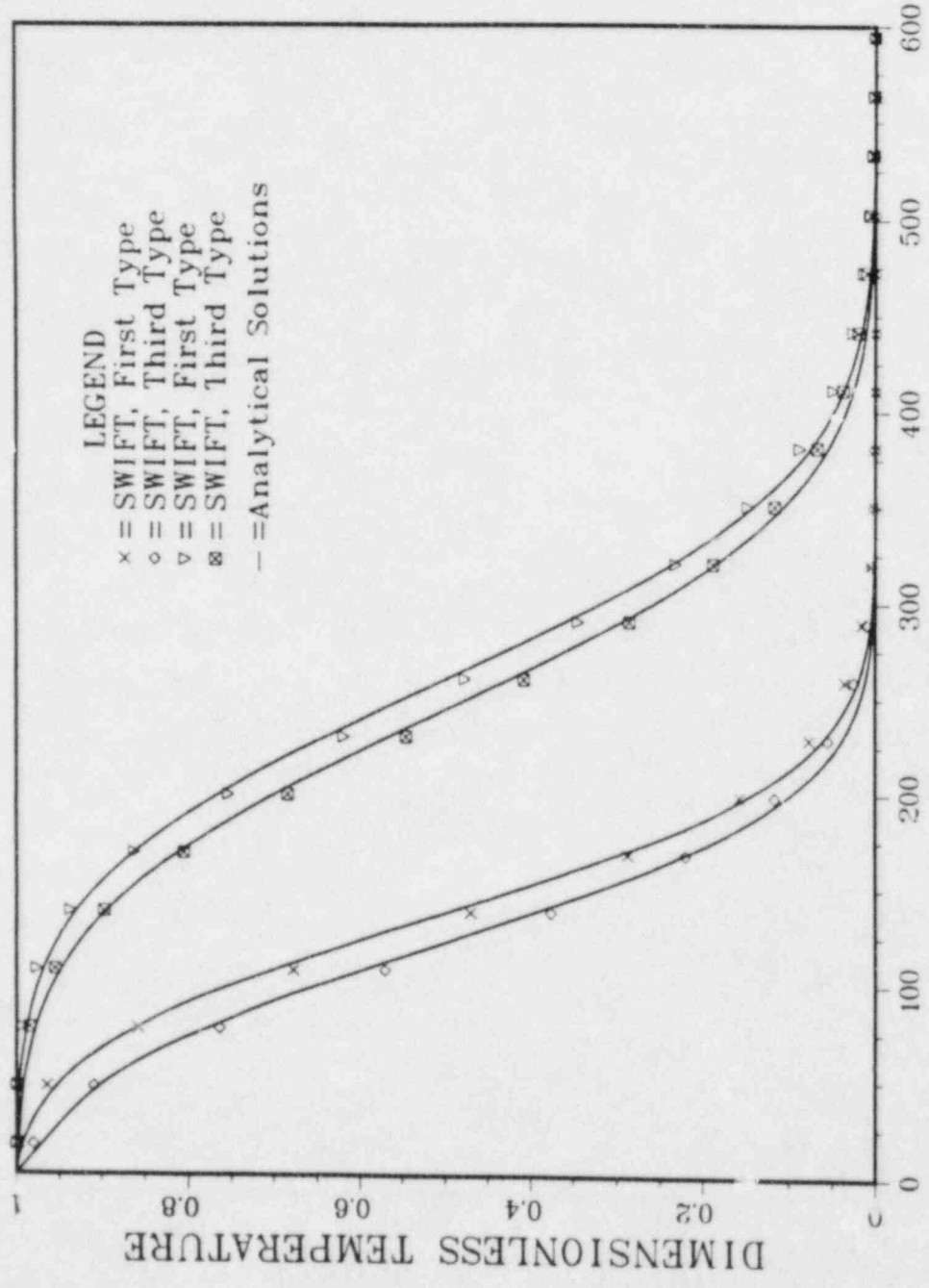

Figure 3-1. Dimensionless Temperature Profiles at Two Values of Time, Problem 3.1.

3.2 LINEAR AND RADIAL HEAT TRANSPORT DURING INJECTION [AVDONIN, 1964]*

3.2.1 Objectives

The purposes for simulating this problem are to test the following aspects of the SWIFT Code:

- thermal convection,
- thermal conduction,
- thermal retardation,
- thermal conduction in confining layers,
- heat loss to confining layers,
- radial and Cartesian coordinates,
- SI and English Engineering units.

3.2.2 Description of Problem

An incompressible fluid of temperature, T_I, is injected into a confined aquifer of temperature, T_o, through a fully penetrating well (see Figure 3-2). Both thermal convection and thermal conduction occur within the aquifer, but only thermal conduction is operative within the over/underburden. Furthermore, heat transport in these confining layers is assumed to be in the vertical (z) direction only. Thus, for the over/underburden, the equation to be solved, at any given distance (x or r) from the wellbore, is:

$$K'_m \frac{\partial^2 T'}{\partial z^2} = \rho'_m c'_{pm} \frac{\partial T'}{\partial t} \qquad (3\text{-}8)$$

and the initial/boundary conditions are

$$T'(x,z,t=0) = T_o, \qquad z > 0 \qquad (3\text{-}9a)$$

---

* Benchmark Problem 5.1 [Ross et al, 1982].

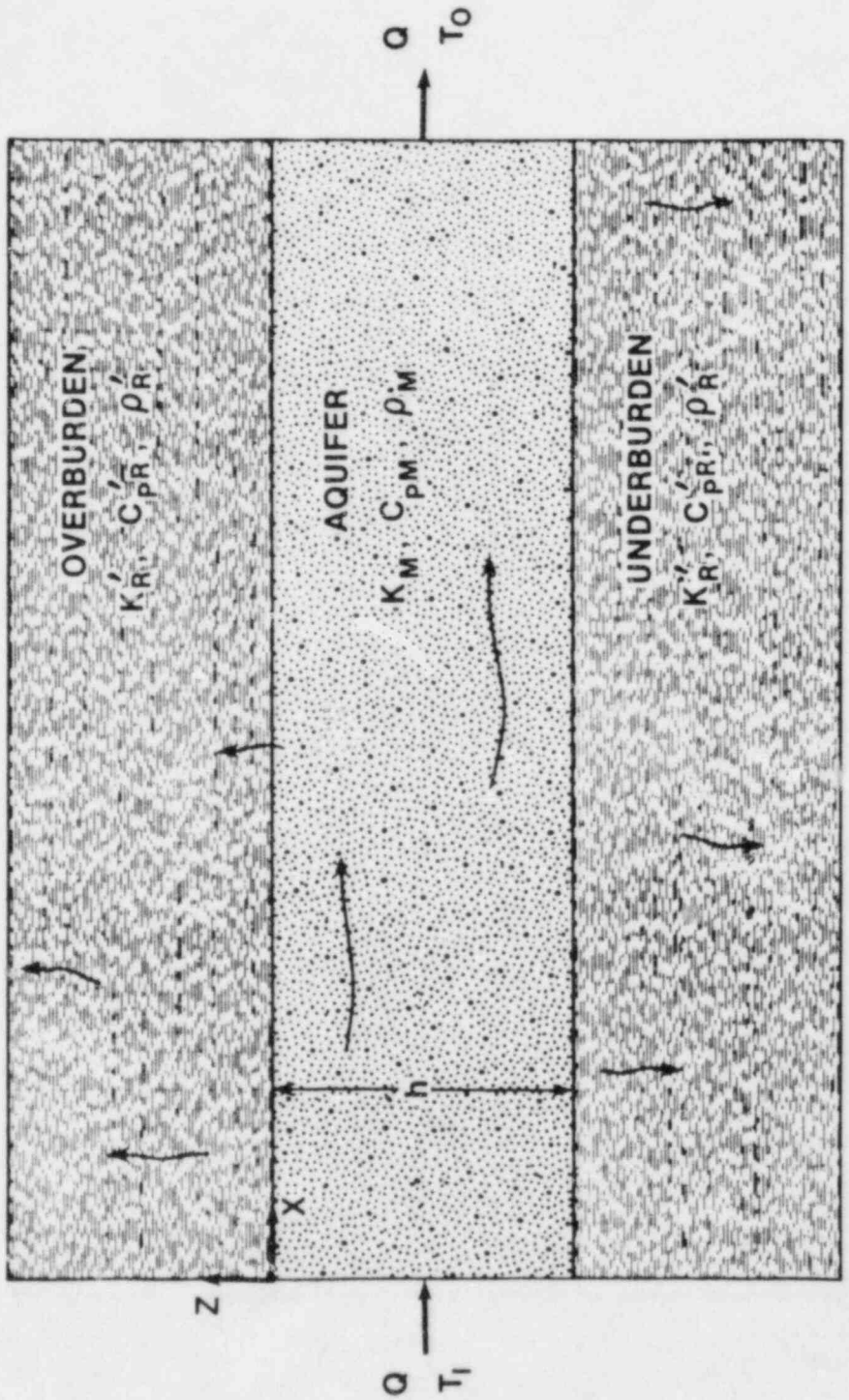

Figure 3-2a. Linear Heat Transport Through an Aquifer System, Problem 3.2.

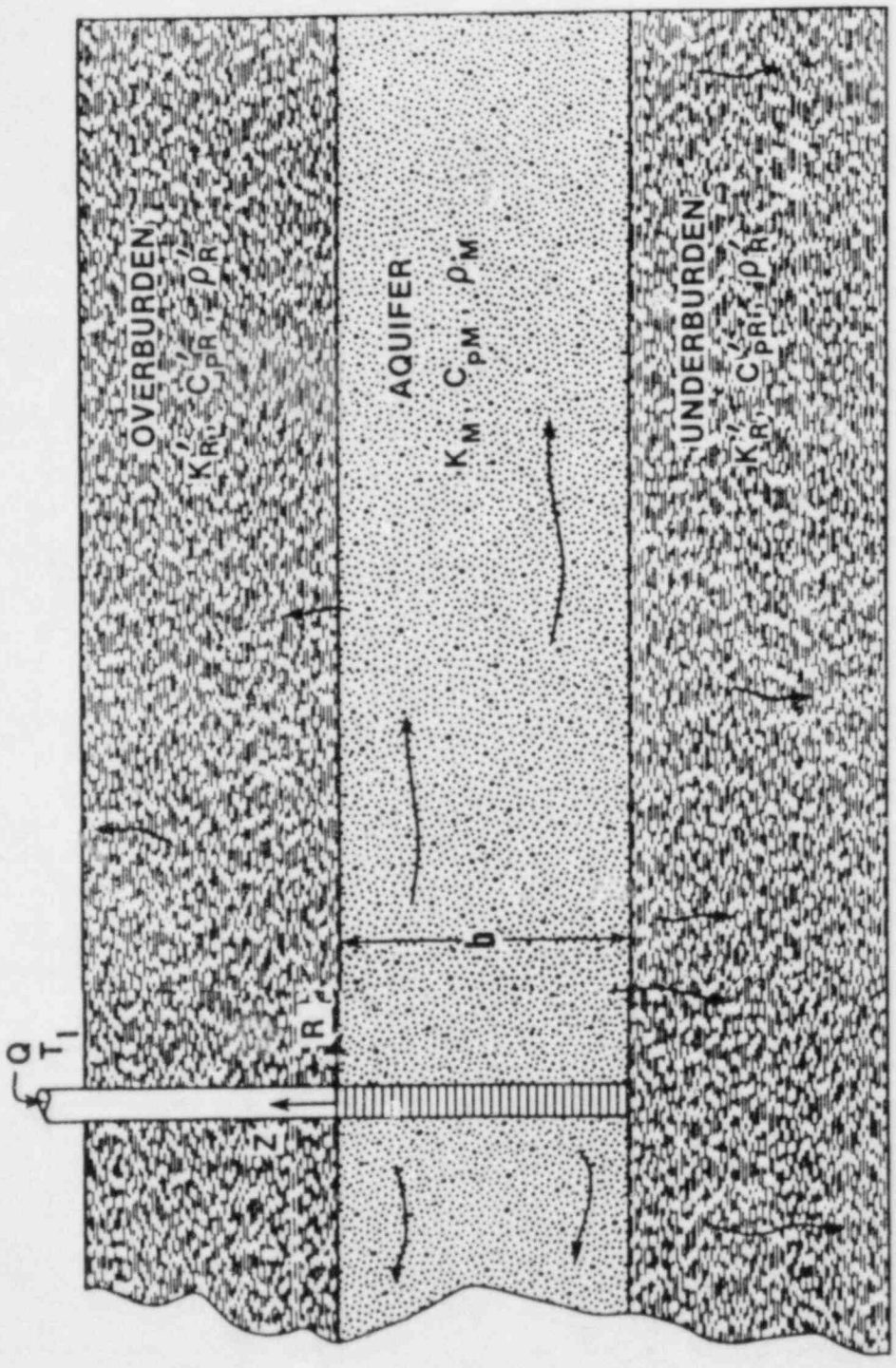

Figure 3-2b. Radial Heat Transport Through an Aquifer System.

$$T'(x,z = \pm\infty,t) = T_o, \qquad t \geq 0 \tag{3-9b}$$

$$T'(x,z=0,t) = T(x), \qquad t \geq 0 \tag{3-9c}$$

$$T'(x,z=-b,t) = T(x), \qquad t \geq 0 \tag{3-9d}$$

Here a prime is used to define over/underburden parameters and the z-axis is positive upward originating at the aquifer-overburden interface.

Both one-dimensional Cartesian (linear) and radial geometries are considered for the aquifer. For the former, the equation to be solved is:

$$-u\rho c_p \frac{\partial T}{\partial x} + K_m \frac{\partial^2 T}{\partial x^2} - \Gamma_H = \rho_m c_{pm} \frac{\partial T}{\partial t} \tag{3-10}$$

For the latter, the equation is:

$$-u\rho c_p \frac{\partial T}{\partial r} + K_m \frac{1}{r} \frac{\partial}{\partial r} \left(r \frac{\partial T}{\partial r}\right) - \Gamma_H = \rho_m c_{pm} \frac{\partial T}{\partial t} \tag{3-11}$$

The over/underburden coupling term is given, in either case, by:

$$\Gamma_H = -(2/b) K'_m \frac{\partial T}{\partial z} \tag{3-12}$$

where b is the aquifer thickness.

Subscripts in Equations (3-10) to (3-12) refer to water (no additional subscript), to rock, R, and to medium, m, (rock and water). In addition, the Darcy velocity, u, is related to the volumetric rate of injection, Q, by:

$$u = \begin{cases} Q/b, & \text{linear case} \\ Q/2\pi rb, & \text{radial case} \end{cases} \tag{3-13}$$

Other notational matters are treated in the section on notation.

Initial/boundary conditions are specified, in the linear case, as:

$$T(x,t=0) = T_o, \qquad x \geq 0 \tag{3-14a}$$

$$T(x = \infty, t) = T_o, \qquad t > 0 \tag{3-14b}$$

$$T(x=0, t) = T_I, \qquad t > 0 \tag{3-14c}$$

where T_o is the initial temperature of aquifer and confining zones and T_I is the injection temperature. For the radial case, Equations (3-14), as well as Equations (3-9), still hold providing that the independent variable is changed from x to r.

3.2.3 Assumptions

The assumptions involved in the above analyses include the following:

- The areal extent of the aquifer is infinite.
- The vertical extent of the confining beds is infinite.
- Hydraulic and thermal parameters are constant.
- The rate of injection is constant and steady-state flow conditions exist within the aquifer. Hence, the Darcy velocity varies inversely as distance from the origin increases in the radial case, and is constant for the linear case.
- Thermal dispersion may be neglected in both aquifer and under/overburden.
- Buoyancy may be neglected within the aquifer and confining layers.
- Convection is negligible within the confining layers.
- Lateral thermal conduction is negligible within the confining layers.

3.2.4 Analytical Solution

Avdonin [1964] solves the above equations in a linear geometry. The resulting aquifer temperature is given by:

$$\theta(x,\tau) = [\chi/(\pi\tau)^{1/2}] \int_o^1 \exp\{-[s\gamma\tau^{1/2} - \chi/(2s\tau^{1/2})]^2\} \cdot \operatorname{erfc}\{\alpha s^2 \tau^{1/2}/[2(1-s^2)^{1/2}]\}\, ds/s^2 \tag{3-15}$$

Here the dimensionless variables are:

$$\theta = (T-T_o)/(T_I-T_o) \tag{3-16a}$$

$$\chi = 2x/b \tag{3-16b}$$

$$\tau = 4K_m t/(\rho_m c_m b^2) \tag{3-16c}$$

and the dimensionless parameters are defined by:

$$\gamma = Q\rho c_p/4K_m \tag{3-17a}$$

$$\alpha = (K'_m\rho'_m c'_{pm})^{1/2}/(K_m\rho_m c_{pm})^{1/2} \tag{3-17b}$$

(In the original reference, γ is defined with 8 in the denominator; this appears to be a typographical error).

Avdonin [1964] also solves the above equations in a radial geometry. The resulting aquifer temperature in this case is given by an expression which is quite similar to Equation (3-15). It is:

$$\theta(\omega,\tau) = (\omega^2/4\tau)^2/(\Gamma(\nu)\int_o^1 \exp\{-\omega^2/4\tau s\} \cdot \operatorname{erfc}\{\alpha s\tau^{1/2}/[2(1-s)^{1/2}]\}\, ds/s^{\nu+1} \tag{3-18}$$

where the dimensionless distance is:

$$\omega = 2r/b \tag{3-19}$$

the parameter ν is given by:

$$\nu = Q\rho c_p/4\pi bK_m \tag{3-20}$$

and Γ is the familar gamma function.

3.2.5 Input Specifications

Input parameters for this problem are taken directly from Ross et al [1982], pp. 60,61. They are presented here in Table 3-3. The input given in this table may be used directly in the analytic solutions given in Section 3.2.4. This input may also be used for the numerical solutions. However, some rather trivial unit changes are necessary for SWIFT. Also, the code requires that the terms ρ_m and c_{pm} be combined from their component parts for water and for aquifer rock. This may be done through the relation:

$$\rho_m c_{pm} = \phi \rho c_p + (1-\phi)\rho_R c_{pR} \qquad (3\text{-}21)$$

A listing of the SWIFT input data file is included in the microfiche.

3.2.6 Output Specifications

The output for this problem consists of temperature as a function of distance at a specified value of time and temperature as a function of time at a specified value of distance.

3.2.7 Numerical Solution

As suggested by Ross et al [1982], a finite system is employed for each numerical solution. The length is taken to be L = 50 m for the linear case and r_e = 1000 m for the radial case. (Ross et al suggested that 1000 m be used in the radial case). In addition, a nonzero well radius is required for the numerical simulation of the radial case in contrast to the analytical solution. Nevertheless, the effect of this should be quite small since the chosen well radius (~ 0.1 m) is much smaller than the observation radius (37.5 m). Centered differencing is used in both time and space domains for the linear case, and in the space domain for the radial case. The space and time steps are chosen to be consistent with the appropriate criteria (see Reeves et al [1984a], Chapter 7). For the radial case, in which the appropriate criteria are unknown, backward-in-time and centered-in-space differencing are chosen, and the mesh is refined to achieve convergence to the analytical solution.

Table 3-3. Parameter Specifications for Problem 3.2.

Parameter	Symbol	Value	
		SI	English
Injection rate	Q	10 kg/s	1.90×10^6 lb/d
Injection temperature	T_I	160 ^{o}C	320 ^{o}F
Initial temperature	T_o	170 ^{o}C	338 ^{o}F
Thermal conductivity, over/underburden	K'_m	20 W/(m·^{o}C)	277.5 Btu/(ft·d·^{o}F)
Density, over/underburden	ρ'_m	2500 kg/m^3	156.1 lb/ft^3
Heat capacity, over/underburden	c'_{pm}	1000 J/(kg·^{o}C)	0.239 Btu/(lb·^{o}F)
Thermal conductivity, aquifer	K_m	20 W/(m·^{o}C)	277.5 Btu/(ft·d·^{o}F)
Density, aquifer	ρ_m	2500 kg/m^3	156.1 lb/ft^3
Heat capacity, aquifer	c_{pm}	1000 J/(kg·^{o}C)	0.239 Btu/(lb·^{o}F)
Density, water	ρ	919 kg/m^3	57.4 lb/ft^3
Heat capacity, water	c_p	4185 J/(kg·^{o}C)	1 Btu/(lb·^{o}F)
Aquifer thickness	b	100 m	328.1 ft
Aquifer porosity	ϕ	0.2	0.2

It is interesting to contrast the length scales used in this problem (50 m for the linear case and 1000 m for the radial case) with that used for the linear Problem 3.1 (2000 ft). Retardation within the fluid results from the heat capacity of the rock comprising the aquifer and from heat transfers to the confining beds. To set up maximum grid sizes, one may neglect the latter. Thus, for the two linear cases the movement of the thermal front is given approximately by $x = v_R t$, where v_R is the retarded velocity. For the radial case the retarded velocity varies inversely with the radius r, i.e., $v \sim v_o/r$ where v_o is a constant. In this case the approximate formula for location of the thermal front is $r^2 = 2v_o t$. In all cases the grid was chosen to be sufficiently large to contain the fronts and their smearing due to conduction at the maximum times simulated.

3.2.8 Results

The output of this problem consists of temperature as a function of distance at a fixed time and temperature as a function of time for a fixed distance. For the linear geometry the fixed time was taken to be 1.3×10^5 s (1.5 d) and the fixed distance was taken to be 37.5 m. Results are presented in Figures 3-3 and 3-4. The agreement between numerical and analytical results is quite satisfactory.

For the radial geometry the fixed time was taken to be 1×10^9 s (32 y) and the fixed distance was taken to be 37.5 m, as suggested by Ross et al. Results for this case are presented in Figures 3-5 and 3-6. Again, the agreement between numeric and analytic results is quite satisfactory.

It is of interest to note the effects of the over/underburden by comparing dashed and solid lines. It may be seen that, in the radial simulation (Figures 3-5 and 3-6), a sufficient amount of time has elapsed so that heat may be transported from confining zones to aquifer thereby increasing the temperature above the 160 ^{o}C of the injected fluid. However, for the linear simulation (Figures 3-3 and 3-4) the elasped time is sufficiently short that such an effect is barely noticeable. Here the confining layers play only a minor role in shaping the temperature front. The effect is to sharpen the leading edge (temperatures near 170 ^{o}C) and to diffuse the trailing edge (temperatures near 160 ^{o}C).

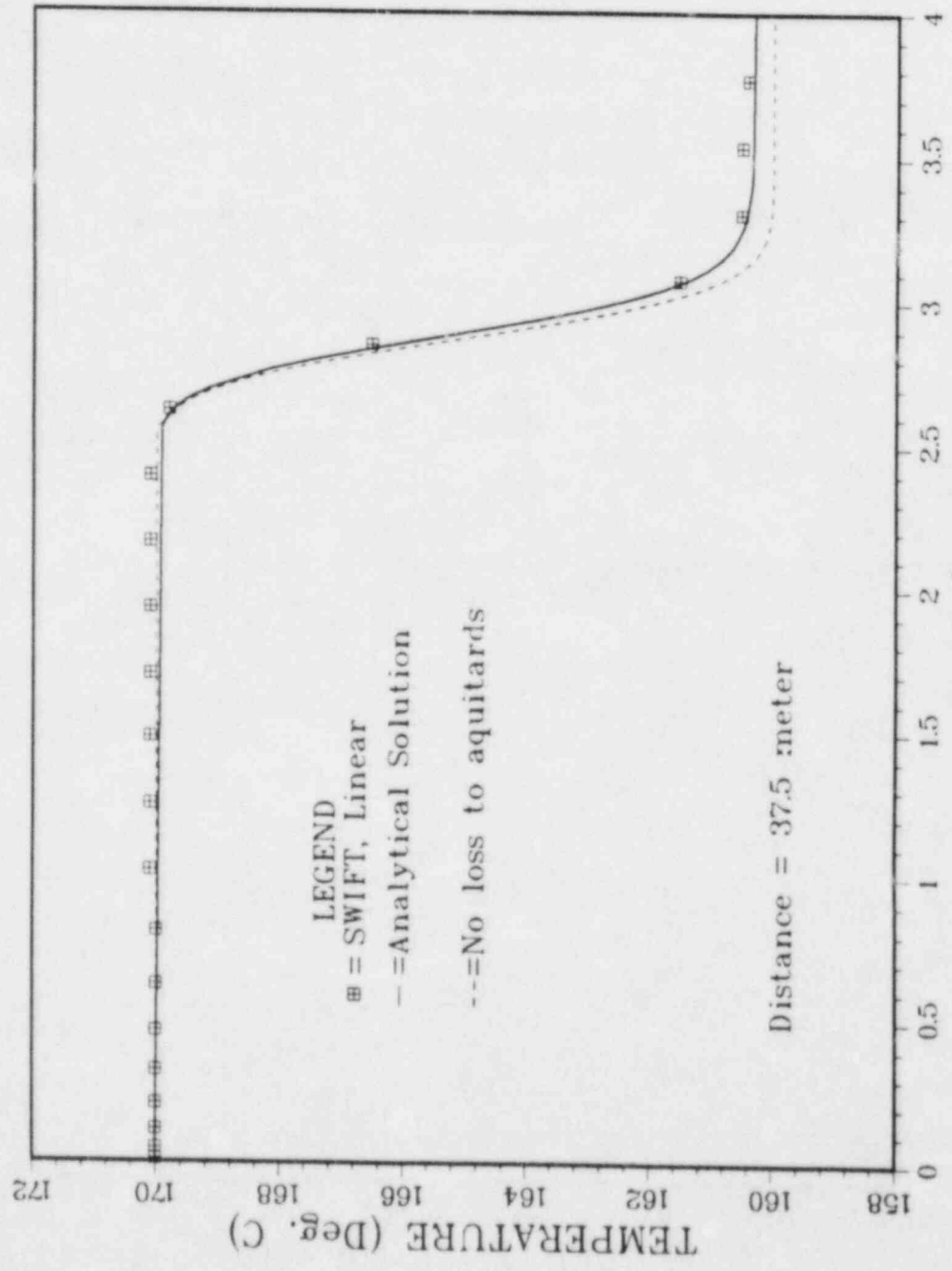

Figure 3-3. Temperature as a Function of Time at a Fixed Distance for a Linear Aquifer System.

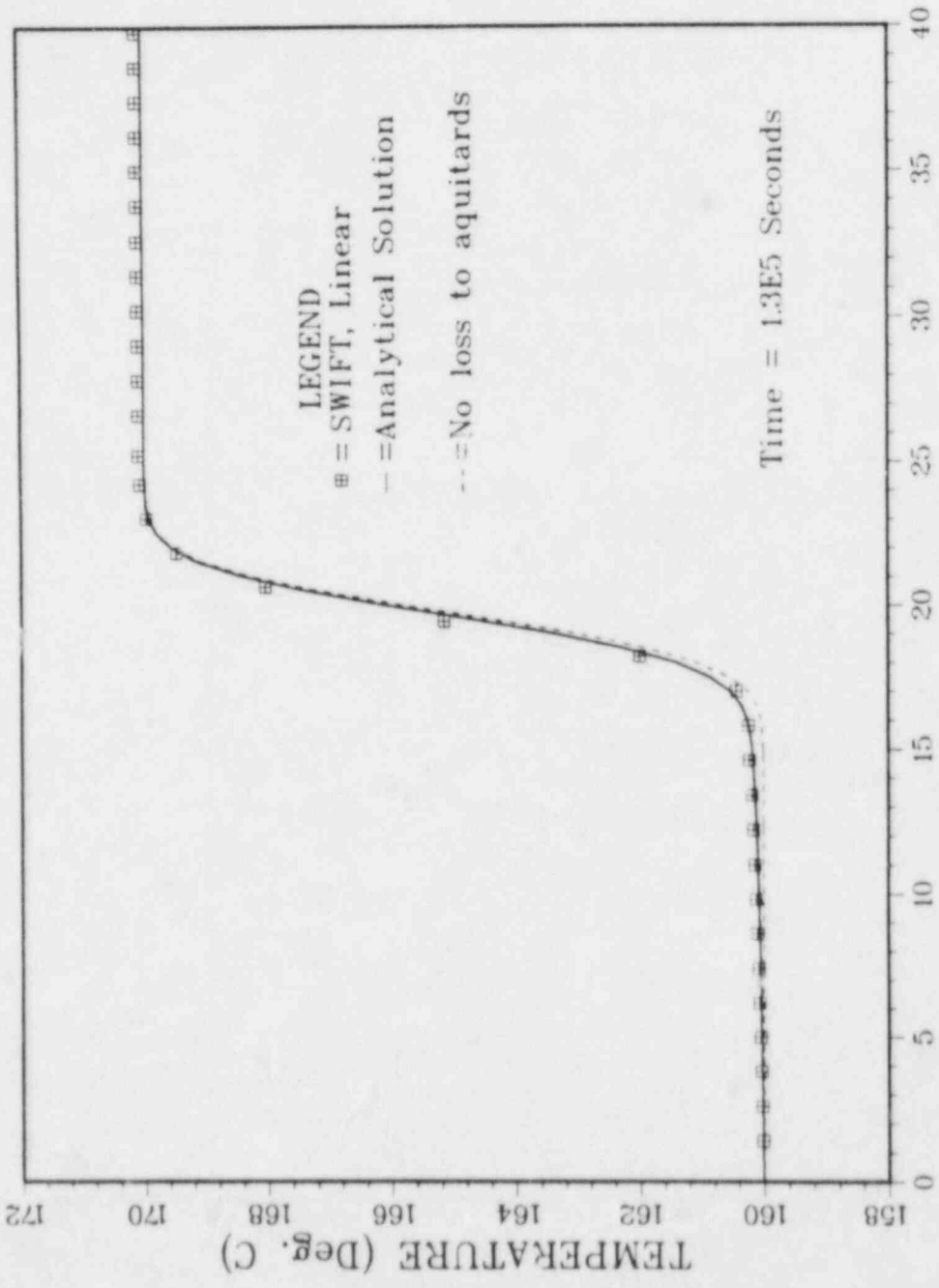

Figure 3-4. Temperature as a Function of Distance at a Fixed Time for a Linear Aquifer System.

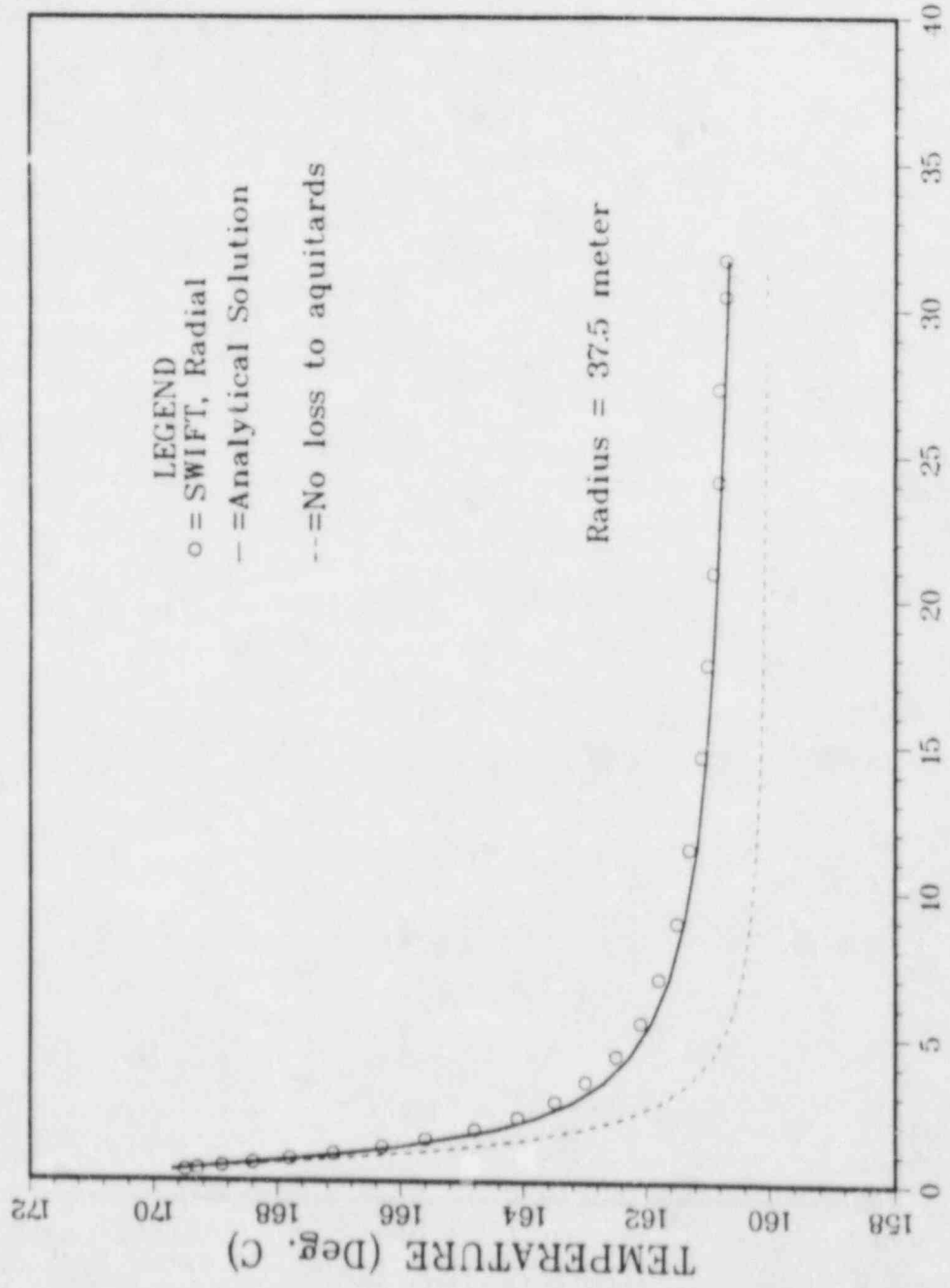

Figure 3-5. Temperature as a Function of Time in a Radial Aquifer System.

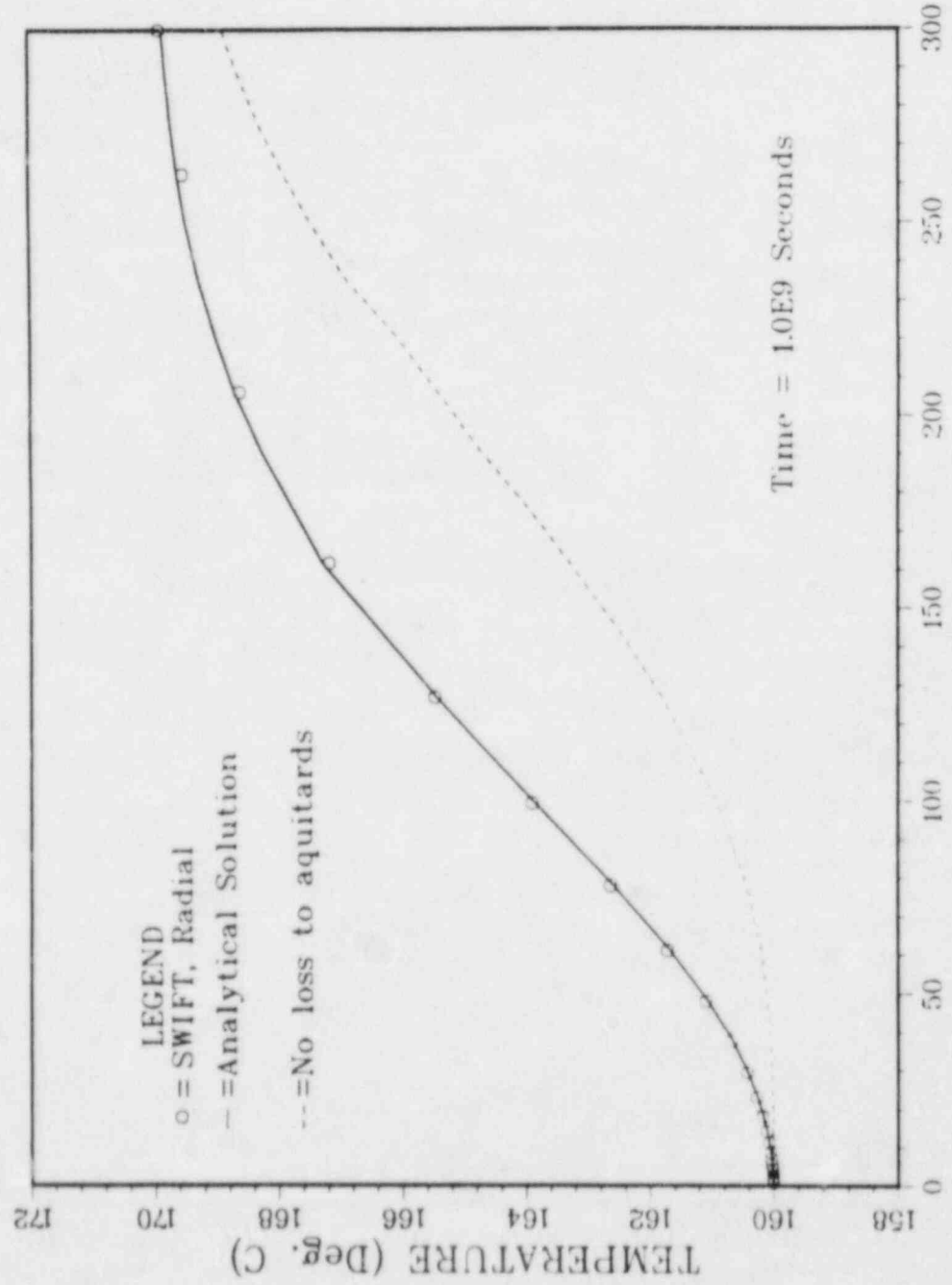

Figure 3-6. Temperature as a Function of Distance in a Radial Aquifer System.

The above calculations were also performed in English Engineering units. As expected, the results are virtually identical to those presented in Figures 3-3 to 3-6.

4 VERIFICATION OF THE SOLUTE TRANSPORT

4.1 ONE-DIMENSIONAL TRANSPORT WITH CHAIN DECAY AND EQUAL RETARDATION PARAMETERS [COATS AND SMITH, 1964]

4.1.1 Objectives

The purposes for simulating this problem are to test the following aspects of the SWIFT Code:

- contaminant transport,
- radionuclide decay and generation of daughter components,
- waste-leach radionuclide-source model,
- Cartesian coordinates,
- English Engineering units.

4.1.2 Description of Problem

A schematic drawing of this problem is given in Figure 4-1. As shown there, a three-component radionuclide chain is released into a porous medium where it is subject to convection, dispersion and sorption. Here, the sorption is assumed to yield a single retardation which is constant in space and time and which is the same for all three components. Assuming a one-dimensional transport system, the equations to be solved are:

$$- v \frac{\partial C_r}{\partial x} + D \frac{\partial^2 C_r}{\partial x^2} + k_{r,r-1} \lambda_{r-1} C_{r-1} - \lambda_r C_r = \frac{\partial C_r}{\partial t}, \quad r = 1,2,3 \qquad (4\text{-}1)$$

where r is the component number.

Parameter k_{rs} is the product of a branching ratio and a daughter-to-parent mass fraction. The velocity appearing in Equation (4-1) is the retarded interstitial velocity, which is defined in terms of the Darcy velocity, u:

$$v = u/\phi K \qquad (4\text{-}2a)$$

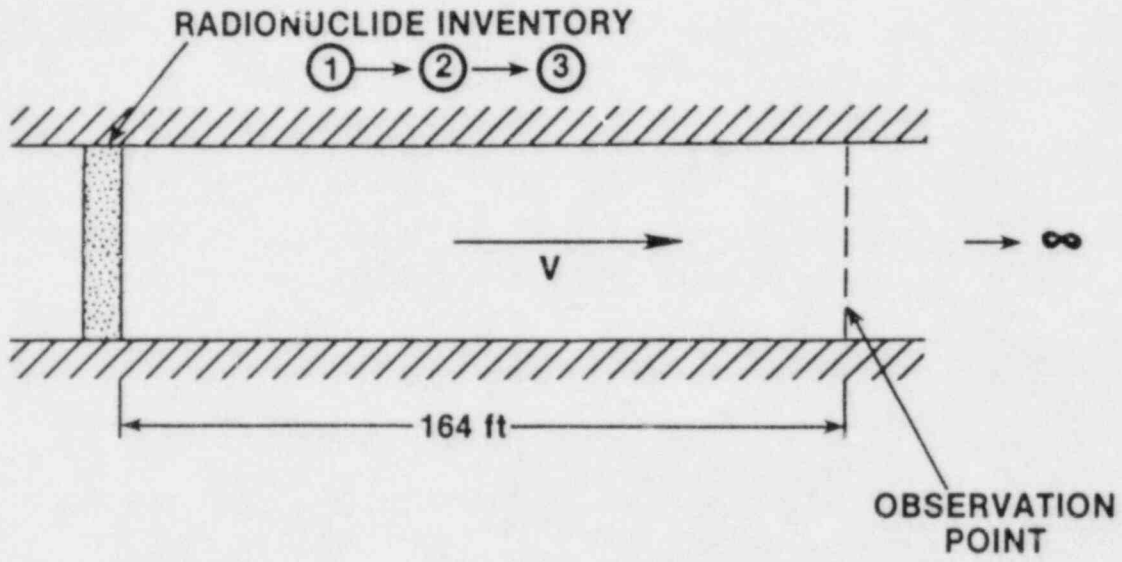

Figure 4-1. One-Dimensional Transport of a Three-Component Chain, Problem 4.1.

where K is the retardation. Dispersion is given in terms of this velocity, i.e.,

$$D = \alpha_L v \tag{4-2b}$$

Initially the concentration in the porous medium is zero for each component:

$$C_r(x,t=0) = 0 , \qquad x > 0 \tag{4-3a}$$

Furthermore, the infinite boundary is held at the initial condition for each component:

$$C_r(x = \infty,t) = 0 , \qquad t > 0 \tag{4-3b}$$

However, a time-dependent flux, $v\tilde{C}_r$, enters the system through a third-type boundary condition:

$$vC_r - D \frac{\partial C_r}{\partial x} = v\tilde{C}_r , \qquad x = 0, \; t > 0 \tag{4-3c}$$

The time-dependent boundary value, $\tilde{C}_r(t)$, arises from a radionuclide inventory undergoing Bateman decay/production relative to the initial boundary values

$$\tilde{C}_r(t=0) = \tilde{C}_{ro} \tag{4-4}$$

4.1.3 Assumptions

The assumptions involved in the above analysis are the following:

- Flow and transport are in one dimension only.
- The domain is semi-infinite.
- Hydraulic parameters are constant throughout the domain.
- The source of radionuclides is leach limited rather than solubility limited.
- The leach time and the inventory of radionuclides are infinite.

- Radionuclides are present in tracer quantities only, and, as such, they do not influence flow.
- Diffusion is insignificant within the fluid.
- There is no diffusion into either the rock matrix or the confining layers.
- Sorption may be approximated by a linear equilibrium isotherm.
- Dispersivity and retardation are constant throughout the semi-infinite domain.
- The radionuclide components have equal retardations.

4.1.4 Analytical Solution

Because of the assumption of equal retardations, the solution of the transport equation, Equation (4-1), may be written in the factored form:

$$C_r(x,t) = \tilde{C}_r(t)O^{(3)}(x,t) \tag{4-5}$$

where $\tilde{C}_r$ contains only decay/production terms, and $O^{(3)}$ contains only transport terms. The function $\tilde{C}_r$ is given by:

$$\tilde{C}_r(t) = \begin{cases} \tilde{C}_{10}e^{-\lambda_r t}, & r=1 \\ \tilde{C}_{ro}e^{-\lambda_r t} + \{\sum_{k=1}^{r-1}[\tilde{C}_{ko}\sum_{j=k}^{r-1} Y_{rj}(t)S_j \cdot \prod_{\substack{\ell=k \\ \ell\neq j}}^{r-1} S_\ell/(\lambda_\ell - \lambda_j)]\}, & r > 1 \end{cases} \tag{4-6}$$

where

$$S_j = k_{j+1,j}\lambda_j \tag{4-7a}$$

$$\prod_{\substack{\ell=k \\ \ell\neq j}}^{r-1} S_\ell/(\lambda_\ell - \lambda_j) = 1, \qquad k = r-1 \tag{4-7b}$$

and

$$Y_{rj} = (e^{-\lambda_j t} - e^{-\lambda_r t})/(\lambda_r - \lambda_j) \qquad (4\text{-}7c)$$

The dimensionless function $\Theta^{(3)}$ in Equation (4-5), which contains the transport terms, reduces to that of a nondecaying species subject to a special third-type boundary condition. This condition has the form of Equation (4-3b), but the input concentration $\tilde{C}$ is set at unity. This function is derived in Coats and Smith [1964] and is the same as that used in Equation (3-6), namely:

$$\begin{aligned}\Theta^{(3)} &= (1/2)\{\mathrm{erfc}[(x-vt)/2\sqrt{Dt}] - \exp(vx/D)\mathrm{erfc}[(x+vt)/2\sqrt{Dt}]\} \\ &- (v/2D)(x+vt)\exp(vx/D)\mathrm{erfc}[(x+vt)/2\sqrt{Dt}] \\ &+ \sqrt{v^2 t/\pi D}\,\exp[-(x-vt)^2/4Dt]\end{aligned} \qquad (4\text{-}8)$$

4.1.5 Input Specifications

Input parameters for this problem are specified in Tables 4-1 and 4-2.

4.1.6 Output Specifications

The output desired here consists of breakthrough curves of concentration versus time for each of the three components at x = 164 ft from the inlet.

4.1.7 Numerical Solution

For numerical solution of this problem, a finite system was chosen to represent the semi-infinite domain used in the analytical solution, and the required Darcy velocity was maintained by means of an imposed pressure drop. This finite domain was chosen, however, to be of sufficient length (L = 254 ft) that the boundary condition imposed there on the transport, a type-three condition, would have negligible influence upon the concentration fronts as they passed through the observation point at 164 ft. Radionuclides were introduced into the system by means of the waste-leach model (see Reeves et al [1984a], Chapter 3).

Table 4-1. Flow and Transport Parameters for Problem 4.1.

Parameter	Symbol	Value	
		SI	English
Darcy velocity	u	2.31×10^{-6} m/s	0.656 ft/d
Porosity	ϕ	0.1	0.1
Dispersivity	α_L	2.59 m	8.5 ft
Retardation	K	9352	9352
Retarded interstitial velocity	v	2.47×10^{-9} m/s	7.01×10^{-4} ft/d
Dispersion	D	6.39×10^{-9} m^2/s	5.96×10^{-3} ft^2/d

Table 4-2. Component-Dependent Parameters for Problem 4.1.

Component Number	Parameter* $k_{r,r-1}$	Half-Life (y)	Decay Constant, λ (y^{-1})	Initial Concentration, $\tilde{C}_{ro}$
1	0	433	1.60×10^{-3}	1
2	1	15	4.62×10^{-2}	0
3	1	6,540	1.06×10^{-4}	0

* Product of branching ratio and mass fraction of daughter to parent.

Centered-in-space differencing was chosen, and the spatial increments were chosen to be consistent with the appropriate criterion ($\Delta x \leq 2\alpha_L$). These increments were:

20 @ 8.2 , 3 @ 5.47 and 9 @ 8.2 ft

The source was distributed uniformly across Grid-Block 1. Within the SWIFT Code a source cannot be placed precisely upon the boundary, as is done in the analytic solution, c.f., Equation (4-3c). However, since the source-block width is much less then the observation length, this is an acceptable approximation.

Centered differencing was also chosen for the time domain. Here, however, the relevant criteria (see Reeves et al [1984a], Chapter 7) were selectively violated in order to minimize computer time. Since Component 2 is in secular equilibrium with its parent, it was unnecessary to adhere to the resulting half-life limit (15 y). However, the criterion arising from the convection term ($\Delta t \leq 20$ y) was used (approximately) until breakthrough occurred at about 640 y. Beyond that time, the concentration gradient within the system dissipates and becomes virtually uniform over the length of the system. In the absence of sharp concentration gradients, overshoot does not appear in the solution since the convection term causing the overshoot disappears. This, of course, would be expected due to the complementary error function in Equation (4-8), erfc ((x-vt)...), which then is controlling.

Thus, after 640 y it was necessary only to observe constraints arising from the half-life of Component 1 (433 y). As this component became insignificant, then, it was necessary only to track Component 3, which had a considerably longer half-life (6540 y). At the end of the simulation, with Component 3 itself becoming insignificant, even this criterion was violated by a factor of about three. Nevertheless, as will be shown in the next section, tne numerical simulations showed remarkable agreement with the analytical simulations.

A list of the additional parameters, over and above those necessary for the analytical calculations, is shown in Table 4-3.

Table 4-3. Additional SWIFT Parameters for Problem 4.1.

Parameter	Symbol	Value	
		SI	English
System length	L	77.5 m	254 ft
Spatial increments	Δx	1.68-2.5 m	5.5-8.2 ft
Time increments	Δt		
$t \leq 270$ y		4.73×10^{8} s	15 y
270 y $\leq t \leq 1.2 \times 10^{5}$ y		4.73×10^{8} - 6.31×10^{10} s	15 - 2,000 y
Boundary pressure	p_o	3.33×10^{5} Pa	48.3 psi
Boundary pressure	p_l	6.98×10^{4} Pa	10 psi
Hydraulic conductivity	K	6.7×10^{-6} m/s	1.9 ft/day
Spatial differencing	CIS*	---	---
Time differencing	CIT*	---	---

* CIS means centered-in-space, and CIT means centered-in-time.

4.1.8 Results

Computed breakthrough curves are exhibited in Figure 4-2. As shown there, the analytical and numerical results agree extremely well. The finite-difference concentrations do tend to breakthrough slightly earlier than the analytical concentrations. However, this is of no consequence, considering the relatively small magnitudes of the concentrations.

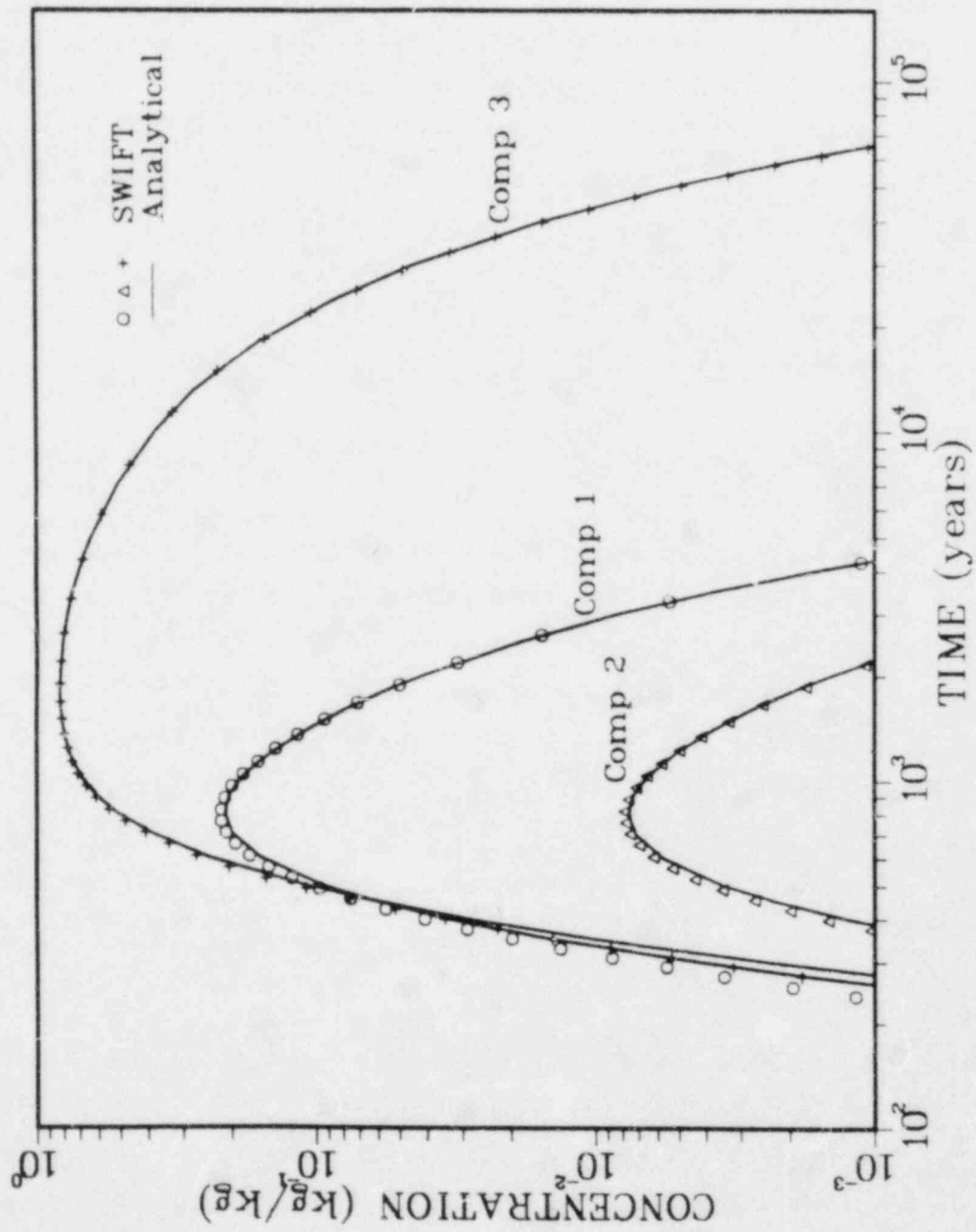

Figure 4-2. Radionuclide Discharge Concentration as a Function of Time.

4.2 ONE-DIMENSIONAL TRANSPORT WITH CHAIN DECAY AND UNEQUAL RETARDATION PARAMETERS (INTRACOIN PROBLEM 1)*

4.2.1 Objectives

The purposes for simulating this problem are to test the following aspects of the SWIFT Code:

- contaminant transport of species with different retardation factors,
- radionuclide decay and generation of daughter components,
- waste-leach radionuclide-source model,
- Cartesian coordinates,
- SI units.

4.2.3 Description of Problem

A schematic drawing of this problem is given in Figure 4-3. As shown there, an inventory of three radionuclides is leached and transported through a one-dimensional system. Both dispersion and sorption processes are present. Retardation, which arises from the latter, is spatially constant. However, in contrast to Problem 4.1, retardations are radionuclide dependent.

The transport equations are:

$$- v_r \frac{\partial C_r}{\partial x} + D_r \frac{\partial^2 C_r}{\partial x^2} + k'_{r,r-1} \lambda_{r-1} C_{r-1} - \lambda_r C_r = \frac{\partial C_r}{\partial t}, \quad r = 1,2,3 \qquad (4\text{-}9)$$

Parameter k'_{rs} contains the product of three terms, i.e., the branching ratio, the daughter-to-parent mass fraction and the parent-to-daughter retardation ratio. Also, as indicated by the component index, both the retarded interstitial velocity and the retarded dispersion are dependent upon the component. The former is defined in terms of the Darcy velocity by the equation:

---

* INTRACOIN [1983].

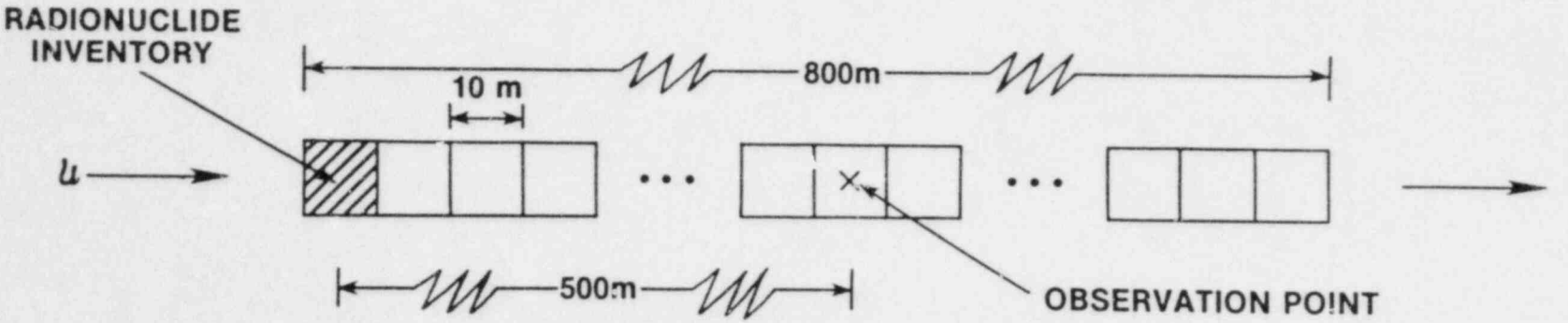

Figure 4-3. One-Dimensional Transport of a Three-Component Chain, Problem 4.2.

$$v_r = u/\phi K_r \tag{4-10a}$$

where K_r is the retardation of species r. The latter, i.e., the retarded dispersion, is then defined by

$$D_r = \alpha_L v_r \tag{4-10b}$$

Initially the concentrations in the porous medium are zero for each component:

$$C_r(x,t=0) = 0 , \qquad x \geq 0 \tag{4-11a}$$

Furthermore, the infinite boundary is held at the initial concentration

$$C_r(x = \infty,t) = 0 , \qquad t \geq 0 \tag{4-11b}$$

A time-dependent type-three condition is then introduced by the leaching of the radionuclide inventory:

$$v_r C_r - D_r \frac{\partial C_r}{\partial x} = v_r \tilde{C}_r , \qquad x = 0 , \; t > 0 \tag{4-11c}$$

where

$$\tilde{C}_r(t) = \begin{cases} I_r/A\rho v_r T , & 0 \leq t \leq T \\ 0 , & t > T \end{cases} \tag{4-12a}$$

Here I_r, the inventory of component r, undergoes Bateman decay/production

$$\frac{dC_r}{dt} = k_{r,r-1}\lambda_{r-1}C_{r-1} - \lambda_r C_r \tag{4-12b}$$

starting from an initial inventory $I_{ro} = I_r(0)$. Quantity A is the cross-sectional area of the one-dimensional flow system.

4.2.3 Assumptions

The assumptions involved in the above analysis are the following:

- Flow and transport are in one dimension only.
- The domain is semi-infinite.
- Hydraulic parameters are constant throughout this domain.
- The source of radionuclides is leach limited rather than solubility limited.
- The leach rate is constant and nonzero only during the time period $t < T$.
- Radionuclides are present in trace quantities only, and, as such, they do not influence flow.
- Diffusion is insignificant within the fluid.
- There is no diffusion into either the rock matrix or the confining layers.
- Sorption may be approximated by a linear equilibrium isotherm.
- Hydrodynamic dispersion is a linear function of velocity.
- Dispersivity and retardation are constant throughout the semi-infinite domain.

4.2.4. Analytical Solution

The solution to this problem may be written as:

$$C_r(x,t) = N_r(x,t) - N_r(x,t-T) \qquad (4\text{-}13a)$$

where

$$N_r(x,t-T) = 0, \qquad t < T \qquad (4\text{-}13b)$$

The superpositon is necessary for the termination of the $x = 0$ boundary condition at time, $t = T$. Function N_r is a generalization of the function $O^{(3)}$ given in Equation (3-5) and, as such, is quite involved. The reader is referred to Harada et al [1980] or to Lester et al [1975] for specification of this function.

4.2.5 Input Specifications

For the x = 0 boundary condition (B, in INTRACOIN notation) and the boundary condition (E) at x = ∞ , as stated above, INTRACOIN specifies variations of leach time (T), observation distance (L), dispersivity α_L (or Peclet number P, in their notation), retardation factor K (R) and inventory (I). We have chosen here to consider only sets R (Table 4-4) and I (Tables 4-5 and 4-6) using base values (Table 4-7) for the other quantities. Thus, there are four cases to be considered here. In the notation of INTRACOIN they are designated as follows:

$$(I_1, R_1, T_2, B_2, L_1, P_2, E_1)$$

$$(I_1, R_2, T_2, B_2, L_1, P_2, E_1)$$

$$(I_2, R_1, T_2, B_2, L_1, P_2, E_1)$$

$$(I_2, R_2, T_2, B_2, L_1, P_2, E_1)$$

4.2.6 Output Specifications

The output consists of breakthrough curves for each of the three radionuclides for each of the four cases listed above. In addition, each such curve is characterized by the following four parameters:

- C_{max}, the maximum concentration
- T_{max}, the time corresponding to C_{max}
- T+, the time of the first occurrence of the concentration, $C_{max}/2$
- T-, the time of the last occurrence of the concentration, $C_{max}/2$

4.2.7 Numerical Solution

In order to obtain the numerical solution of these problems, the two boundary conditions were treated in the following manner. To approximately simulate the effects of the infinite boundary condition given in Equation (4-11b), the migration length, L = 500 m, was considered, and, the condition

Table 4-4. Reference Retardation Factors.

Element	Retardation	
	Set R_1	Set R_2
Cm	5000	60
Np	700	200
U	300	60
Th	2×10^4	500
Ra	1×10^4	20

Table 4-5. Reference Inventories for Problem 4.2.

Set	Nuclides	Inventory (Ci)	Inventory (kg)
I_1	^{234}U	1.0	0.158
	^{230}Th	0.01	4.9×10^{-4}
	^{226}Ra	0.004	4.0×10^{-6}
I_2	^{245}Cm	0.7	4.0×10^{-3}
	^{237}Np	1.0	1.4
	^{233}U	0.004	4.1×10^{-4}

Table 4-6. Half Lives.

Element	Half Life (y)
^{245}Cm	8.500×10^{3}
^{237}Np	2.140×10^{6}
^{233}U	1.592×10^{5}
^{234}U	2.445×10^{5}
^{230}Th	7.700×10^{4}
^{226}Ra	1.600×10^{3}

Table 4-7. Base Parameter Values.

Parameter	Symbol	Value
Leach time	T	10^5 y
Darcy velocity	u	0.01 m/y
Porosity	ϕ	0.01
Interstitial velocity	v	1 m/y
Observation distance	L	500 m
Dispersivity	α_L	50 m
System Peclet number	P_e	10

$$\frac{\partial C_r}{\partial x}(x = 800\ m, t) = 0 \qquad (4\text{-}14)$$

was set 300 m down dip from the observation point. This condition calls for no dispersion, i.e., convection only, at the boundary. It is imposed automatically by the code wherever a fluid withdrawal occurs.

For the type-three condition of Equation (4-11c), applied at the origin, radionuclides were introduced into the system via the leach model (see Reeves et al [1984a]). This model solves the Bateman equations, as required for the inventory, and uniformly introduces the radionuclides into the system throughout the leach time, T. However, the source is distributed over a grid block of length $\Delta x = 10$ m rather than being confined to a point, as is assumed in the expression of Equation (4-11c). Therefore, the observation point is placed at L = 500 m from the midpoint of the source.

A relatively fine spatial gridding ($\Delta x = 10$ m) was used, as compared to the Peclet-number criterion (see Reeves et al [1984a]),

$$\Delta x \leq 2\alpha_L = 100\ m \qquad (4\text{-}15a)$$

in order to minimize the effects of the distributed source. (A centered-in-space, centered-in-time differencing was used throughout). For the time gridding careful consideration was given to the time criterion, secular equilibrium, half life and the expected travel times to the observation point (again refer to Reeves et al [1984a]). However, in each case, the time criterion:

$$\Delta t \leq \min_r (2\Delta x/v_r) \cdot \frac{1}{11} \qquad (4\text{-}15b)$$

predominated. This notation indicates that the minimum travel time, $2\Delta x/v_r$, is to be used, considering all components, r. The factor of 11 results from the factor $(1 + 2\alpha/\Delta x) = 11$, which arises in the second-order centered-in-time criterion.

4.2.8 Results

Calculated breakthrough curves are shown in Figures 4-4 to 4-7 for the cases (I_1, R_1 ...), (I_1, R_2 ...), (I_2, R_1 ...) and (I_2, R_2 ...). For the first case, Figure 4-4, the chain

$$^{234}U \rightarrow ^{230}Th \rightarrow ^{226}Ra$$

is shown to be in secular equilibrium at the observation point. All curves in the first figure, Figure 4-4, have approximately the same shape except that the breakthrough curve for ^{230}U is shifted horizontally toward lower values of time due to its lower value of retardation (see Table 4-4). It is noteworthy, however, from the half lives in Table 4-7 that the condition for secalar equilibrium holds more strongly for ^{230}Th and ^{226}Ra than for ^{234}U and ^{230}Th.

For the second, Figure 4-5, only the last two components of this chain are in equilibrium, a circumstance which results both from the retardations and from the half lives of the components. Perhaps the most apparent observation of Figure 4-6 is the fact that the curve for the parent nuclide ^{245}Cm does not appear. This is due to the fact that this species undergoes approximately 300 half lives before reaching the observation point, and consequently its concentrations there are negligible.

A major observation to be made of all of these figures, including Figure 4-7, is that there is a variety of shapes, and, thus, these four cases constitute a rather stringent test of the radionuclide-chain transport within the code. Table 4-8 compares the SWIFT results with analytic results from the code UCB-NE [Harada et al, 1980] using the four parameters specified in Section 4.2.6. As shown, the comparisons are quite acceptable in each case.

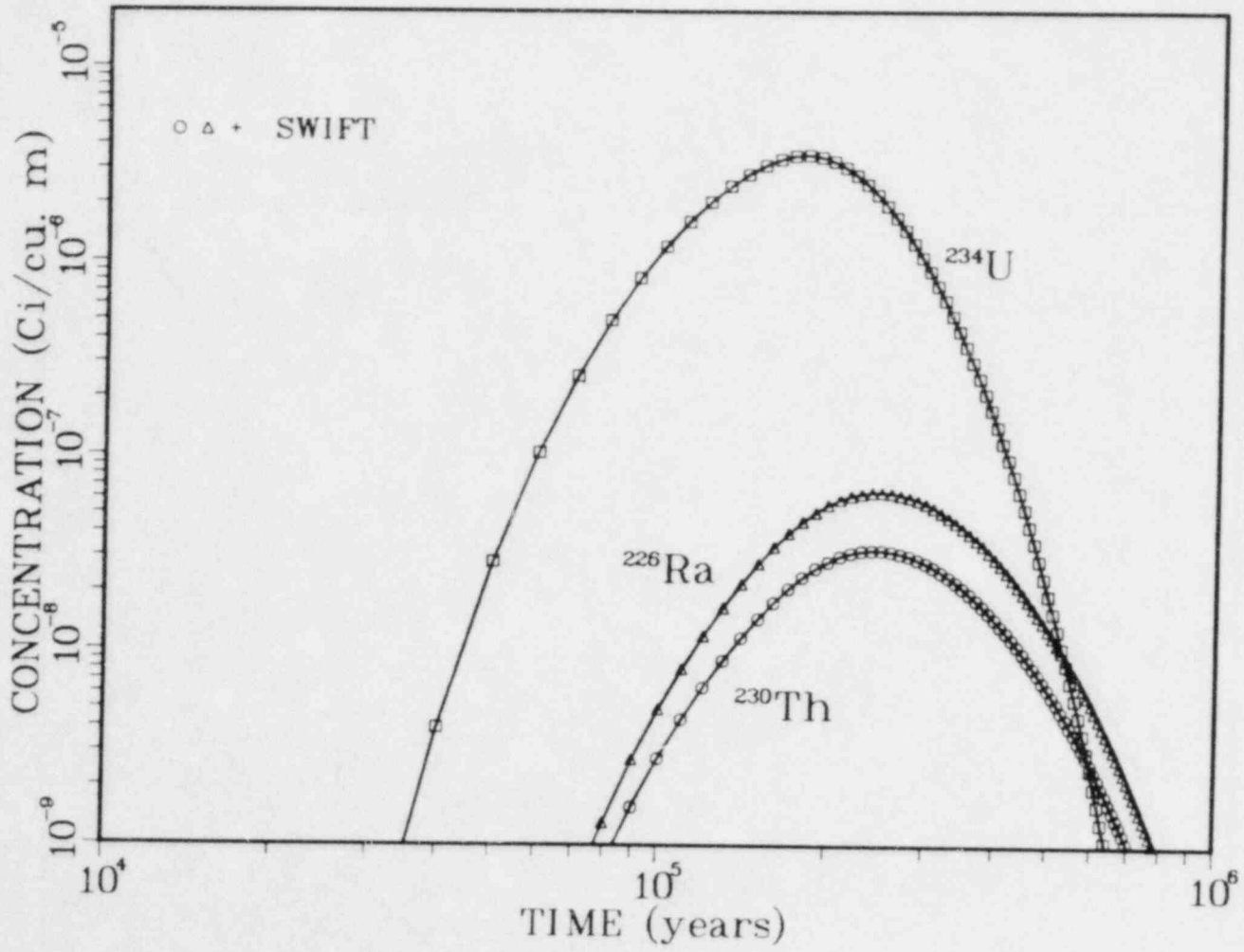

Figure 4-4. Radionuclide Discharge Concentration as a Function of Time.

INTRACOIN LEVEL 1, CASE 1 [I_1, R_1, T_2, B_2, L_1, P_2, E_1].

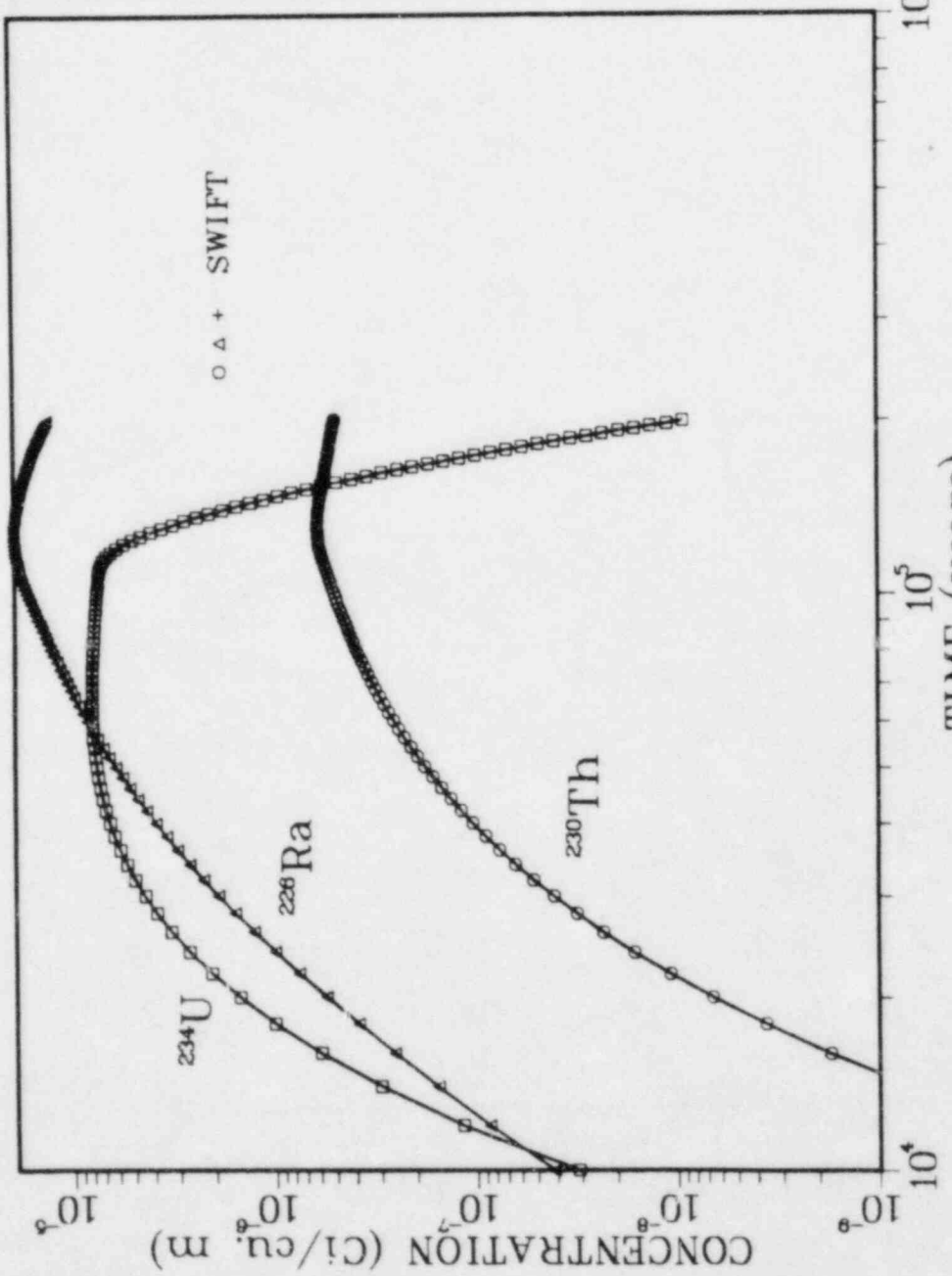

Figure 4-5. Radionuclide Discharge Concentration as a Function of Time.

INTRACOIN LEVEL 1, CASE 1 [I_1, R_2, T_2, B_2, L_1, P_2, E_1].

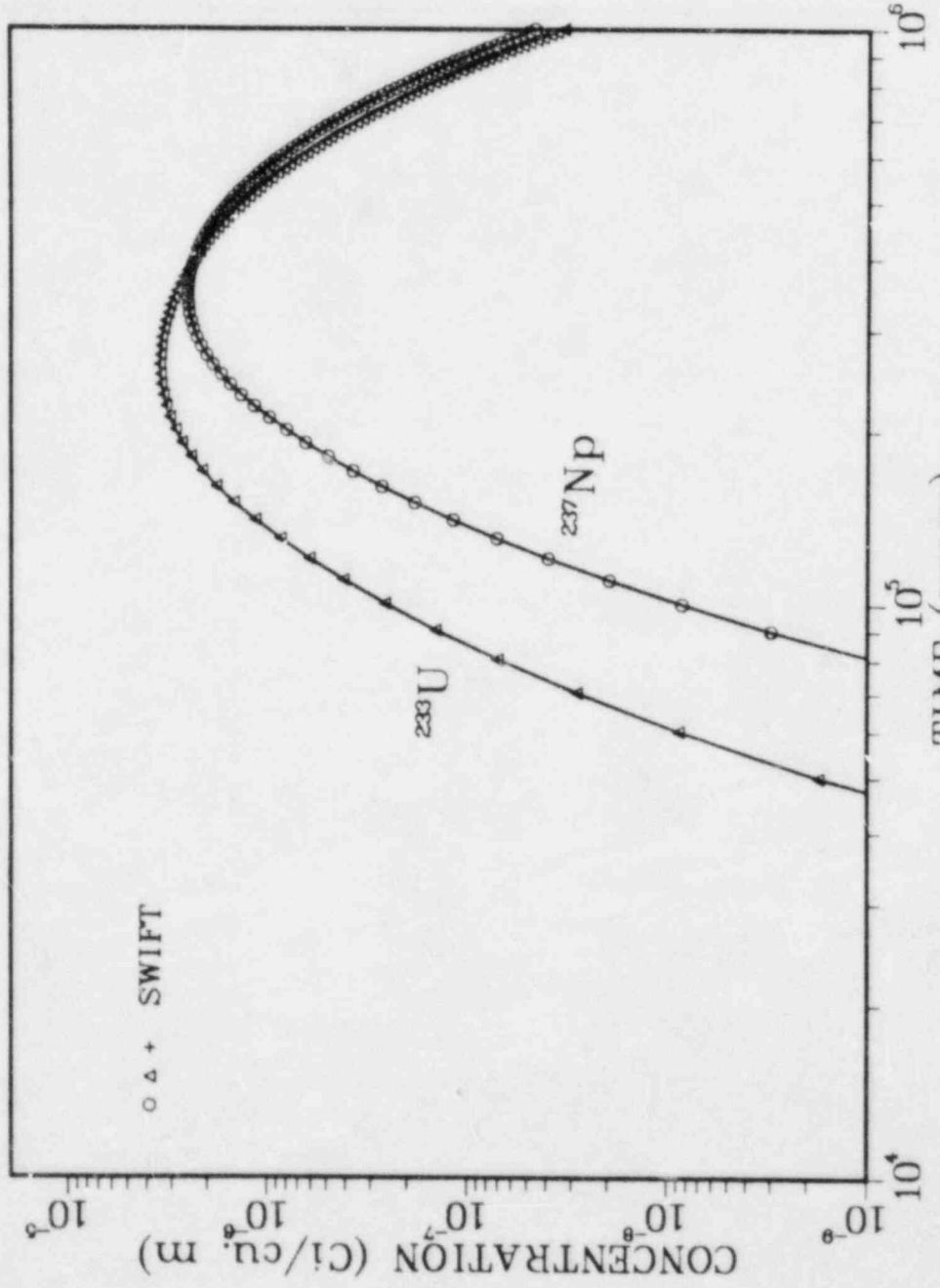

Figure 4-6. Radionuclide Discharge Concentration as a Function of Time.

INTRACOIN LEVEL 1, CASE 1 [I_2, R_1, T_2, B_2, L_1, P_2, E_1].

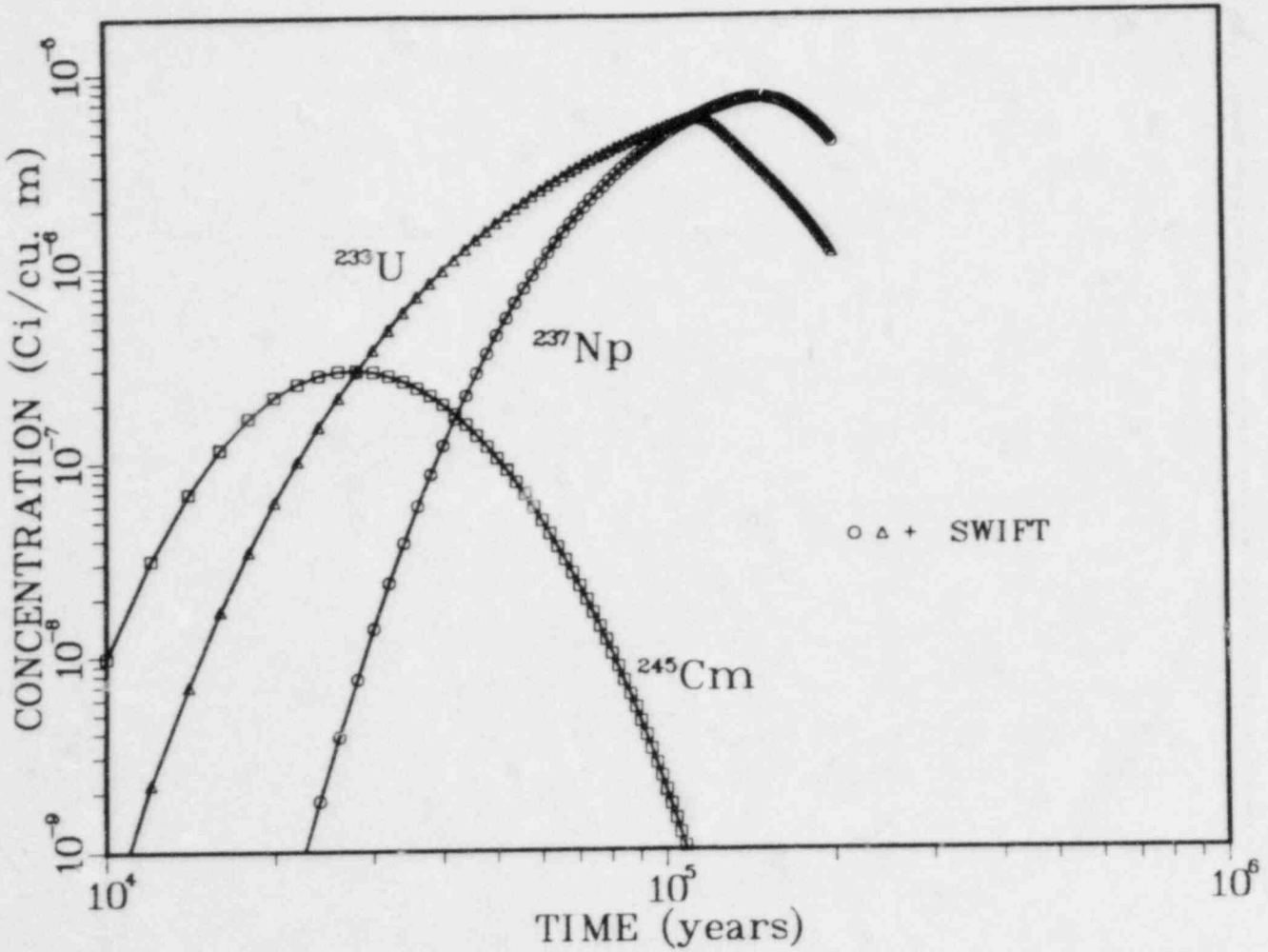

Figure 4-7. Radionuclide Discharge Concentration as a Function of Time. INTRACOIN LEVEL 1, CASE 1 [I_2, R_2, T_2, B_2, L_1, P_2, E_1].

Table 4-8a. Comparison of SWIFT and UCB-NE for Cases $[I_1, R_1]$ and $[I_1, R_2]$ [1,2,3].

Case	Nuclide	Code	C_{max} (Ci/m^3)	T_{max} (y)	T+50% (y)	T-50% (y)
I_1,R_1	^{234}U	SWIFT	3.53×10^{-6}	1.77×10^{5}	1.14×10^{5}	2.57×10^{5}
I_1,R_1	^{234}U	UCB-NE	3.16×10^{-6}	1.83×10^{5}	1.19×10^{5}	2.78×10^{5}
I_1,R_1	^{230}Th	SWIFT	3.21×10^{-8}	2.43×10^{5}	1.56×10^{5}	3.86×10^{5}
I_1,R_1	^{230}Th	UCB-NE	3.01×10^{-8}	2.58×10^{5}	1.63×10^{5}	4.00×10^{5}
I_1,R_1	^{226}Ra	SWIFT	6.42×10^{-8}	2.46×10^{5}	1.57×10^{5}	3.88×10^{5}
I_1,R_1	^{226}Ra	UCB-NE	6.03×10^{-8}	2.59×10^{5}	1.66×10^{5}	4.04×10^{5}
I_1,R_2	^{234}U	SWIFT	8.03×10^{-6}	6.59×10^{4}	2.85×10^{4}	1.28×10^{5}
I_1,R_2	^{234}U	UCB-NE	7.90×10^{-6}	7.09×10^{4}	3.09×10^{4}	1.38×10^{5}
I_1,R_2	^{230}Th	SWIFT	5.93×10^{-7}	1.31×10^{5}	6.61×10^{4}	$(4.80 \times 10^{5})^3$
I_1,R_2	^{230}Th	UCB-NE	5.72×10^{-7}	1.40×10^{5}	6.76×10^{4}	2.71×10^{5}
I_1,R_2	^{226}Ra	SWIFT	1.93×10^{-5}	1.26×10^{5}	6.53×10^{4}	$(2.20 \times 10^{5})^3$
I_1,R_2	^{226}Ra	UCB-NE	1.84×10^{-5}	1.34×10^{5}	6.69×10^{4}	2.41×10^{5}

1 Results from the code UCB-NE presented by permission of the INTRACOIN Project Director, Kjell Andersson, Swedish Nuclear Power Inspectorate.

2 Base-case parameters T_2, B_2, L_1, P_2 and E_1 are used throughout.

3 Estimated values (...) are based on graphical extrapolation.

Table 4-8b. Comparison of SWIFT and UCB-NE for Cases $[I_2, R_1]$ and $[I_2, R_2]$[1,2,3].

Case	Nuclide	Code	C_{max} (Ci/m^3)	T_{max} (y)	T+50% (y)	T-50% (y)
I_2,R_1	^{245}Cm	SWIFT	0.	--	--	--
I_2,R_1	^{245}Cm	UCB-NE	0.	--	--	--
I_2,R_1	^{237}Np	SWIFT	2.49×10^{-6}	3.44×10^{5}	2.25×10^{5}	5.37×10^{5}
I_2,R_1	^{237}Np	UCB-NE	2.28×10^{-6}	3.68×10^{5}	2.36×10^{5}	5.78×10^{5}
I_2,R_1	^{233}U	SWIFT	3.45×10^{-6}	2.61×10^{5}	1.58×10^{5}	4.52×10^{5}
I_2,R_1	^{233}U	UCB-NE	3.31×10^{-6}	2.84×10^{5}	1.65×10^{5}	4.89×10^{5}
I_2,R_2	^{245}Cm	SWIFT	2.96×10^{-7}	2.76×10^{4}	1.73×10^{4}	4.47×10^{4}
I_2,R_2	^{245}Cm	UCB-NE	3.73×10^{-7}	2.80×10^{4}	1.57×10^{4}	4.25×10^{4}
I_2,R_2	^{237}Np	SWIFT	7.32×10^{-6}	1.47×10^{5}	8.94×10^{4}	$(2.00 \times 10^{5})^3$
I_2,R_2	^{237}Np	UCB-NE	7.79×10^{-6}	1.40×10^{5}	8.14×10^{4}	2.05×10^{5}
I_2,R_2	^{233}U	SWIFT	5.74×10^{-6}	1.14×10^{5}	6.54×10^{4}	1.55×10^{5}
I_2,R_2	^{233}U	UCB-NE	5.32×10^{-6}	1.20×10^{5}	5.89×10^{4}	1.54×10^{5}

1 Results from the code UCB-NE presented by permission of the INTRACOIN Project Director, Kjell Andersson, Swedish Nuclear Power Inspectorate.

2 Base-case parameters T_2, B_2, L_1, P_2 and E_1 are used throughout.

3 Estimated values (...) are based on graphical extrapolation.

5 FIELD COMPARISON FOR THE FLOW

5.1 HYDRAULIC TESTING FOR THERMAL-ENERGY STORAGE IN AN AQUIFER [PARR ET AL, 1983]

5.1.1 Objectives

The purposes for simulating this field problem are to test the following aspects of the SWIFT Code:

- pressure solution,
- anisotropic aquifer characteristics,
- injection and observation wells,
- flow from aquitards.

5.1.2 Description of Problem

Since 1975, investigators at Auburn University have conducted a testing program to examine the feasibility of using a confined aquifer for temporary storage of heated water. At a project site, located near Mobile, Alabama, three different sets of field experiments have been performed. Initial experiments were carried out in 1975-1976 [Molz et al, 1978] and were simulated numerically by Papadopulos and Larson [1978]. A second group of experiments was performed in 1978-1979 [Molz et al, 1979, 1981]. These results were simulated numerically both by Tsang et al [1981] and by Sykes et al [1982].

In 1981 the third set of experiments was initiated. In this case a new location was selected at the eastern side of the original well field in order to eliminate effects arising from earlier experiments. Hydraulic, thermal and geochemical tests were made to determine basic properties [Parr et al, 1983a,b], and three energy-storage experiments were performed [Molz et al, 1983]. These consisted of two injection-storage-recovery cycles, known as Cycles 3-1 and 3-2, and a two-well test. These experiments are of interest

since injection temperatures (up to 88 °C for Cycle 3-2) are sufficient to cause significant buoyancy effects. Recently Buscheck et al [1983] numerically analyzed the thermal experiments for both cycles. Using the hydraulic and thermal parameters taken from the estimates of Parr et al [1983a], Buscheck was able to achieve good agreement with the data for both Cycles 3-1 and 3-2.

Here, in this document, the objective is to assess the adequacy of the SWIFT code by comparison with field data. This problem, Problem 5.1, focuses on the hydraulic tests of Parr, and then Problem 6.1 focuses on the Cycle 3-1 experiment of Molz. The basic objective is to simulate the field data. At the same time, however, we would like to investigate three questions raised by the work of Buscheck and by the work of Parr. One question pertains to the possibility of a consistent set of aquifer parameters. In the work of Parr, values determined for the storativity and for the vertical-to-horizontal permeability ratio vary by as much as 20 percent depending on the observation well. Considering the coupling of these parameters, all of the data could be matched equally well by a single value of the storativity and a single value of the permeability ratio. This possibility will be examined.

The second question is that of aquifer boundaries. Parr inferred from pump tests the presence of such boundaries, with their presence being felt as early as 45 min after the tests begin. Since the withdrawal rates used for the hydraulic tests are of comparable magnitude to those used in the thermal tests, and since the duration of the pumping periods are much longer for the thermal tests (about 30 days) than for the hydraulic tests, boundary effects should also be present in the thermal work. The work of Buscheck ignored such geometrical effects. Here these effects are considered.

The final question relates to the characterization of the upper aquitard. Because of the buoyancy of heated water, one of the primary pathways for energy loss is through the upper aquitard. Most likely, thermal conduction is the dominant mechanism for heat transport. However, there will be some convective movement of the heat, which, of course, depends on the hydraulic properties of the aquitard. Parr estimated the hydraulic

diffusivity at 8.22×10^{-6} m^2/s whereas Buscheck adopted a value of 6.25×10^{-7} m^2/s for his simulation of the thermal-energy-storage experiment. The data appear to be inconclusive and therefore will not be examined. Consequently, a resolution of this issue will be reserved for Problem 6.1, where a limited sensitivity analysis will be performed.

5.1.3 Summary of Hydraulic Tests

According to Parr et al [1983a], the aquifer of interest is a 21-m-thick bed of sand, which extends from a depth of 40 m to a depth of 61 m below the surface. It is underlain by a sequence of clays, sands and thinly bedded limestones and is overlain by a 5.6-m-thick clay layer, above which is another aquifer. The hydraulic examination of the aquifer for the Cycle-3 experiments consisted of three separate tests, two of which are of interest here.

Anisotropy Test. Vertical permeability, in conjunction with the buoyancy effect, contributes to the upward movement of a thermal plume and the consequent energy loss to the aquitard. The anisotropy test, which was designed to measure this permeability, is shown schematically in Figure 5-1. It consisted of a pumping well completed in a lower horizon of the aquifer and three observation wells completed in an upper horizon of the aquifer. Water was withdrawn from the pumping well at a rate of

$$Q = 818 \ m^3/d \qquad (5-1)$$

and drawdown was measured at each observation well. Pumping lasted 1.4 days.

Standard Pumping Test. This test was performed in order to determine the average horizontal permeability of the aquifer and the corresponding storage coefficient. It consisted of a fully penetrating pumping well and an observation well (see Figure 5-2). Through the pumping well, water was withdrawn from the aquifer at a rate of

$$Q = 600 \ m^3/d \qquad (5-2)$$

and from the observation well, drawdown measurements were made.

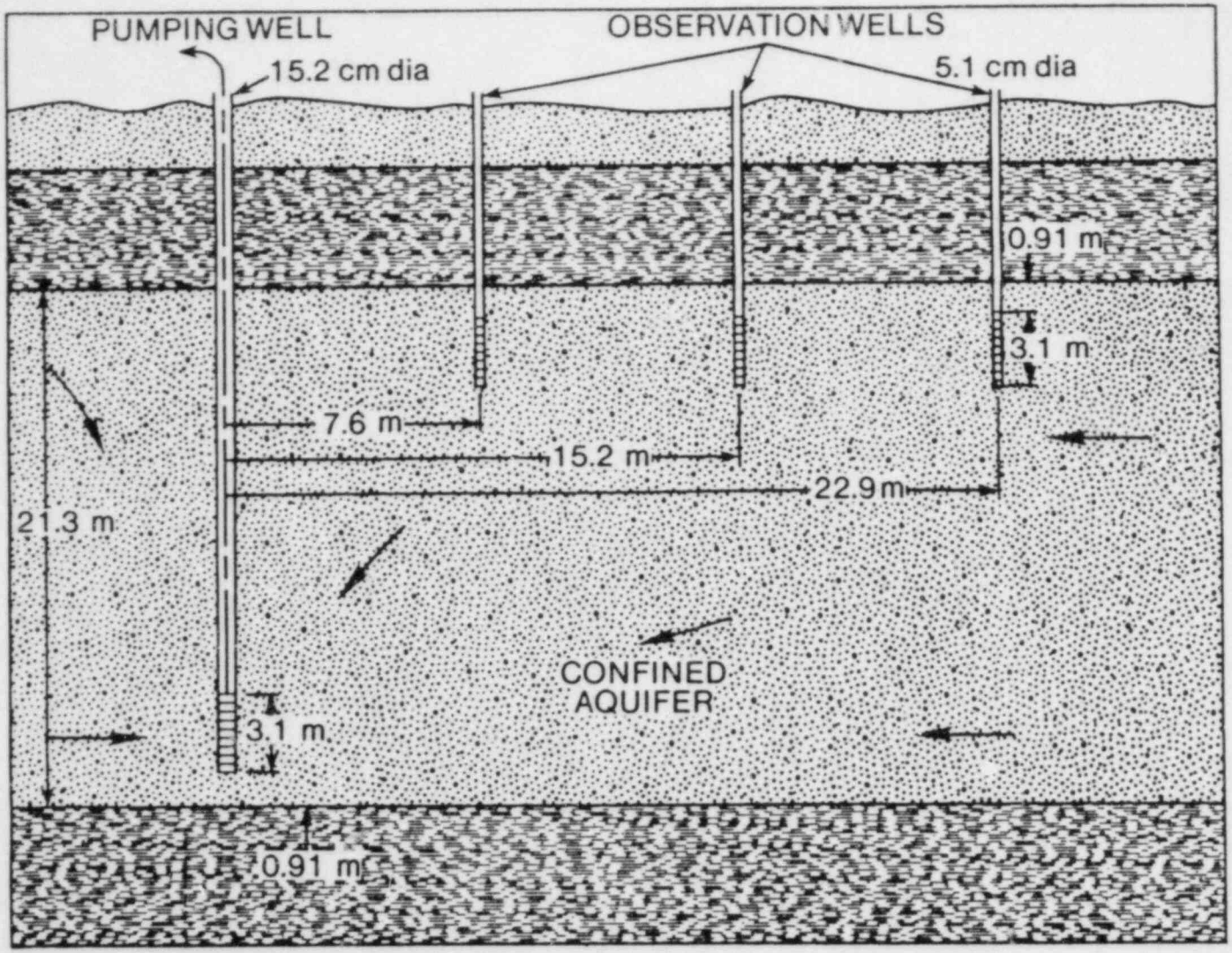

Figure 5-1. Schematic Diagram Depicting the Pumping and Observation Wells Used in the Anisotropy Test, Problem 5.1.

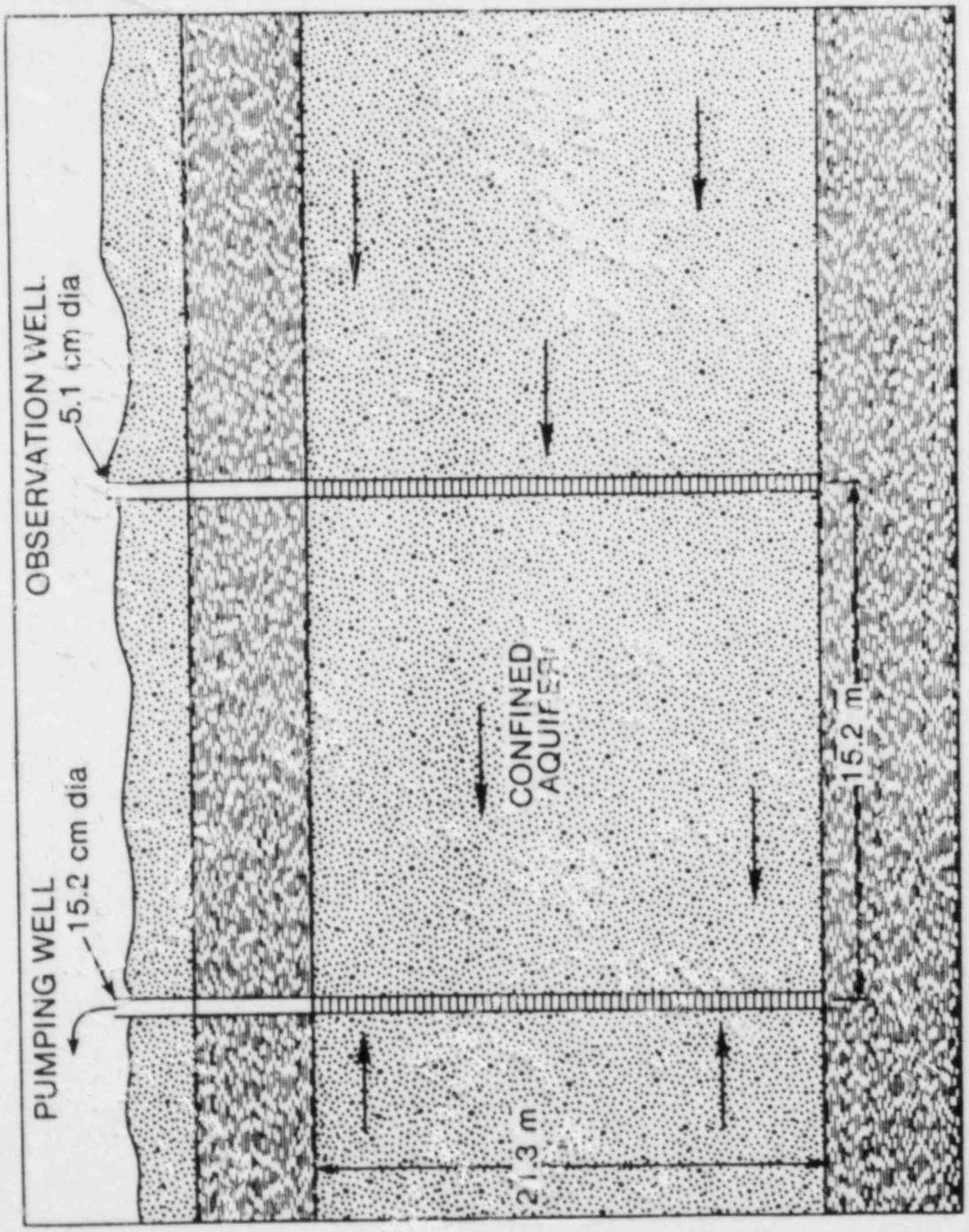

Figure 5-2. Schematic Diagram Depicting the Pumping and Observation Wells Used in the Standard Pumping Test.

With these two tests, in addition to a leaky-aquifer test, Parr obtained, at the various observation wells, the drawdown profiles shown in Figures 5-3 through 5-5. By comparison with analytically based type curves, he then determined the hydraulic properties given in Table 5-1.

5.1.4. Assumptions

For a conceptual site model on which to base the SWIFT simulations, the following three assumptions were made:

- The aquifer is semi-infinite and bounded on two sides.
- The aquifer consists of three layers.

The first assumption is taken from the observations of Parr et al [1983a]. As shown in Figures 5-3 and 5-4, there are several abrupt changes in the plots of drawdown s versus log (t), with t equal to time. These may be explained by boundary effects, i.e., sharp reductions in transmissivities (see Bear [1979], pp. 479-481).

The second assumption comes from the work of Buscheck et al [1983]. In order to explain the "fingering" which was observed in the temperature distributions, the three-layer aquifer model was adopted there (see Table 5-2).

5.1.5 Numerical Simulation and Results

Anisotropy Test. In preparation for the heat-storage cycle to be considered in Problem 6.1, it is of interest here to examine the permeability ratio. Production temperatures at the beginning of the production period, as simulated by Buscheck et al [1983], are high by about 4 percent relative to field data. Also the storage coefficients, as estimated by Parr et al [1983a], for the anisotropy test are low by as much as 20 percent when compared to the storage coefficient determined by the standard pumping test (see Table 5-1). Both of these circumstances could be related to an anomalously high value of the permeability ratio.

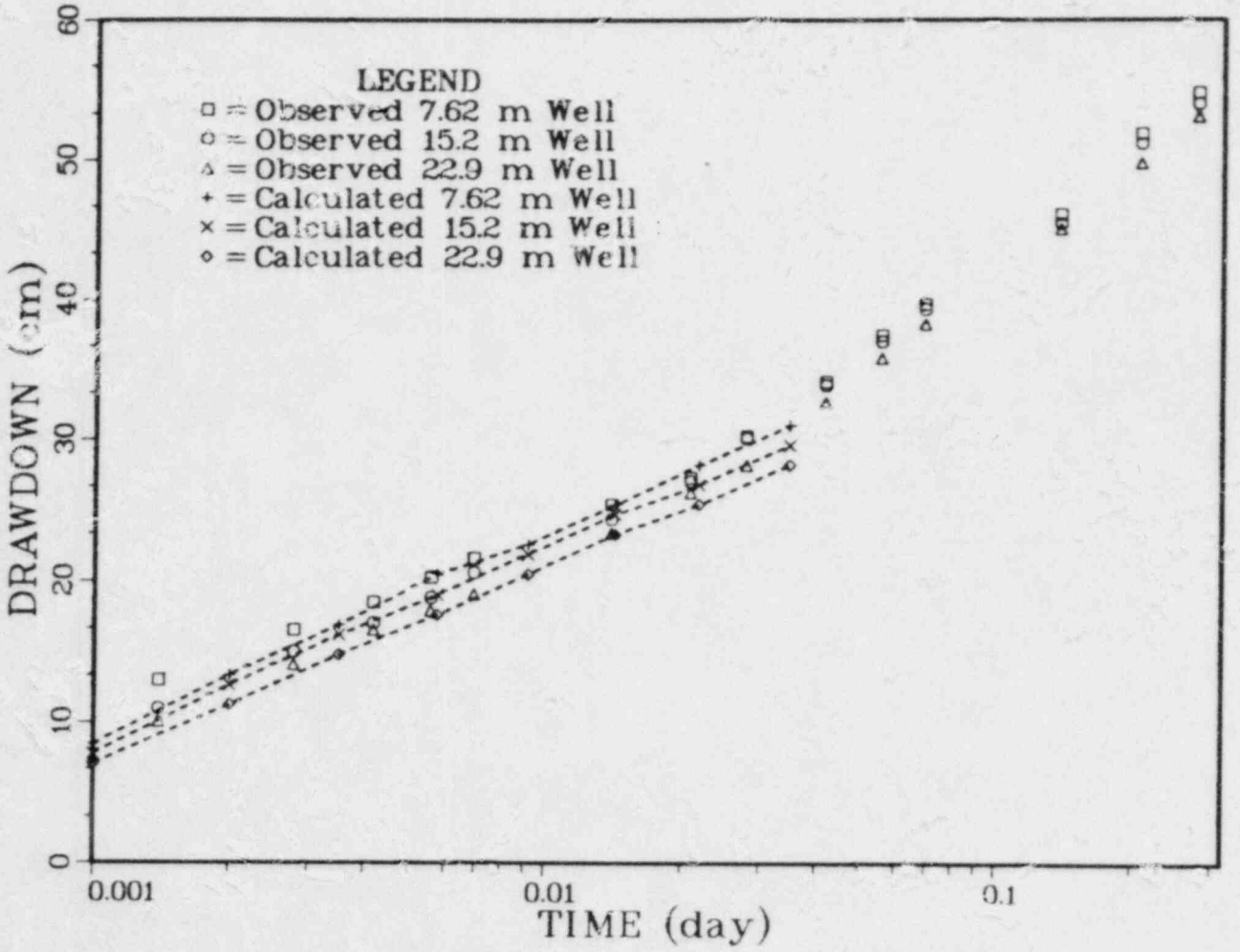

Figure 5-3. Aquifer Drawdown as a Function of Time at Three Observation Wells for the Anisotropy Test.

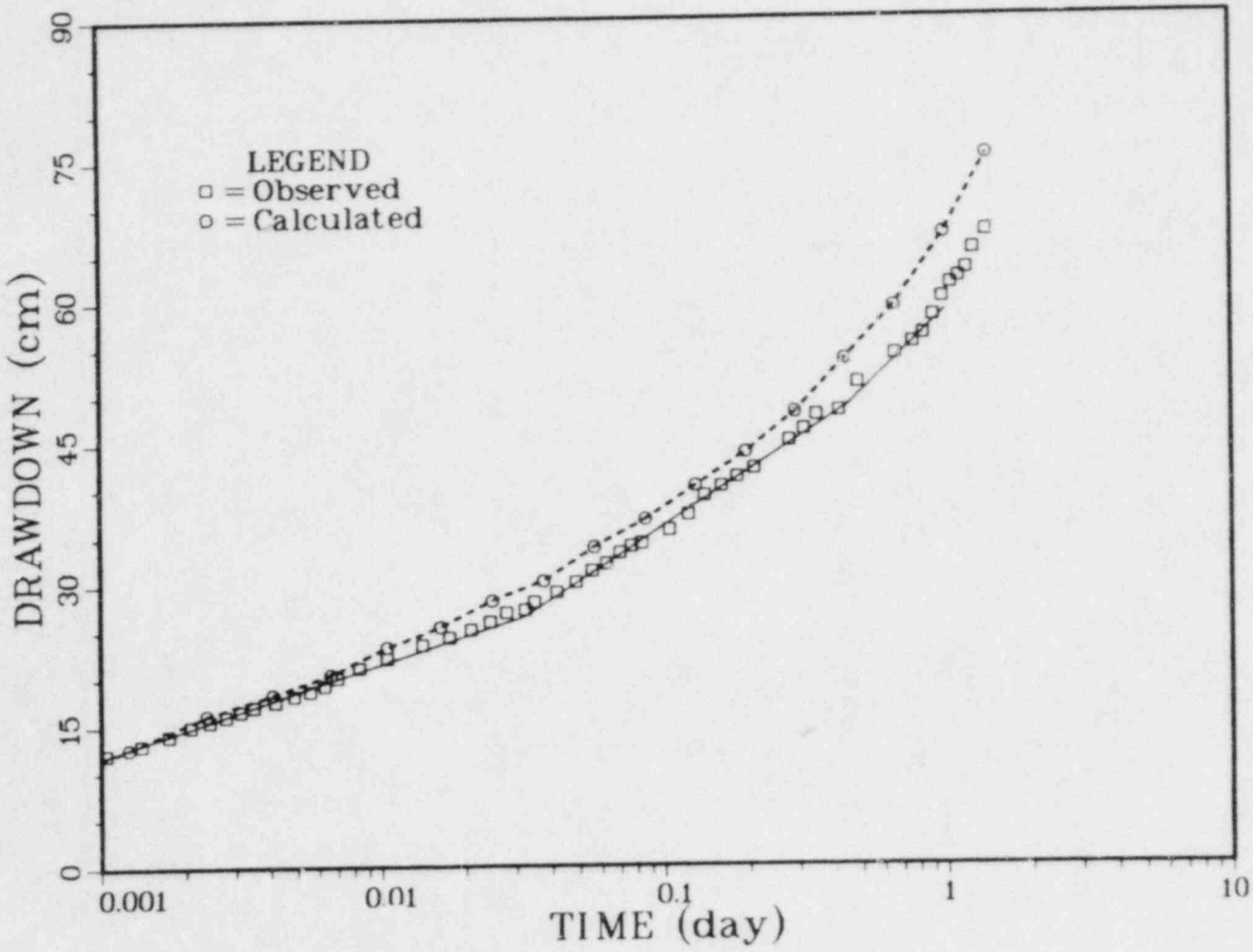

Figure 5-4. Aquifer Drawdown as a Function of Time for the Standard Pumping Test.

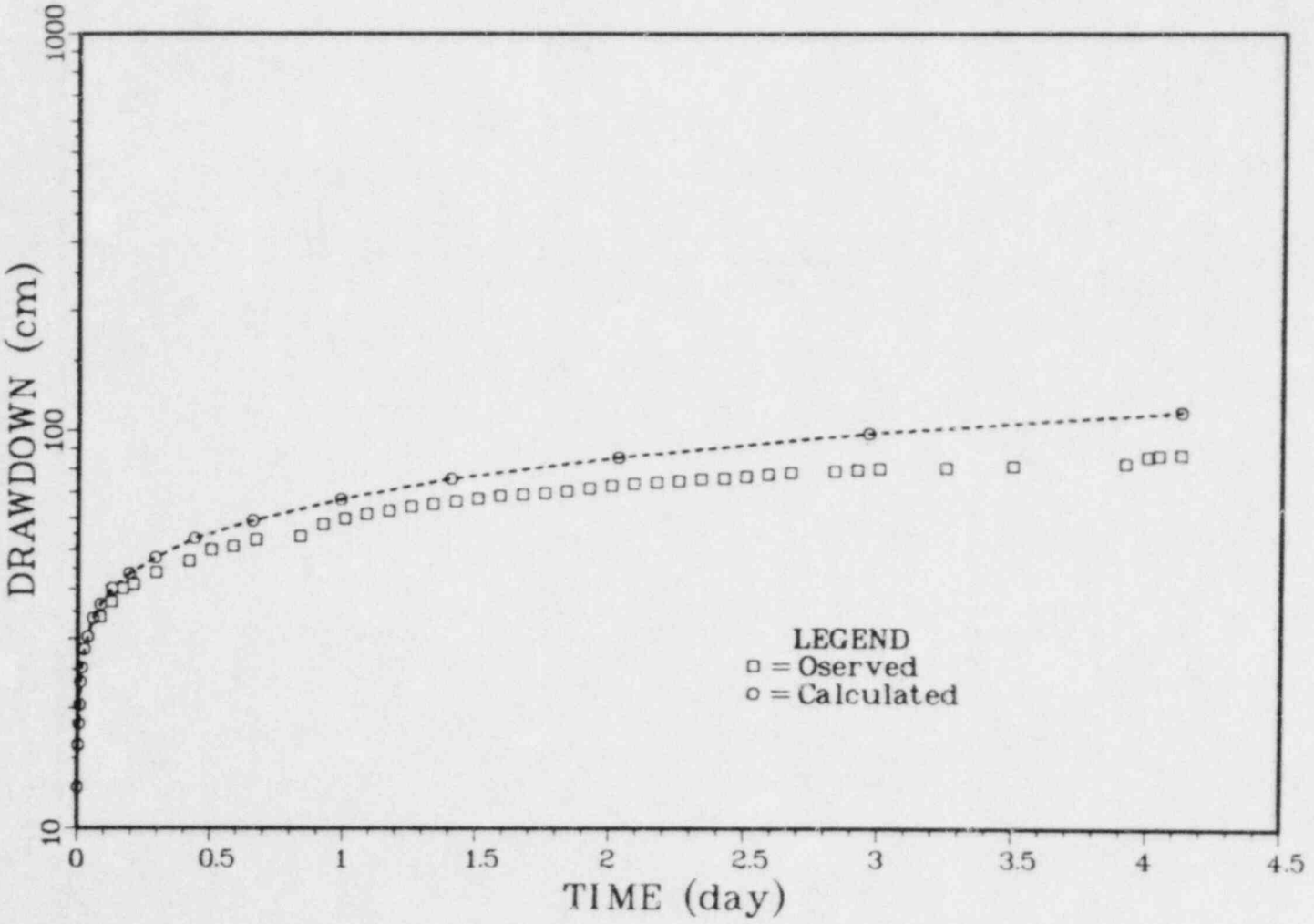

Figure 5-5. Aquifer Drawdown at a Fully Penetrating Observation Well as a Function of Time for the Leaky-Aquifer Test. This curve extends the time response of the standard pumping test.

Table 5-1. Hydraulic Properties of Aquifer and Aquitard (from Parr et al [1983a]).

Parameter	Hydrological Test	Value	
		SI	English
Aquifer Hydraulic Conductivity (Horizontal)	Std. Pump	6.19×10^{-4} m/s	175.5 ft/d
	Anisotropy*	6.31×10^{-4} m/s	178.8 ft/d
		6.09×10^{-4} m/s	172.6 ft/d
		6.19×10^{-4} m/s	175.5 ft/d
Aquifer Hydraulic Conductivity (Vertical)	Anisotropy*	1.05×10^{-4} m/s	29.9 ft/d
		8.3×10^{-5} m/s	23.9 ft/d
		9.17×10^{-5} m/s	26.0 ft/d
Aquifer Storativity	Std. Pump	.00069	
	Anisotropy	.00047	
		.00052	
		.00049	
Aquitard Diffusivity	Leaky (upper)	8.22×10^{-6} m^2/s	7.6 ft^2/d
	Leaky (lower)	1.27×10^{-5} m^2/s	11.8 ft^2/d

* The three values presented correspond to measurements obtained at radii of 7.62, 15.2 and 22.9 m from pumping well.

To examine this issue, only the first limb ($t \leq 45.5$ min) of the drawdown profile of Figure 5-3 was considered. For this time period, boundary effects were negligible. Consequently, only the aquifer was gridded, and an axisymmetric (r-z) coordinate system was used with a Carter-Tracy aquifer-influence function at the boundary. Table 5-2 presents both the spatial and the temporal discretizations. The horizontal conductivities for each layer were fixed at the values used by Buscheck (Table 5-3).

A sensitivity analysis was then performed for the two remaining parameters, i.e., for the storativity, S, and for the vertical-to-horizontal conductivity ratio, R. Table 5-4 summarizes the analysis. The control variables, which are the drawdown s (15.2 m, 10 min) and the incremental drawdown Δs (10 min) = s (7.62 m, 10 min) - s (22.9 m, 10 min), behave in a predictable manner [Hantush, 1961]. There is definitely a coupling between S and R in that both bear an inverse relationship to s. The only distinction between the two lies in the fact that only R affects Δs. Based on a comparison between simulated and experimental data, we concluded that the best pair of values to use in the thermal-storage simulation is

$$S = 6 \times 10^{-4} \qquad (5\text{-}4a)$$

and

$$R = 1{:}5 \qquad (5\text{-}4b)$$

The drawdown profiles determined for these values are shown in Figure 5-3, where they may be compared directly with the field data.

Standard Pumping Test. The drawdown curves of Figure 5-4 and Figure 5-5 exhibit regions of distinguishably different behavior. The first two such regions, or limbs, were characterized as straight lines by Parr:

$$s = 10.24 + 9.69 \log (t) \quad , \quad t \leq 45.5 \text{ min} \qquad (5\text{-}5a)$$

and

$$s = 5.91 + 2(9.69) \log (t) \quad , \quad 45.5 \text{ min} < t \leq 650 \qquad (5\text{-}5b)$$

The factor of two may be interpreted [Bear, 1979] as arising from a totally reflecting boundary, which is mathematically equivalent to an image well pumping at an identical rate. In effect, then, when the first image well begins to be felt, the pumping rate is doubled. Parr positions the first

Table 5-2. Spatial Grid in Axisymmetric Cylindrical Coordinates and Temporal Grid as Used for the Anisotropy Test.

Number	Block Center Radius (ft)	z-Increment (ft)	Time Increment (d)
1	0.60	3.0	1.00×10^{-3}
2	0.88	5.0	1.50×10^{-3}
3	1.28	5.0	2.25×10^{-3}
4	1.88	5.0	3.38×10^{-3}
5	2.75	7.0	5.07×10^{-3}
6	4.00	6.5	7.59×10^{-3}
7	5.90	8.5	1.29×10^{-2}
8	12.4	8.0	
9	18.2	4.0	
10	25.0	5.0	
11	40.0	5.0	
12	50.0	5.0	
13	65.0	3.0	
14	75.0		
15	100.0		
16	165.0		
17	250.0		
18	380.0		
19	587.0		
20	898.0		
21	1370.0		
22	2100.0		

Table 5-3. Values of Hydraulic Conductivity for the Three-Layer Aquifer Model (from Buscheck et al [1985]).

	Thickness		Value	
	(m)	(ft)	(m/s)	(ft/d)
Upper Layer	9.6	31.5	4.51×10^{-4}	128
Middle Layer	5	16.5	11.4×10^{-4}	322
Lower Layer	6.6	22.0	4.51×10^{-4}	128
Composite Value	21.2	70.0	6.17×10^{-4}	175

Table 5-4. Determination of Consistent Values of Storativity and Conductivity Ratio from the Anisotropy Test.

Aquifer Storativity	Permeability Ratio	Relative Drawdown[1] (cm)	Relative Incremental Drawdown[2] (cm)
6.0×10^{-4}	1:5	-0.3	-0.1
6.9×10^{-4}	1:4	-0.4	0.3
4.9×10^{-4}	1:6.7	-0.6	-0.5
6.2×10^{-4}	1:6.7	-1.7	-0.1
6.2×10^{-4}	1:4	0.2	0.7
4.9×10^{-4}	1:4	1.8	0.3

1 Simulated drawdown s (15.2 m, 10 min) less observed drawdown (20.4 cm) at the same location and time.

2 Incremental drawdown Δs (10 min) = s (7.62 m, 10 min) - s (22.9 m, 10 min) less observed incremental drawdown (2.4 cm). For the latter quantity an average over times 4 min $\leq t \leq$ 40 min was used in order to remove effects due to data fluctuations.

boundary at 150 m from the pumping well. Since we use an average storativity of 6.0×10^{-4}, as compared to his value of 6.9×10^{-4}, we position the corresponding boundary at 182 m. We also locate the second boundary at 790 m, as shown in Figure 5-6. This configuration of boundaries may be explained analytically by the presence of an infinite sequence of image wells and, consequently, many limbs.

Since both the pumping well and the observation well fully penetrate the aquifer, it was sufficient to use the average conductivity

$$K = 6.17 \times 10^{-4} \text{ m/s} \qquad (5\text{-}6)$$

and the average storativity given by Equation (5-5), together with a single layer for the aquifer. Figure 5-6 shows an areal view of the system model, and Table 5-5 presents both the spatial and the temporal discretizations.

Since the field data is insufficient for precise location of the boundaries, three separate observation wells were positioned within the system model in order to show the variations which might be expected. Each such well was located at the same 15.2 m from the pumping well as for the actual observation well. Figure 5-4 shows the simulated drawdowns, both with and without boundaries, plotted alongside the observed data for values of time less than 1.4 d. Figure 5-5 then extends these results to 4 days.

Obviously, the effect of the boundaries are significant when viewed in the localized context of small-time behavior ($t \leq 4$d) at a single location. However, the important issue to be addressed is the effect of the boundaries for temporal and spatial scales commensurate with those of the thermal-energy storage experiment, i.e., the duration of the injection or production period (about 30 d) and the radial extent of the thermal migration (about 40 m).

To assess this matter, the calibrated flow model of the site was used to generate the drawdown contours which would occur if the $Q = 600$ m^3/d withdrawal rate were continued for 30 days. Since this rate is comparable to that of the thermal-energy storage experiment (about 800 m^3/d), this pattern should be indicative of the geometrical effects present in that experiment. Figure 5-7 presents the results of that simulation on a regional scale, where the boundary effects are quite marked. Figure 5-8 presents the same results, but on the scale of the thermal-energy experiment. Here, an examination of the corresponding velocity field showed deviations from the radially symmetric

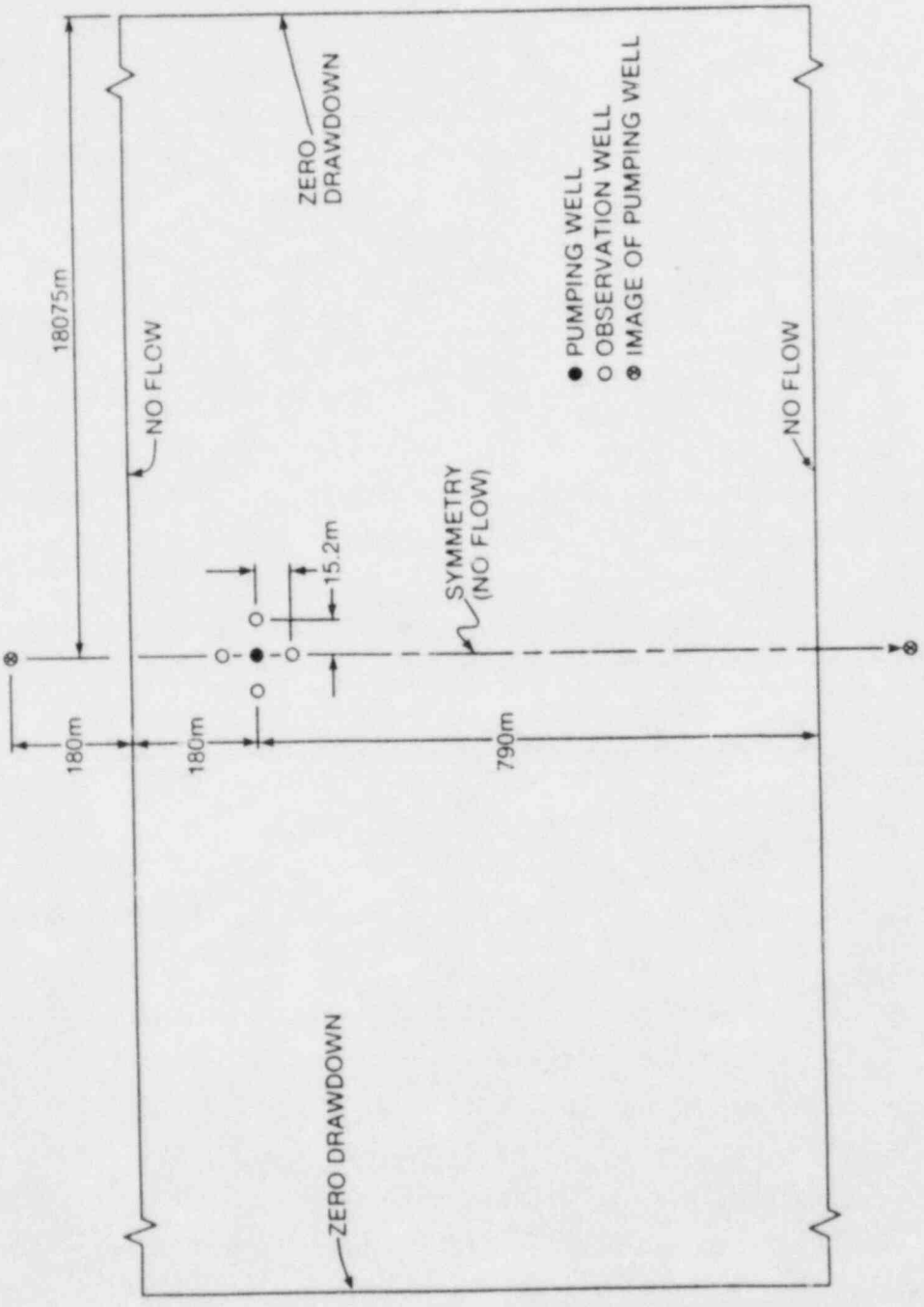

Figure 5-6. System Model Including the Effects of Boundaries.

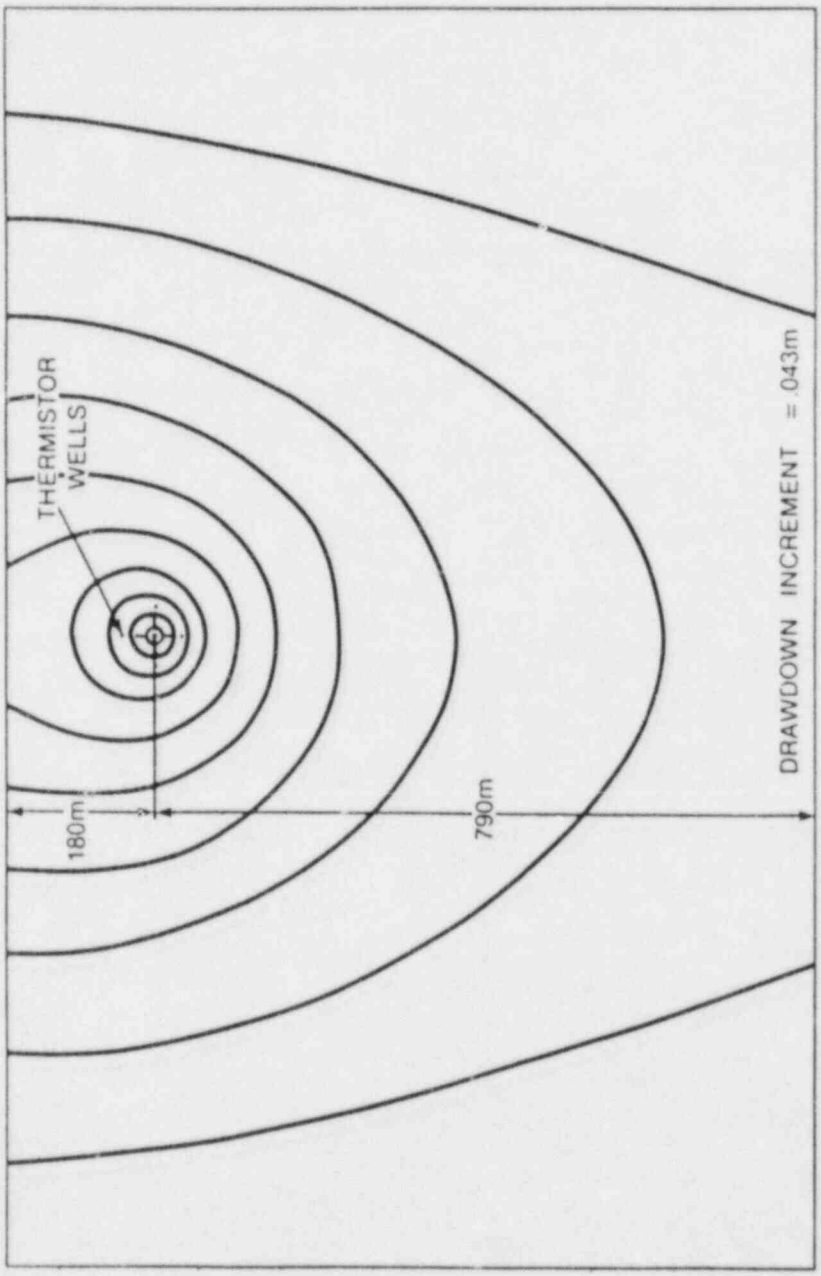

Figure 5-7. Drawdown Contours Viewed on a Regional Scale.

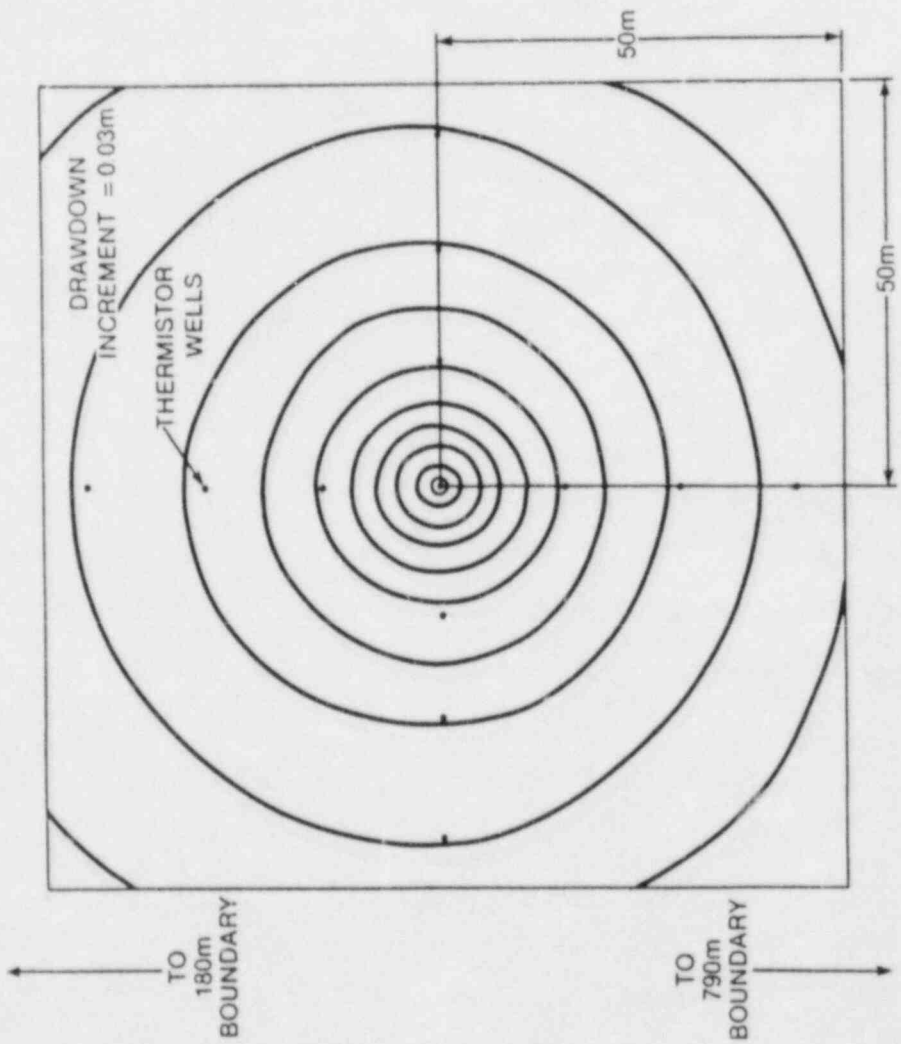

Figure 5-8. Drawdown Contours Viewed on the Scale of the Thermal-Energy Storage Experiment.

Table 5-5. Spatial Grid In Cartesian Coordinates and Temporal Grid as Used for the Standard Pumping Test.

Number	x-Increment (ft)	y-Increment (ft)	Time Increment (d)
1	174	1	7.50×10^{-4}
2	153	4	1.13×10^{-3}
3	97	8	1.69×10^{-3}
4	64	16	2.53×10^{-3}
5	32	32	3.79×10^{-3}
6	16	64	5.70×10^{-3}
7	8	128	8.54×10^{-3}
8	4	256	1.28×10^{-2}
9	2	256	1.92×10^{-2}
10	4	256	2.88×10^{-2}
11	8	256	4.32×10^{-2}
12	8	512	6.49×10^{-2}
13	8	768	9.73×10^{-2}
14	8	1152	0.146
15	8	1728	0.219
16	4	2592	0.329
17	2	3888	0.416
18	4	5832	
19	8	8748	
20	8	13122	
21	8	19682	
22	8		
23	8		
24	4		
25	2		
26	4		
27	8		
28	16		
29	32		
30	64		
31	64		
32	128		
33	203		
34	256		
35	256		
36	256		
37	256		
38	500		
39	500		

(Theis) field ranging from zero at the pumping well to about 40 percent at 40 m. Thus, it was concluded that migration distances, as computed from an approximate radially symmetric model, could differ by as much as 20 percent from those computed by the partially bounded model of the site.

6 FIELD COMPARISON FOR THE HEAT-TRANSPORT

6.1 THERMAL-ENERGY STORAGE IN AN AQUIFER [MOLZ ET AL, 1983]

6.1.1 Objectives

The purposes for simulating this field problem are to test the following aspects of the SWIFT Code:

- coupled pressure and temperature solutions,
- anisotropic aquifer characteristics,
- injection and observation wells,
- aquifer-influence functions,
- heat loss to aquitards.

6.1.2 Description of the Problem

Since 1975, investigators at Auburn University have conducted a testing program to examine the feasibility of using a confined aquifer for temporary storage of heated water. Three sets of experiments have been performed at the project site, which is located near Mobile, Alabama. The most recent set of experiments (Cycle 3) is of interest here. Problem 5.1 focused upon the hydraulic testing and a site model was developed there. That model contained a three-layer discription of the aquifer and it employed a consistent set of aquifer parameters. Ideally this site model would also contain impermeable boundaries as indicated by Figure 5-6. However, it was pointed out there (Section 5.1.4) that for the thermal-energy storage problem an approximate axisymmetric model could be used, but that there would be some discrepancies in the predicted temperature distribution. In particular, the migration length in the direction of the nearest boundary, at the end of the injection period, would be overpredicted by about 20 percent with the axisymmetric representation.

In this problem the basic objective is to simulate the Cycle 3-1 thermal-energy-storage experiment and by comparison with field data to demonstrate the validity of the SWIFT Code. We, like Buscheck et al [1983], in their simulation of these data, will employ an axisymmetric model. Table 6-1 and Table 5-3 list values of all parameters to be used, these properties come from the estimates of Parr and Molz, as supplemented by our analysis of Problem 5.1 and by the analysis of Buscheck.

In this problem we would also like to return to the question raised earlier regarding the hydraulic properties of the upper aquitard. As indicated in Section 5.2, Parr's value of hydraulic diffusivity (8.22×10^{-6} m^2/s) is about an order of magnitude higher than that used in Buscheck's simulation (6.25×10^{-7} m^2/s). Further, because of instrumentation problems [Parr, 1983a], the data are inconclusive. As indicated in Table 6-1, Parr's value is adopted for the basic simulation. Neither of the above-mentioned values would permit significant leakage during the Cycle-3 test. However, to assess the sensitivity of the energy recovery factor to this quantity an additional run will be performed with an order-of-magnitude increase in this quantity, which would yield significant leakage during the test.

6.1.3 Summary of Field Test

The well field used for the Cycle 3-1 experiment is shown in Figure 6-1. A volume of 25,400 m^3 of heated water was injected over a 32-day period. Then, following a 31-day storage period, the same volume of water was recovered over a 26-day period. The twelve observation wells, instrumented as shown in Figure 6-2, were then used to determine temperature distributions (Figures 6-3 and 6-4), which resulted from the injection/production schedules of Figures 6-5 through 6-7.

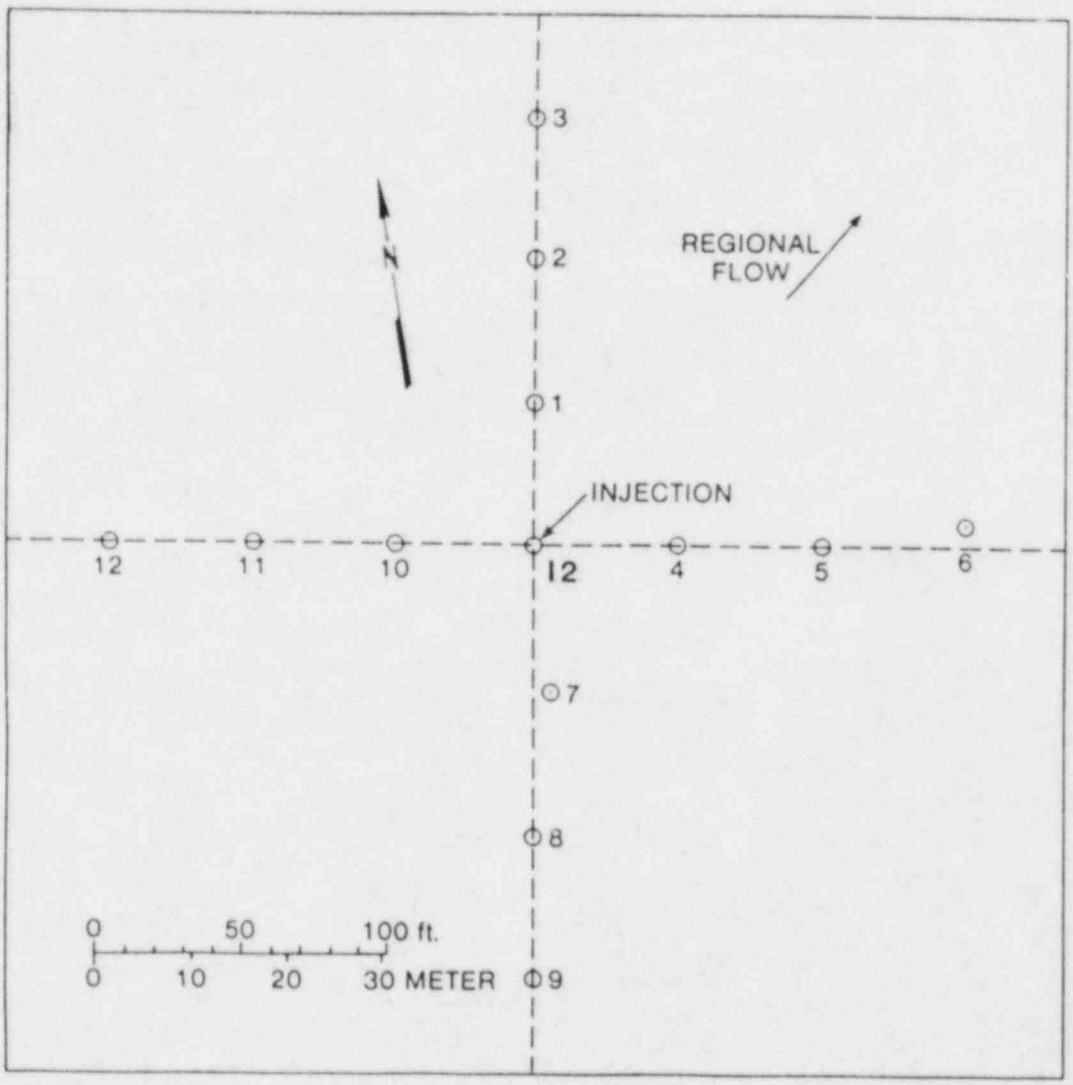

Figure 6-1. Top view of the Well Field Showing the Different Types of Wells (After Molz et al [1983]), Problem 6.1.

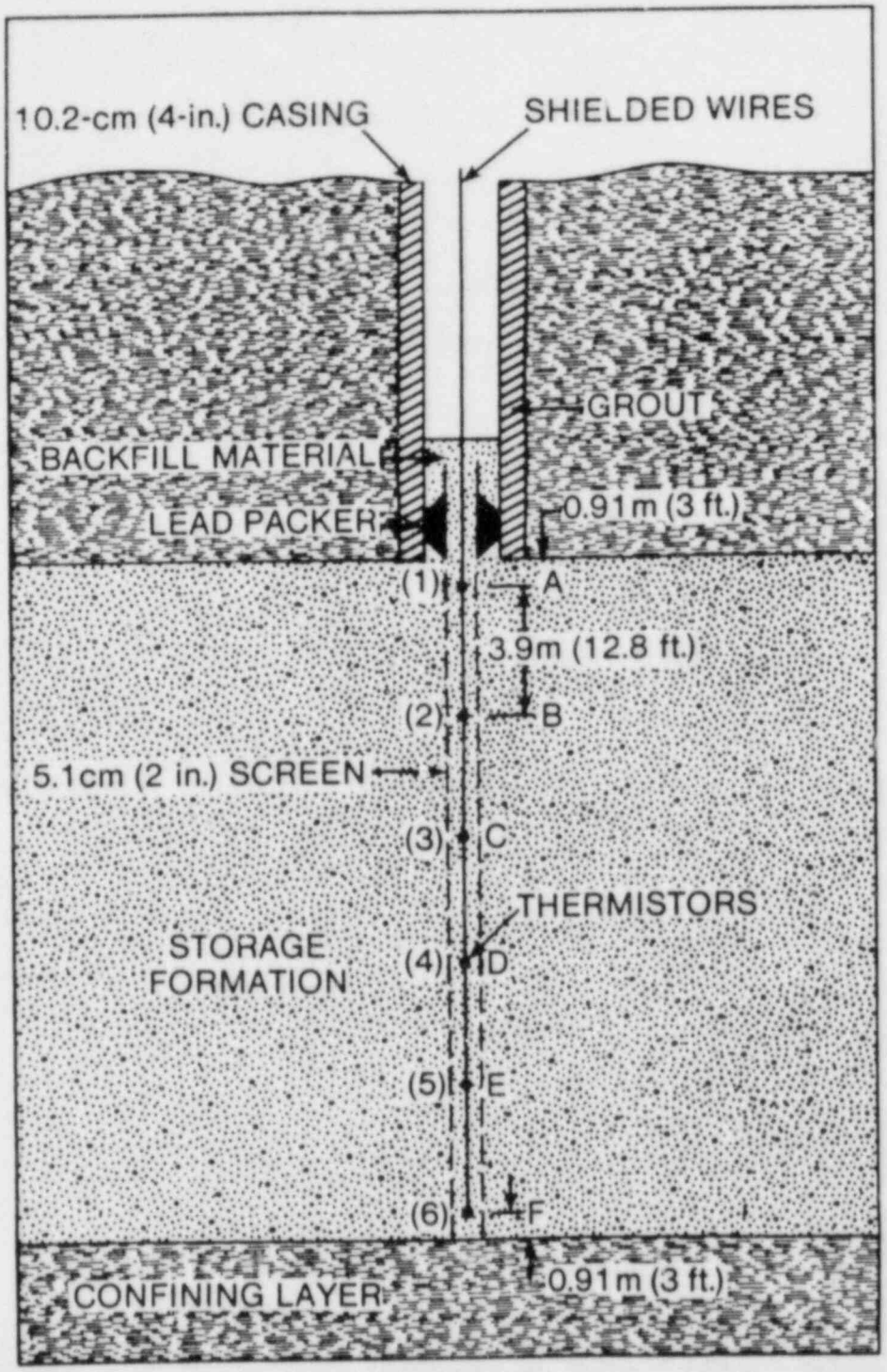

Figure 6-2. Schematic Diagram of a Typical Temperature Observation Well (After Molz et al [1983]).

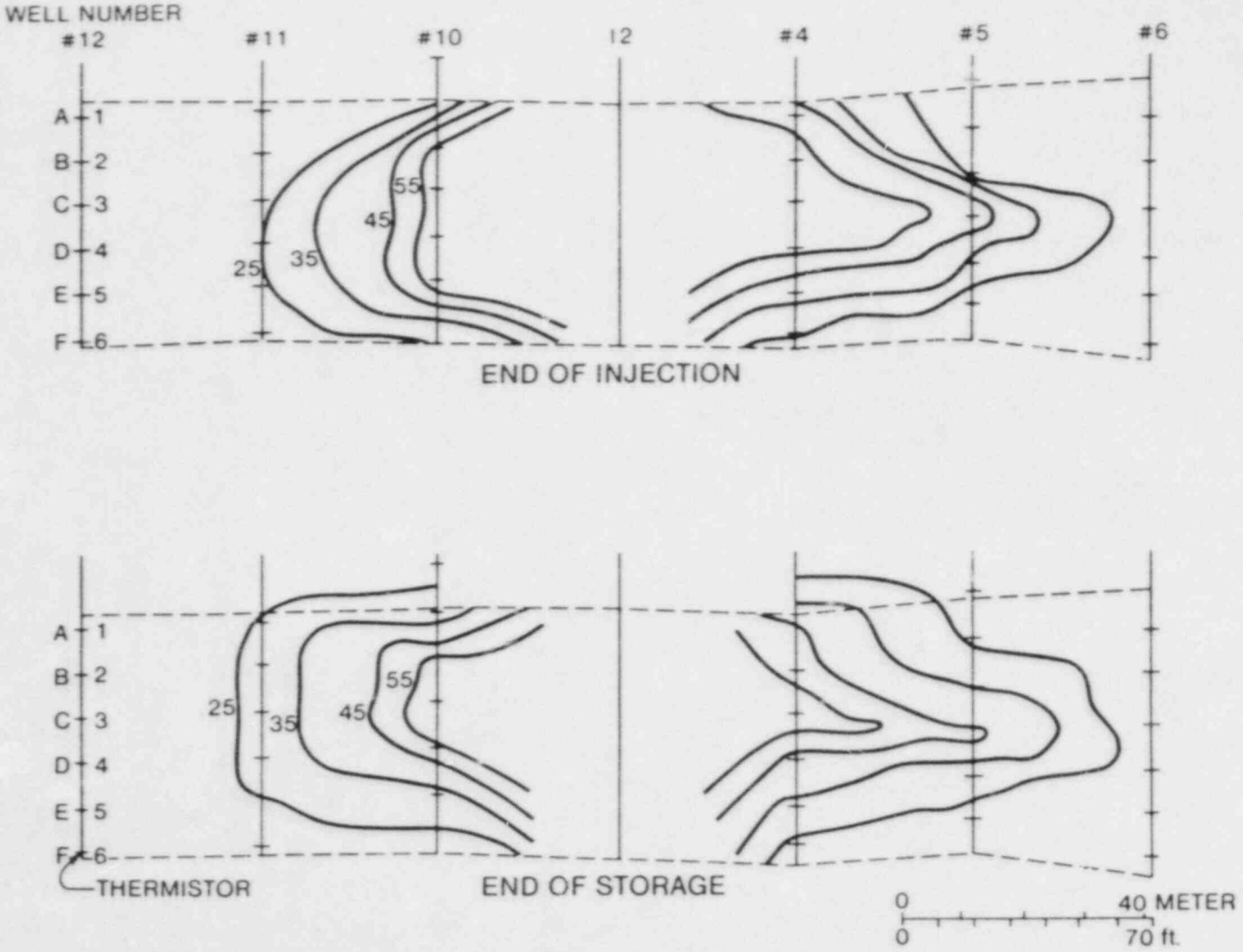

Figure 6-3. East-West Ground-water Temperature Distributions at Selected Times. The vertical sections run between Wells 12 and 6 (Figure 6-1).

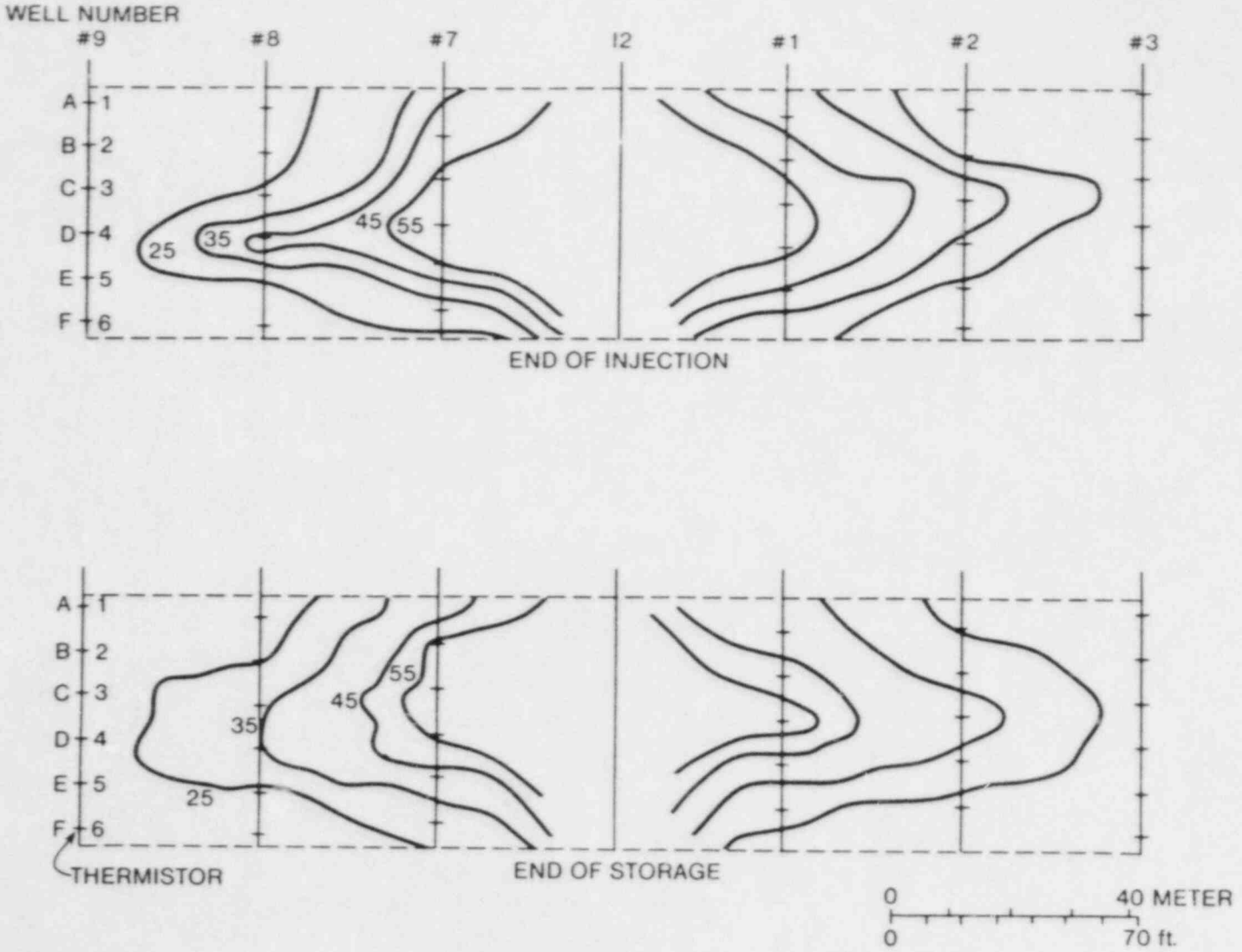

Figure 6-4. North-South Ground-water Temperature Distributions at Selected Times. The vertical sections run between Wells 9 and 3 (Figure 6-1).

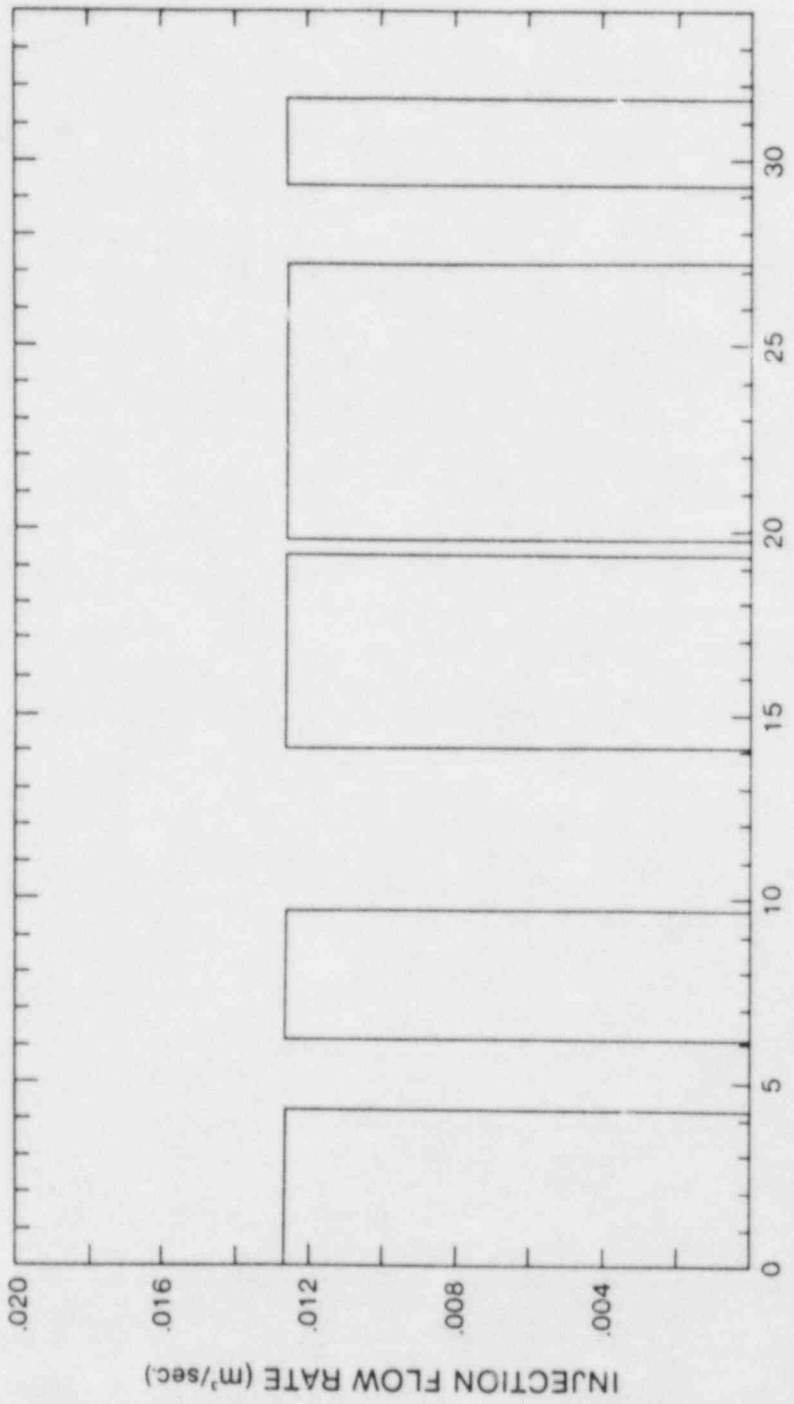

Figure 6-5. Injection Rate as a Function of Time.

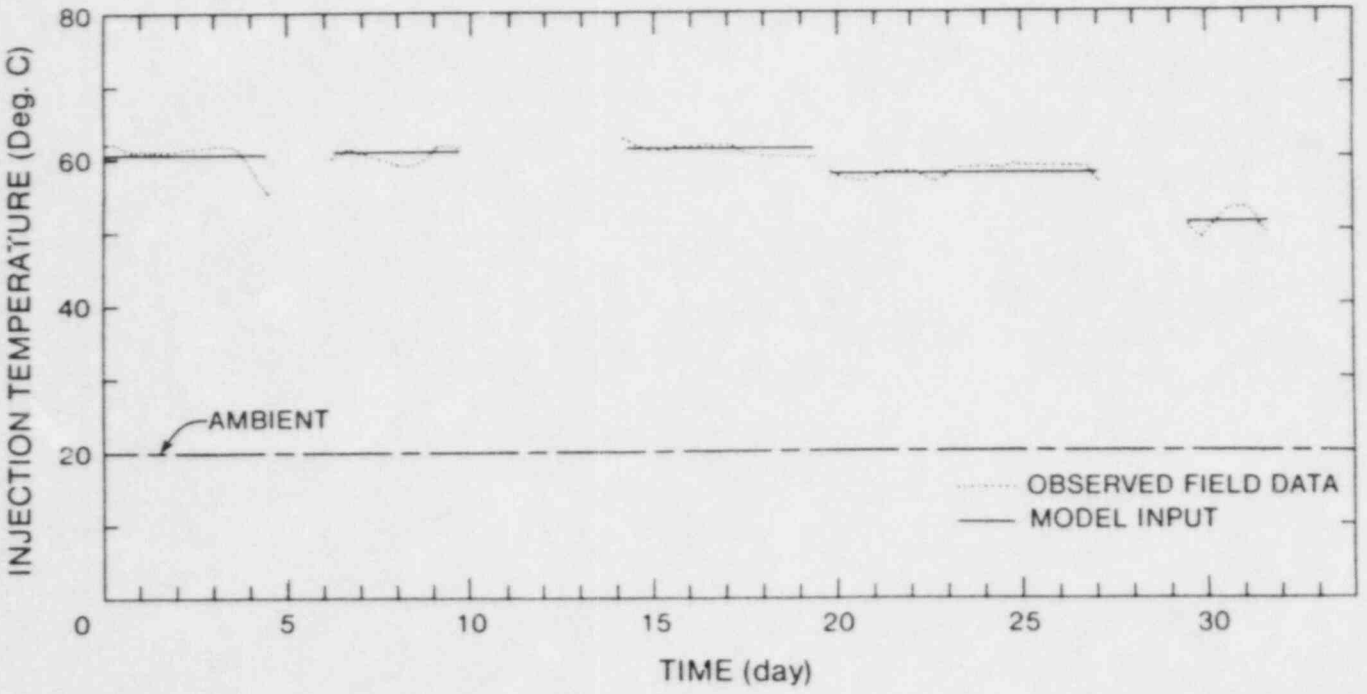

Figure 6-6. Injection Temperature as a Function of Time. The line marked "ambient" indicates the ambient ground-water temperature (after Molz et al [1983]).

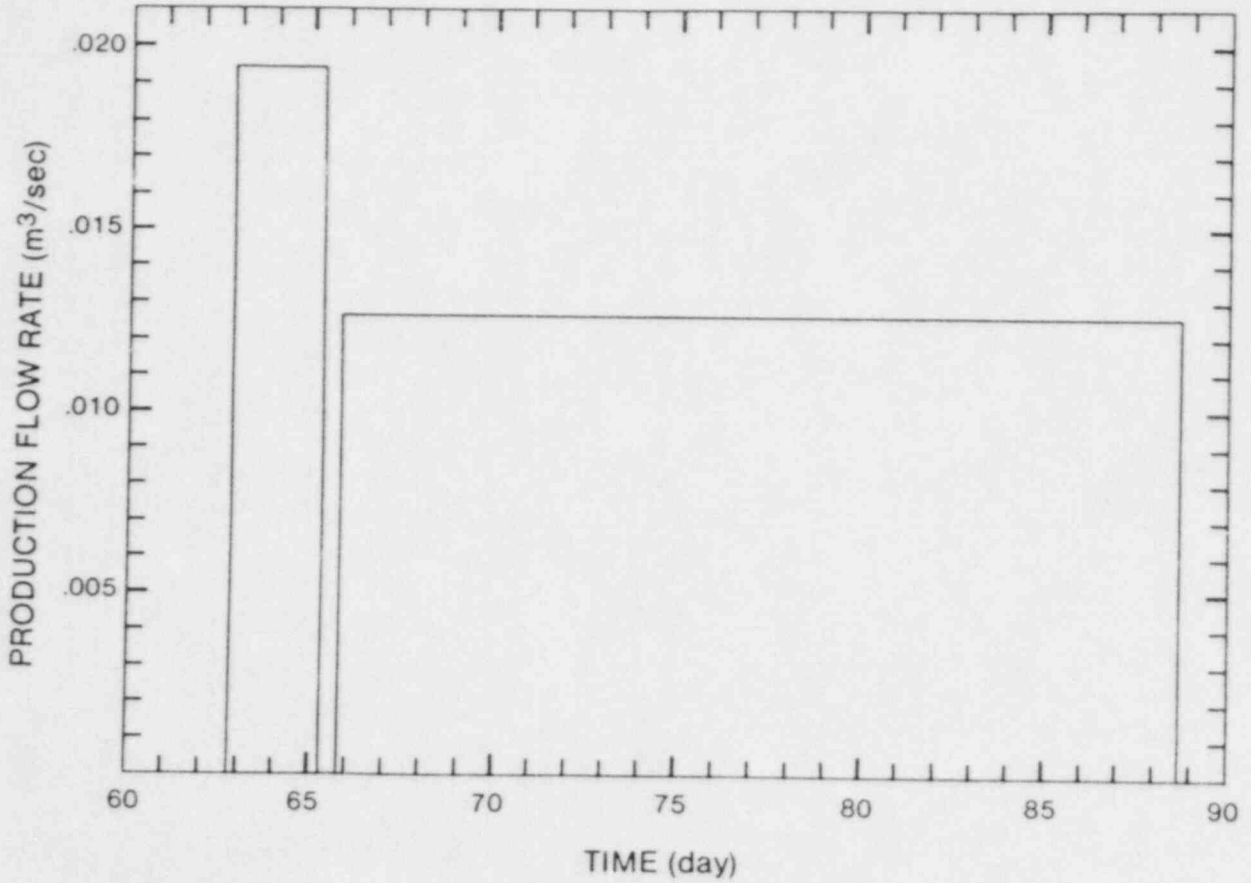

Figure 6-7. Recovery Rate as a Function of Time (After Molz et al [1983]).

Table 6-1. Hydraulic and Heat-Transport Parameters Adopted for Problem 6.1.

Parameter	Source[1]	Symbol	Value	
			SI	English
Aquifer thickness	Parr	b	21.2 m	70.0 ft
Hydraulic conductivity, aquifer[2]	Parr	K	6.17×10^{-4}	175
Storativity, aquifer		S	6×10^{-4}	6×10^{-4}
Porosity, aquifer	Buscheck	ϕ	0.25	0.25
Heat capacity, aquifer	Molz	c_p	1.81×10^{6} J/($m^3 \cdot {}^{o}C$)	27.0 Btu/($ft^3 \cdot {}^{\circ}F$)
Thermal conductivity, aquifer	Molz	K_m	2.29 W/($m \cdot {}^{o}C$)	31.8 Btu/($ft \cdot d \cdot {}^{\circ}F$)
Thickness, upper aquitard	Parr	b'	5.6 m	18.4 ft
Porosity, aquitard	Buscheck	ϕ'	0.35	0.35
Heat capacity, aquitard	Buscheck	c'_{pR}	1.81×10^{6} J/($m^3 \cdot {}^{o}C$)	27.0 Btu/($ft^3 \cdot {}^{\circ}F$)
Thermal conductivity, aquitard	Molz	K'_m	2.56 W/($m \cdot {}^{o}C$)	35.5 Btu/($ft \cdot d \cdot {}^{\circ}F$)
Hydraulic diffusivity, upper aquitard	Parr	D'	8.22×10^{-6} m^2/s	7.64 ft^2/d
Hydraulic diffusivity, lower aquitard	Parr	D''	1.27×10^{-5} m^2/s	11.8 ft^2/d
Rock density	Buscheck	ρ_R	2600 kg/m^3	120 lb/ft^3
Thermal expansion of water	Clark	c_T	5.3×10^{-4} $(^{\circ}C)^{-1}$	2.9×10^{-4} $(^{\circ}F)^{-1}$
Injection duration	Molz	Δt_1	2.74×10^{6} s	31.7 d
Storage duration	Molz	Δt_2	2.70×10^{6} s	31.3 d
Production duration	Molz	Δt_3	2.20×10^{6} s	25.7 d
Initial temperature	Parr	T_o	$20^{o}C$	$68^{o}F$
Aquifer permeability ratio[3]		R	1:6	1:6

1 The references are Parr [1983a], Buscheck [1983], Molz [1983] and Clark [1966]. No reference indicates an assumption by the authors.

2 Composite value of horizontal conductivity. Refer to Table 5-2 for hydraulic conductivities of individual layers.

3 Composite value. The ratio is 1:5 for individual layers.

6.1.4 Assumptions

The conceptual site model employed here for the SWIFT simulations was similiar to that used for Problem 5.1 and was based on the following assumptions:

- The aquifer, though likely bounded, may be approximated by an infinite system.
- The aquifer consists of three layers.

The latter comes from the work of Buscheck et al [1983] and yields the simplest system model which may be used to explain the "fingering" which is present in the temperature distributions (Figures 6-3 and 6-4).

6.1.5 Numerical Simulation and Results

To simulate the thermal-energy-storage experiment, the site model was discretized spatially (Table 6-2) and was then stepped through time (Table 6-3) using the SWIFT Code. By including both a variable density (via the thermal expansion coefficient) and a variable viscosity (Table 6-4), a fully coupled flow/heat-transport simulation was achieved. The results were fluid pressures and temperatures given as functions of both space and time. Here we focus on the thermal results only.

The simulated temperature distributions for the end of the injection period and for the end of the storage period (Figure 6-8) display both preferential flow within the more permeable central layer and thermal buoyancy. They are in general agreement with the observed data (Figures 6-3 and 6-4). However, for the end of the storage period, the simulated temperatures are somewhat high in the upper layer and somwhat low in the lower layer. A refinement in the characterization of the layering, would likely correct this discrepancy. Nevertheless, the time- and space-dependent profiles (Figures 6-9 through 6-12) show reasonable agreement between observed and simulated results. Simulated production temperatures (Figure 6-13) yield an

Table 6-2. Spatial Grid* Selected for the Thermal-Energy Storage Simulation.

Number	Block Center Radius (m)
1	0.60
2	0.78
3	1.02
4	1.32
5	1.72
6	2.24
7	2.91
8	3.78
9	4.92
10	6.41
11	8.33
12	10.84
13	14.90
14	21.00
15	29.60
16	36.00
17	44.10
18	58.00
19	74.00

* Centered-in-space differencing was used.

Table 6-3. Temporal Grid* Selected for the Thermal-Energy Storage Simulation.

Number	Time Increment (d)	Number	Time Increment (d)
1	0.926	33	0.231
2	0.926	34	0.926
3	0.926	35	0.926
4	0.879	36	0.578
5	0.926	37	0.926
6	0.741	38	1.389
7	0.926	39	2.083
8	0.926	40	2.986
9	0.926	41	3.009
10	0.682	42	3.472
11	0.926	43	3.681
12	0.926	44	3.958
13	0.926	45	3.704
14	0.926	46	5.139
15	0.671	47	0.023
16	0.926	48	0.926
17	0.926	49	0.926
18	0.926	50	0.509
19	0.926	51	0.486
20	0.926	52	0.926
21	0.613	53	1.099
22	0.482	54	1.122
23	0.926	55	1.331
24	0.926	56	1.481
25	0.926	57	1.643
26	0.926	58	1.793
27	0.926	59	1.875
28	0.926	60	1.967
29	0.926	61	2.071
30	0.926	62	2.222
31	0.926	63	2.453
32	0.926	64	2.882

* Backward-in-time differencing was used.

Table 6-4. Viscosity as a Function of Temperature.*

Temperature (°C)	Viscosity (Pa-sec)
20	1.00×10^{-3}
30	8.00×10^{-4}
50	5.44×10^{-4}
100	2.79×10^{-4}

* From Meyer et al [1968].

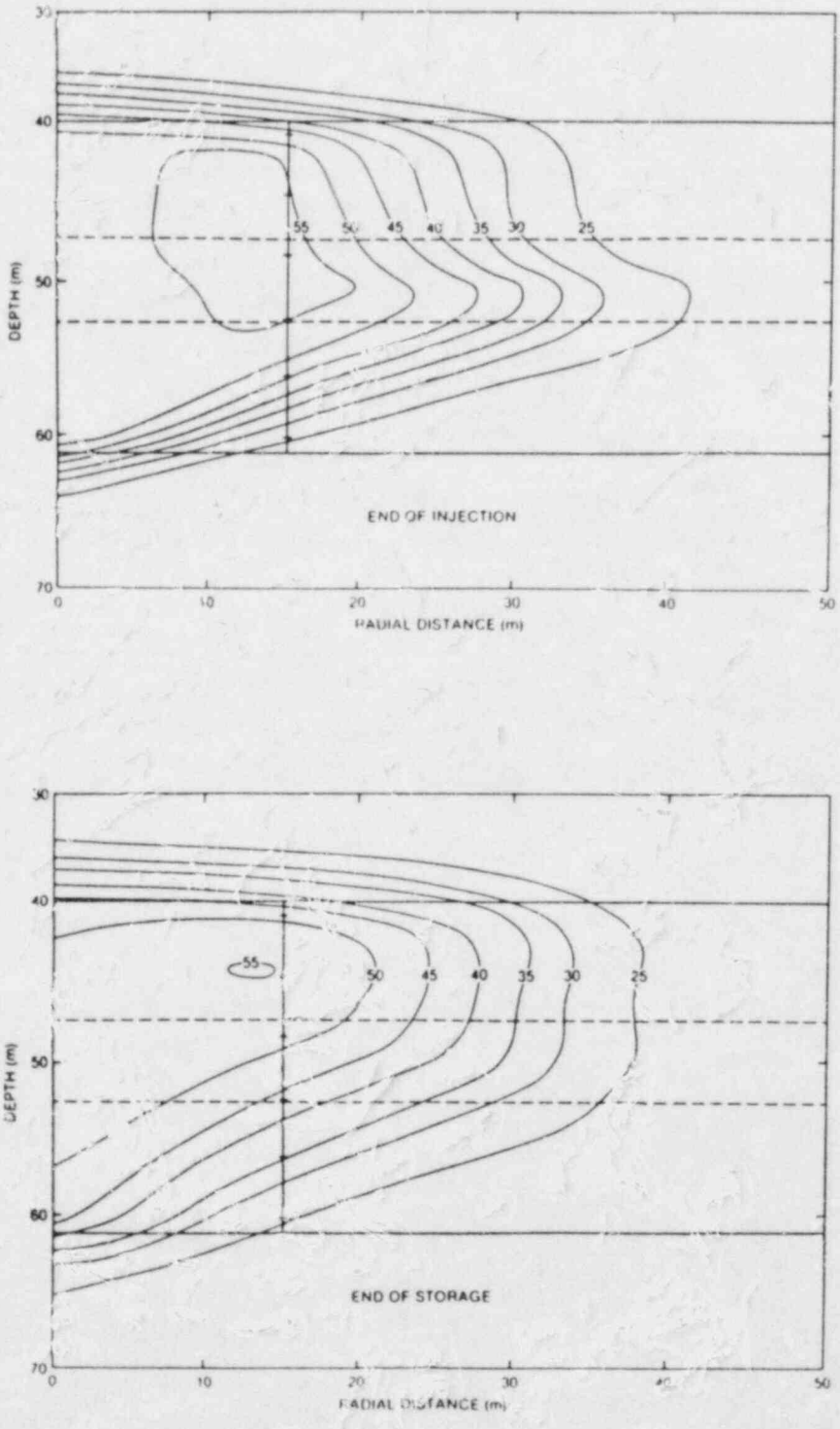

Figure 6-8. Simulated Ground-water Temperature Distributions at Selected Times.

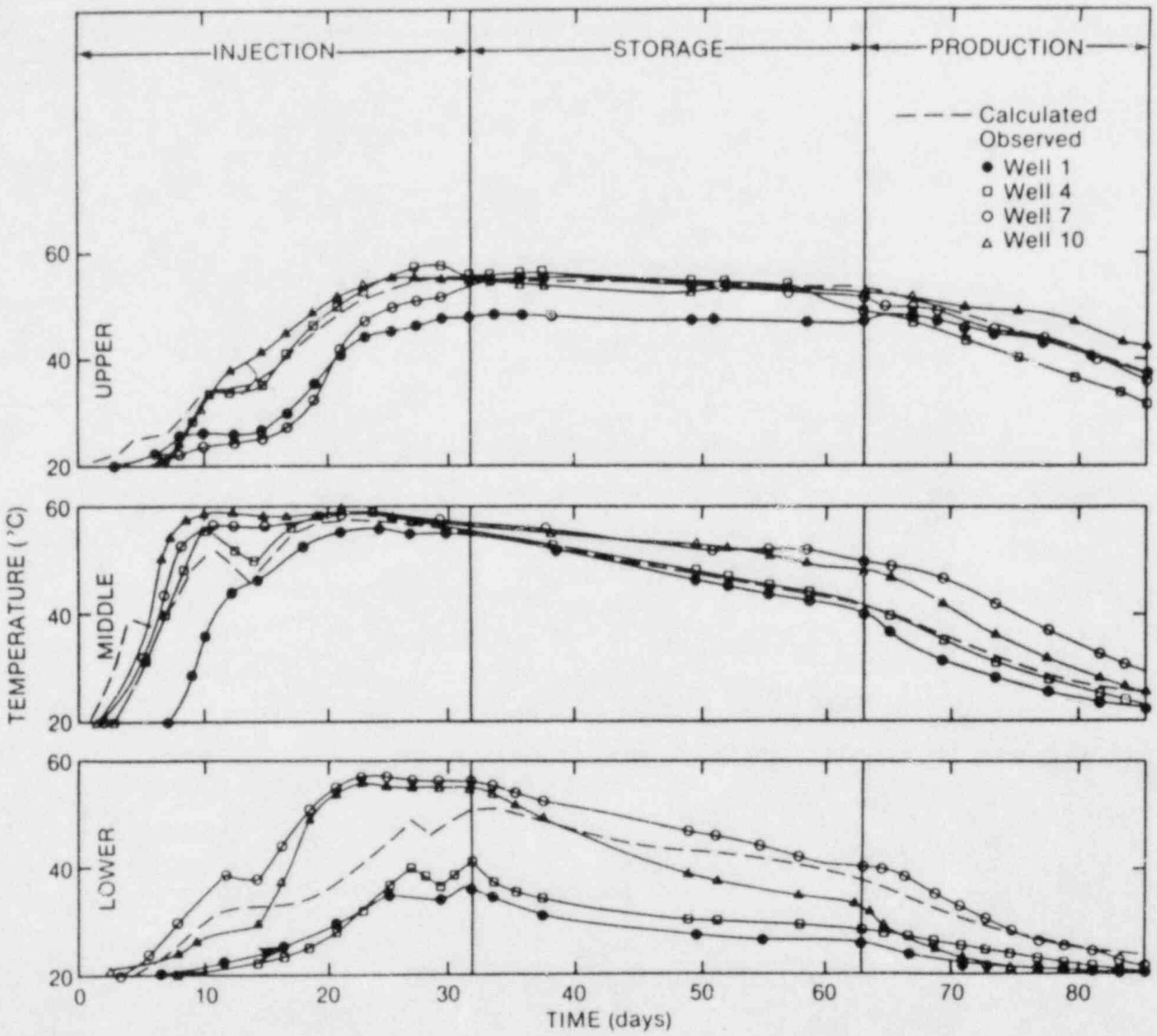

Figure 6-9. Observed and Simulated Temperature as a Function of Time at a Radiai Distance of 15 m in the Upper (Probe B), Middle (Probe D) and Lower (Probe E) Layers of the Aquifer.

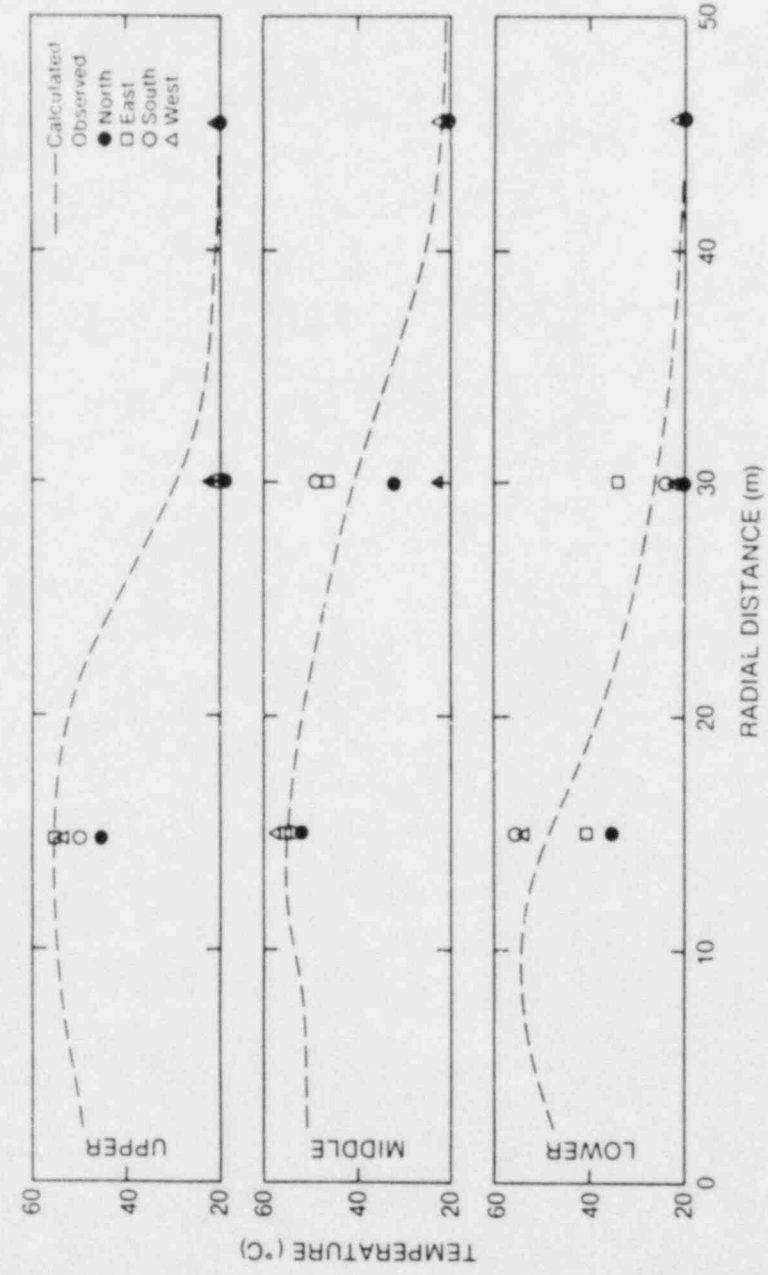

Figure 6-10. Observed and Simulated Temperature as a Function of Distance at the End of the Injection Period in the Upper, Middle and Lower Layers of the Aquifer.

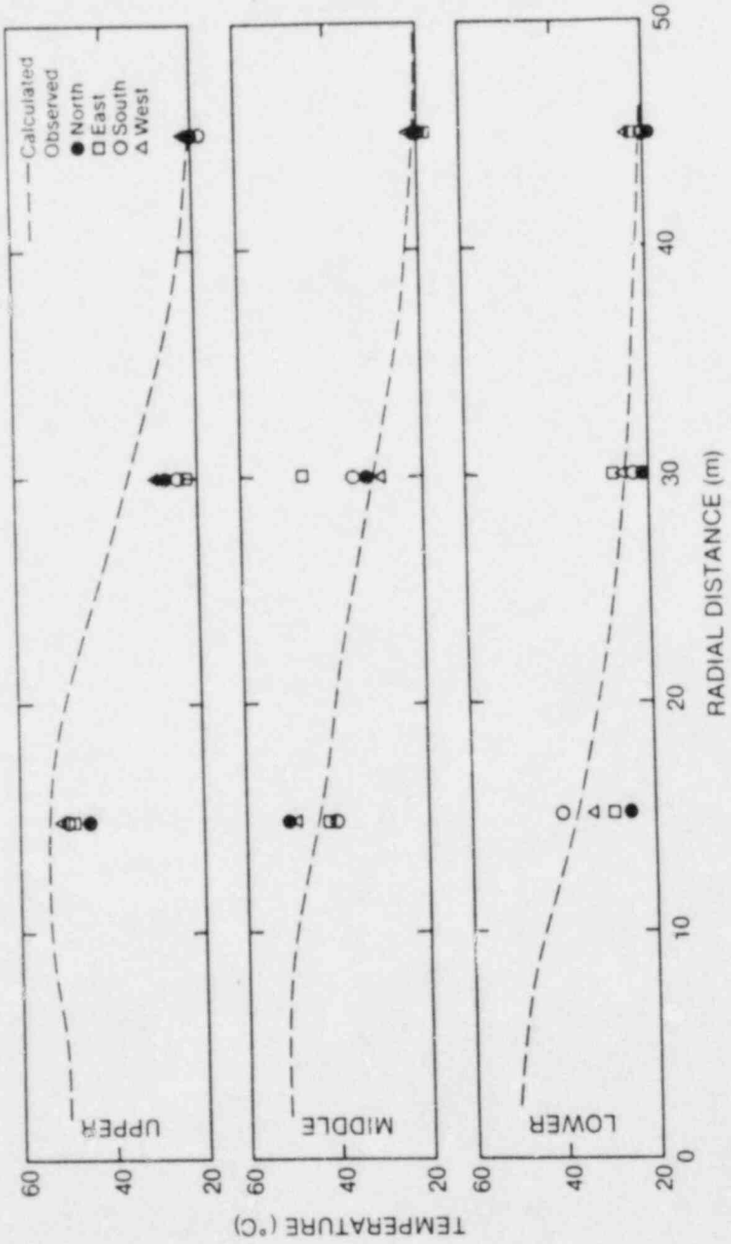

Figure 6-11. Observed and Simulated Temperature as a Function of Distance at the End of the Storage Period in the Upper, Middle and Lower Layers of the Aquifer.

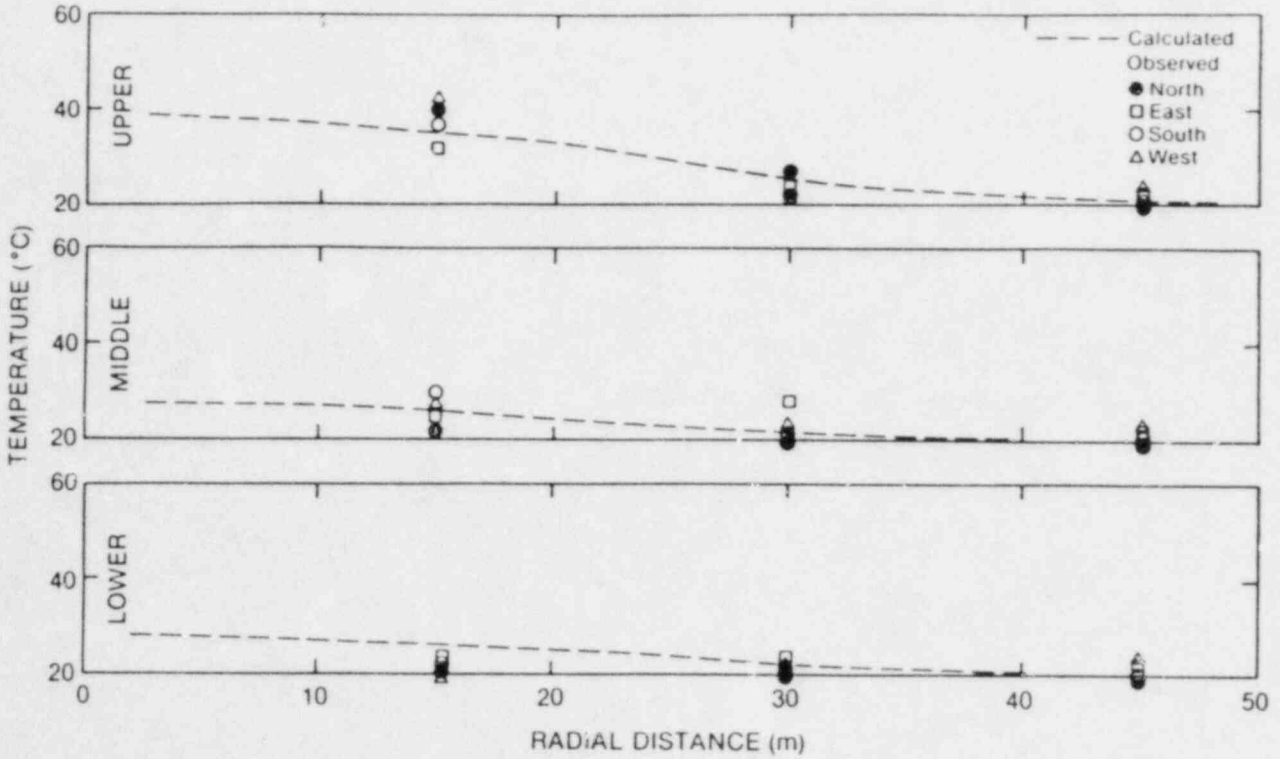

Figure 6-12. Observed and Simulated Temperature as a Function of Distance at the End of the Production Period in the Upper, Middle and Lower Layers of the Aquifer.

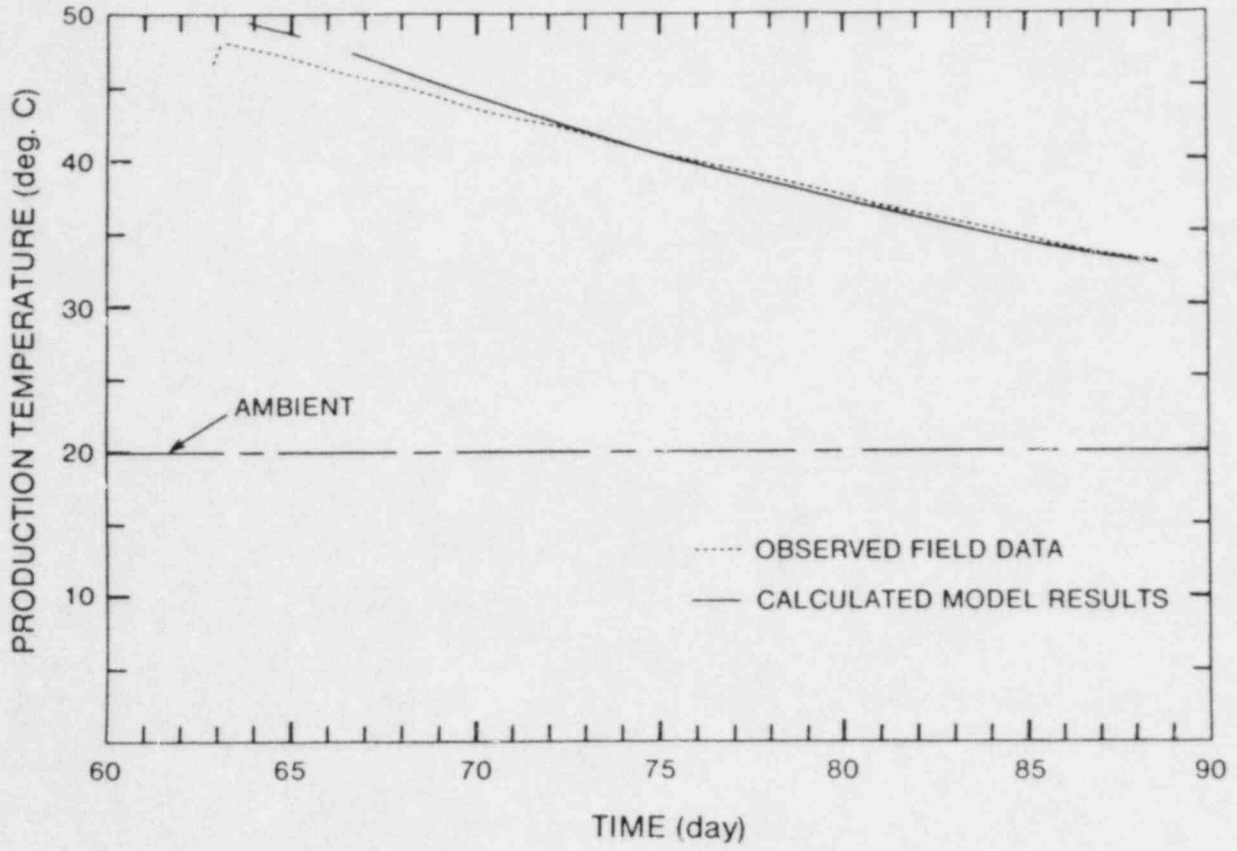

Figure 6-13. Observed and Simulated Production Temperature as a Function of Time (after Molz et al [1983]).

energy recovery factor* of 0.55 as compared to the experimental value which also was 0.55. It is interesting to note here that Buscheck et al [1983] calculated a recovery factor of 0.58. It would appear that our reduced permeability ratio 1:6 (overall) versus his 1:7 (overall) is the source of the difference.

However, the two simulations do differ in the hydraulic characterization of the aquitards, as discussed earlier. As a check, then, our calculation was repeated with the value of hydraulic diffusivity increased by an order of magnitude (to 8.22×10^{-5} m^2/s) in the upper aquitard. Such a value does permit significant leakage (after about 2 days of pumping) and is about two orders of magnitude greater than Buscheck's value (6.25×10^{-7} m^2/s). Nevertheless, the energy recovery factor was unchanged, indicating that the dominant heat-transport mechanism within the aquitard is that of heat conduction.

---

* The energy recovery factor is defined as thermal energy produced divided by thermal energy injected for equal injection and production volumes. In this case energies were measured relative to the ambient aquifer temperature (20 °C).

7 FIELD COMPARISON FOR THE SOLUTE TRANSPORT

7.1 CONTAMINANT MIGRATION FROM A LANDFILL [CLEARY, 1978; KIMMEL AND BRAIDS, 1980]

7.1.1 Objectives

The purposes for simulating this field problem are to test the following aspects of the SWIFT Code:

- contaminant convection and hydrodynamic dispersion,
- steady-state velocity,
- time- and space-dependent contaminant source terms,
- aquifer-influence functions.

7.1.2 Description of Problem

Babylon is located in southwestern Suffolk County, Long Island, New York. The landfill for this town, which began operation in 1947, has been the subject of several field studies by investigators of both Princeton University [Cleary, 1973] and the U.S. Geological Survey [Kimmel and Braids, 1975, and Kimmel and Braids, 1980]. The chloride isopleths obtained by these studies were used in the calculations performed by Gureghian et al [1981]. These authors took the chloride distributions of November, 1975 as initial conditions and then simulated a 13-month evolution of the chloride plume using the isopleths of December, 1976 for model calibration. Here, the work of Gureghian et al is extended in the following manner. It is known that the loading occurred in three different stages in three different locations within the 35-acre landfill. This staging, insofar as it is known, is used herein as a time- and space-dependent source, and the entire 29-year evolution of the chloride plume is simulated, using the measured isopleths of September, 1976, for calibration of the site model.

7.1.3 Summary of Field Tests

The landfill is located in an upper glacial aquifer underlain by a tight clay layer (Figure 7-1). Regional ground-water flow in this aquifer is relatively uniform and constant throughout the year with an interstitial velocity of about 1 ft/d. Major hydrogeologic units for Long Island are described in detail by Cohen et al [1968].

Figure 7-2 gives an areal view of the landfill and the town of Babylon. As shown, the landfill consists of three different piles. Pile 1 was used from 1947 to 1965. Pile 2 began in the mid 1950's and was used until 1968. Pile 3 began in 1968 and was still being used in 1976. It constitutes the major portion of the waste, which consists of approximately 1.3×10^8 ft^3 of refuse.

Field studies of the chloride plume emanating from this landfill have been performed since 1975, and the findings of these studies are published in Kimmel and Braids [1975], Cleary [1978] and Kimmel and Braids [1980]. The basic data come from the approximately 120 wells which have been located in the town of Babylon (see Figure 7-2). Each of these wells is monitored at the three different levels typified by Figure 7-1. Concentrations measured at Level A behave somewhat erratically due to the effects of surface dilution and localized sources of the chloride ion. Concentrations measured at Level B, however, are more stable and are amenable to simulation. Isopleths developed from the Level B data are shown in Figures 7-3 through 7-6 for specific times in the time span of December 1975 through December 1976. Even for the Level B data, however, some "noise" remains. Such erratic behavior, for example, is evident in Figures 7-7 through 7-9. Therefore, some subjective judgement was required in developing the contour plots shown in Figures 7-3 through 7-6.

7.1.4 Assumptions

In setting up the numerical simulation, the following assumptions were made:

- Both flow and transport may be characterized by a two-dimensional geometry.
- The Darcy velocity vector is constant over the region considered.

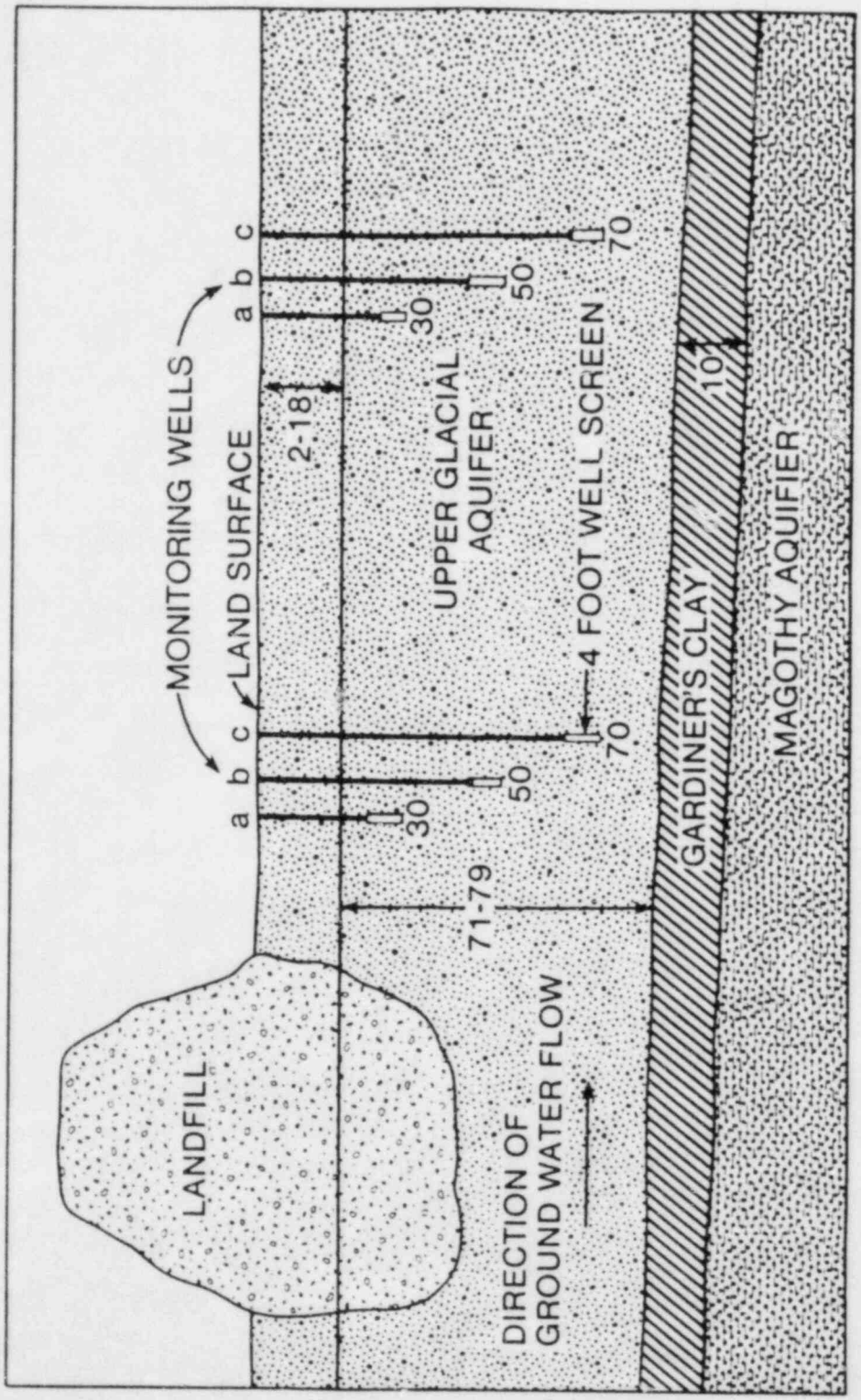

Figure 7-1. Cross Section at Landfill Site Depicting Simplifed Hydrogeology and Monitoring Wells (after Cleary [1978), Problem 7.1.

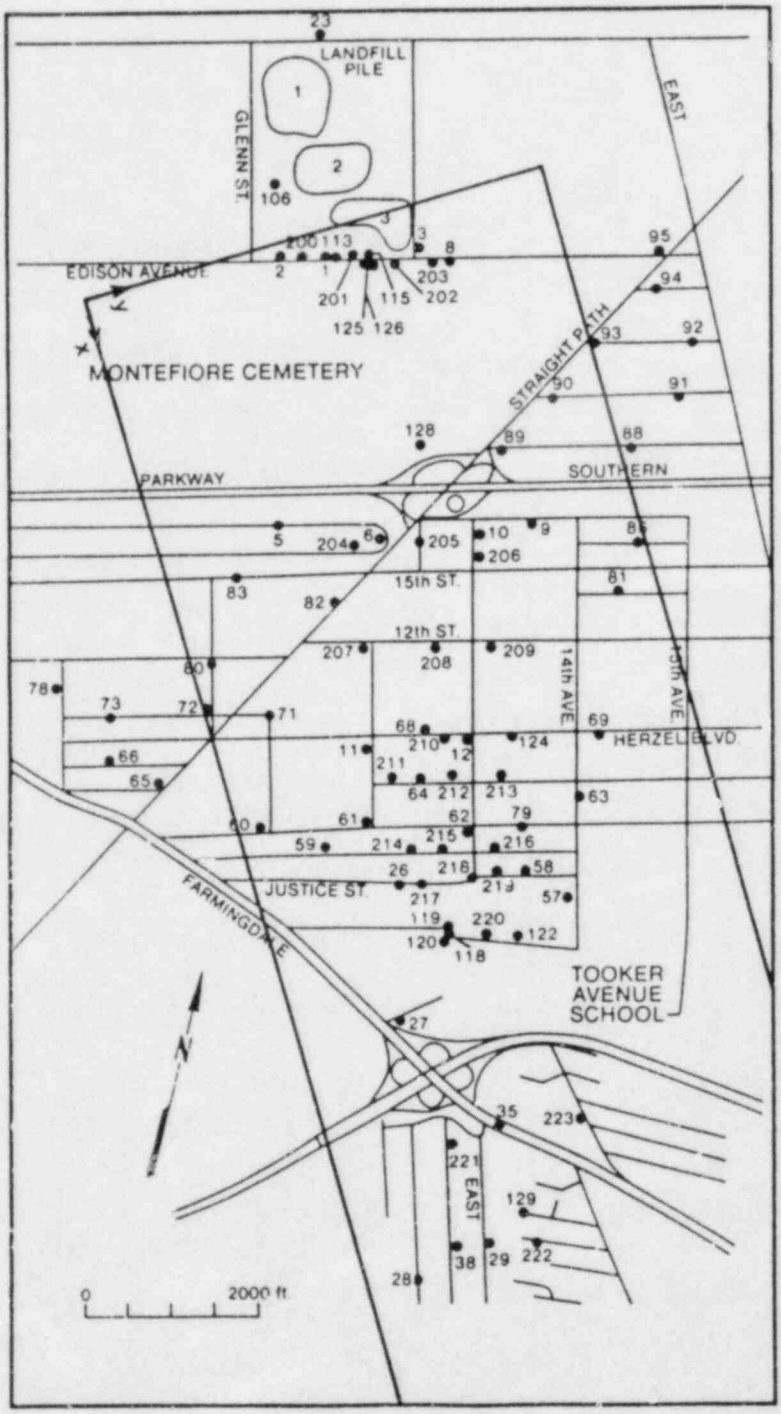

Figure 7-2. Areal View of the Landfill, the Town of Babylon, the Monitoring Wells and a Portion of the Simulated Region. The superimposed rectangle denotes the boundary of the numerical grid.

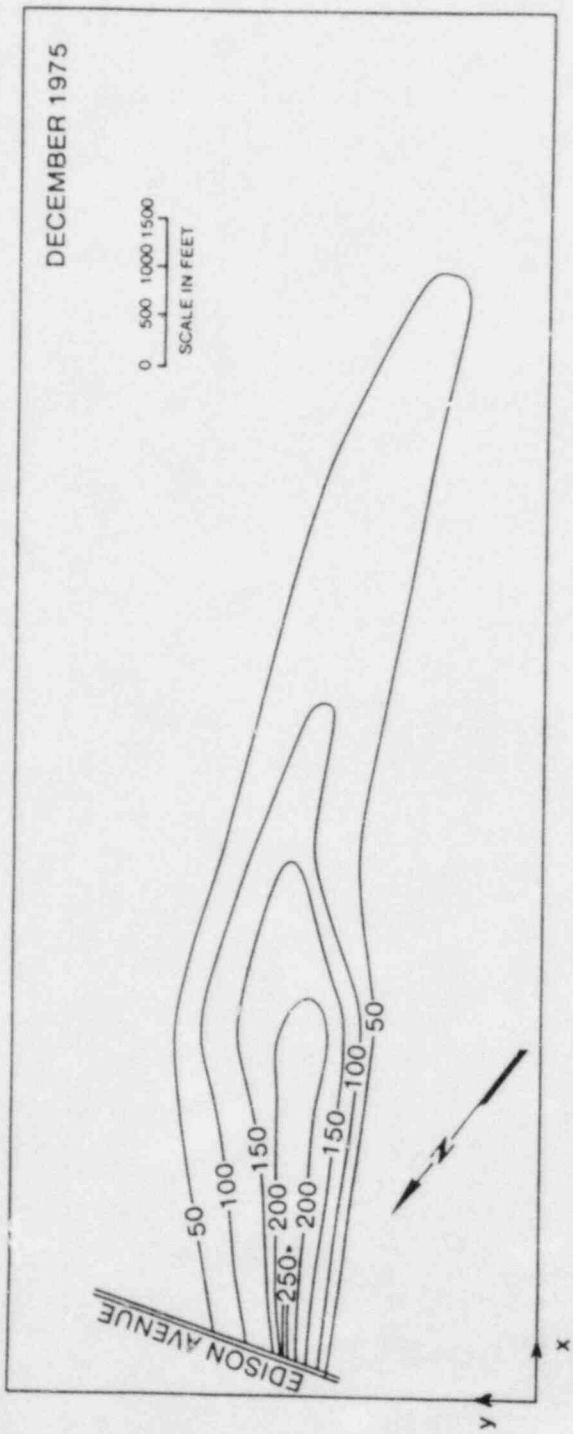

Figure 7-3. Observed Chloride Concentration (mg/l) Derived from the B-Level Data of December, 1975 (after Cleary [1978]). Figure frame coincides with boundary of numerical grid.

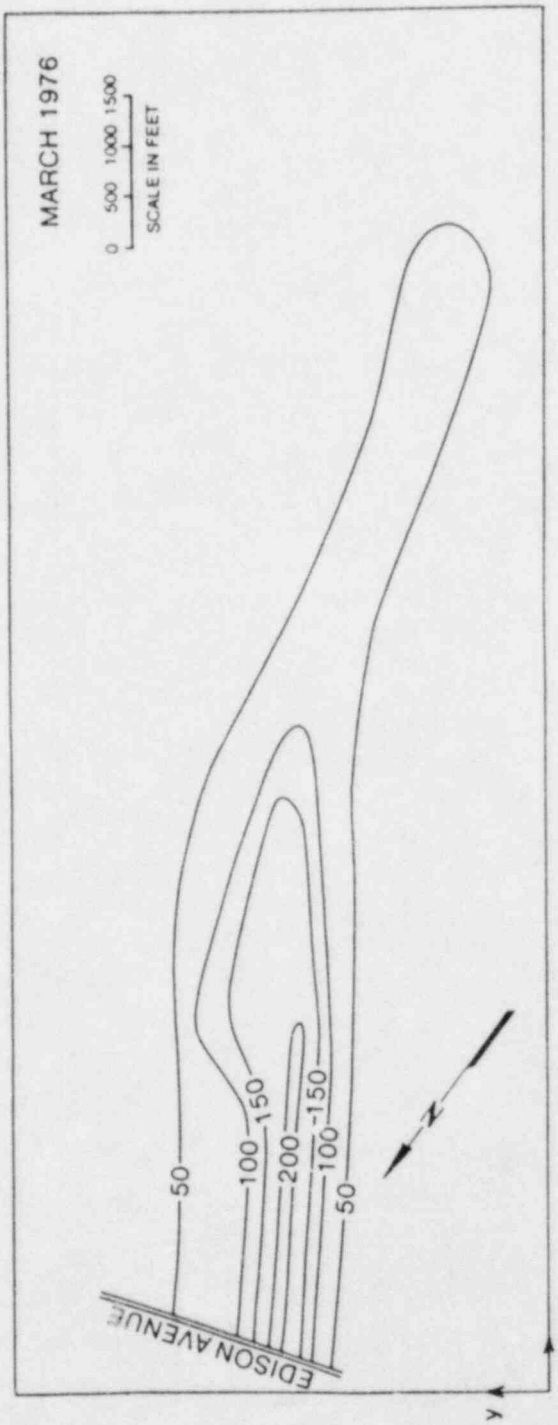

Figure 7-4. Observed Chloride Concentration (mg/l) Derived from the B-Level Data of March, 1976 (after Cleary [1978]). Figure frame coincides with boundary of numerical grid.

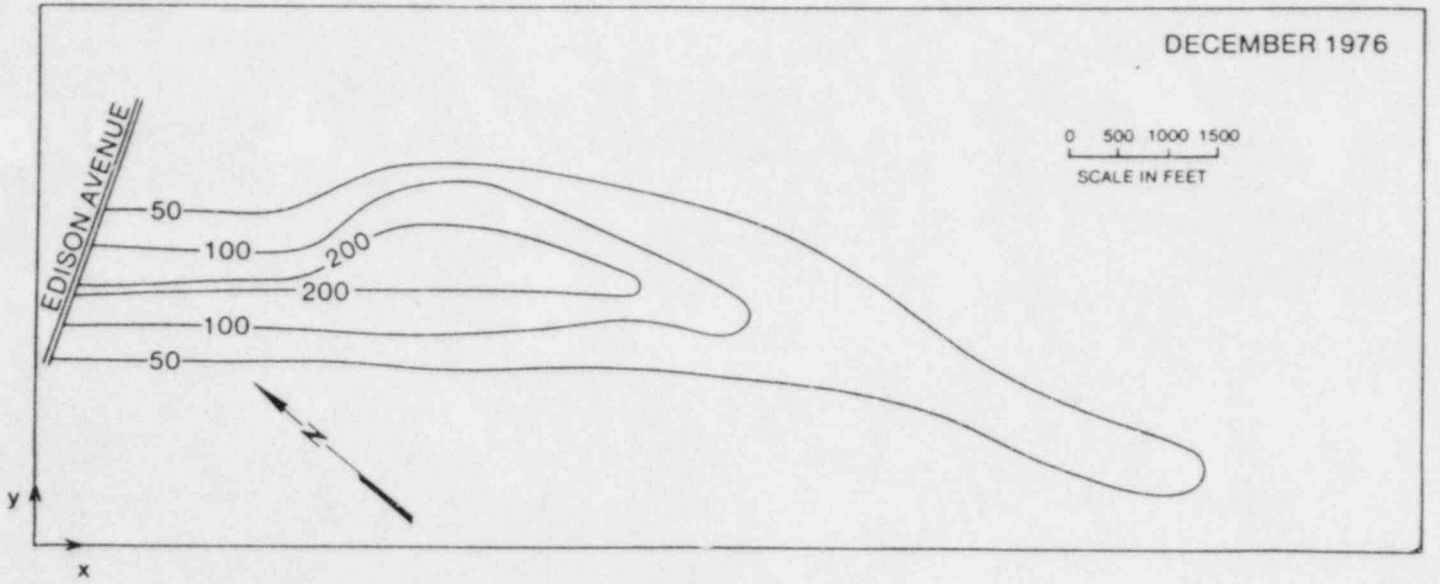

Figure 7-5. Observed Chloride Concentration (mg/l) Derived from B-Level Data of December, 1976 (after Cleary [1978]). Figure frame coincides with boundary of numerical grid.

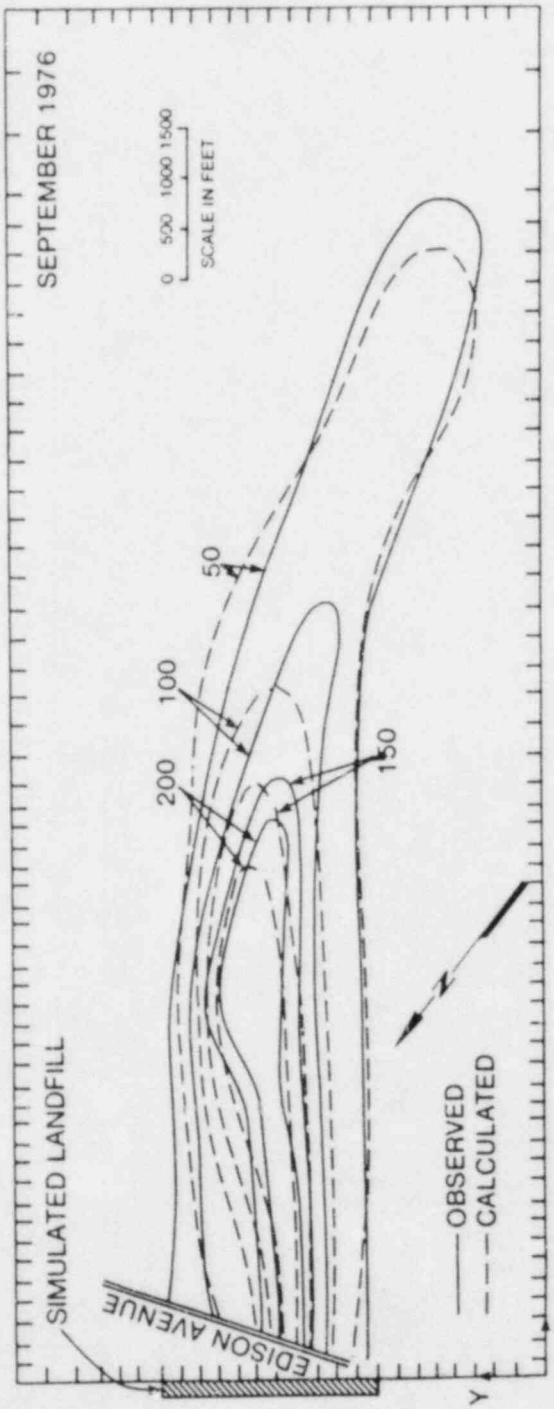

Figure 7-6. Observed (September, 1976) and Simulated Chloride Concentrations (observed data from Cleary [1978]). Tic marks denote the numerical gridding.

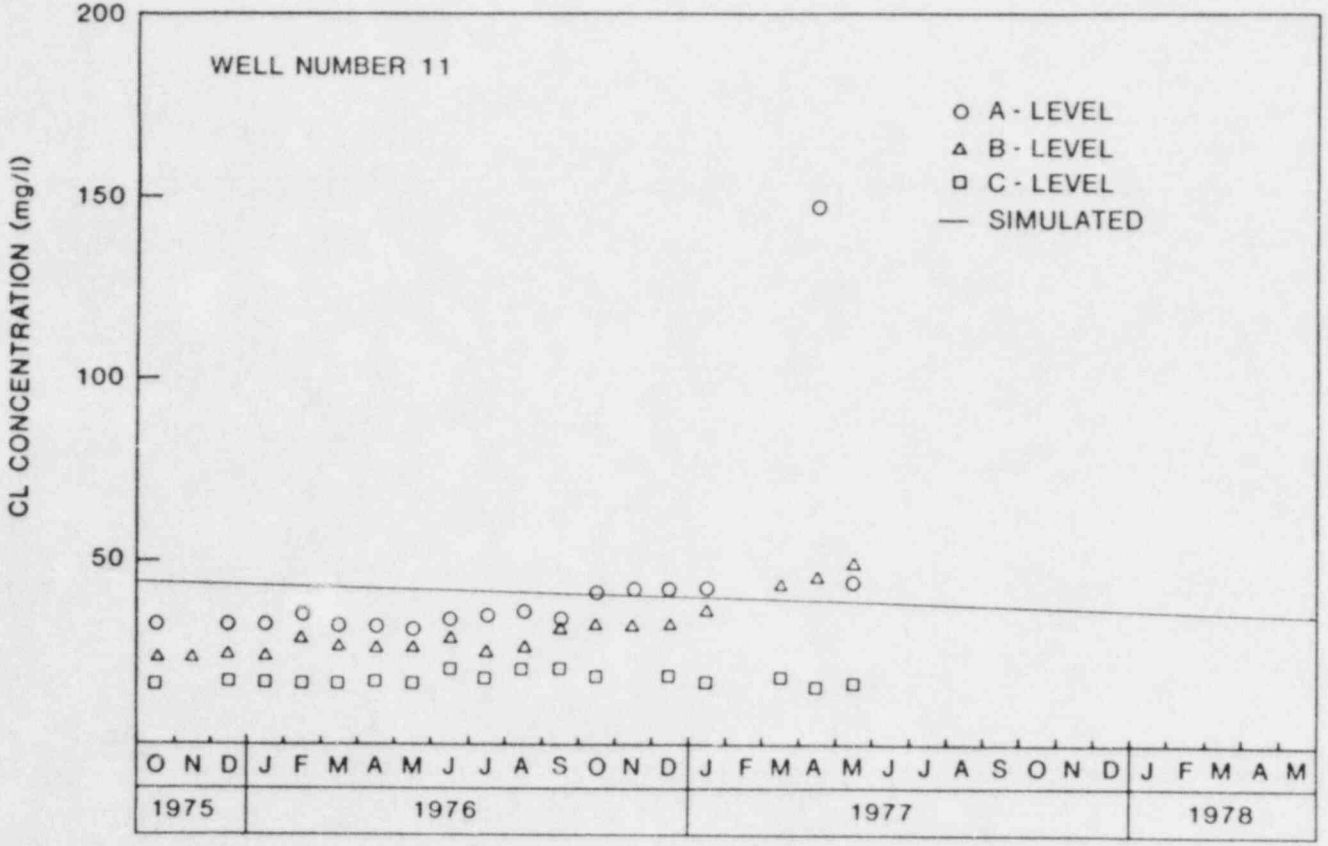

Figure 7-7. Observed and Simulated Chloride Concentration as a Function of Time for Well Number 11 (data from Cleary [1978])

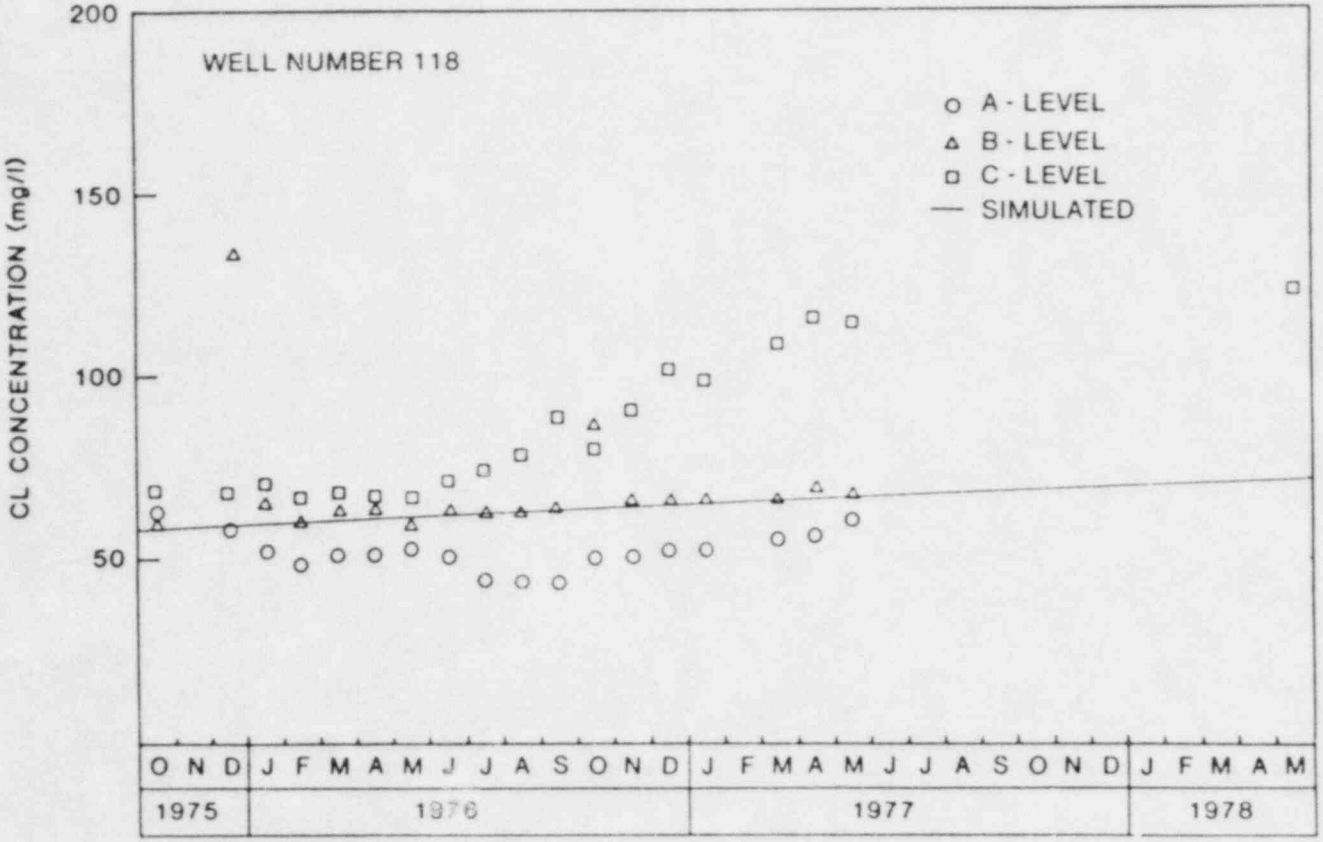

Figure 7-8. Observed and Simulated Chloride Concentration as a Function of Time for Well Number 118 (data from Cleary [1978]).

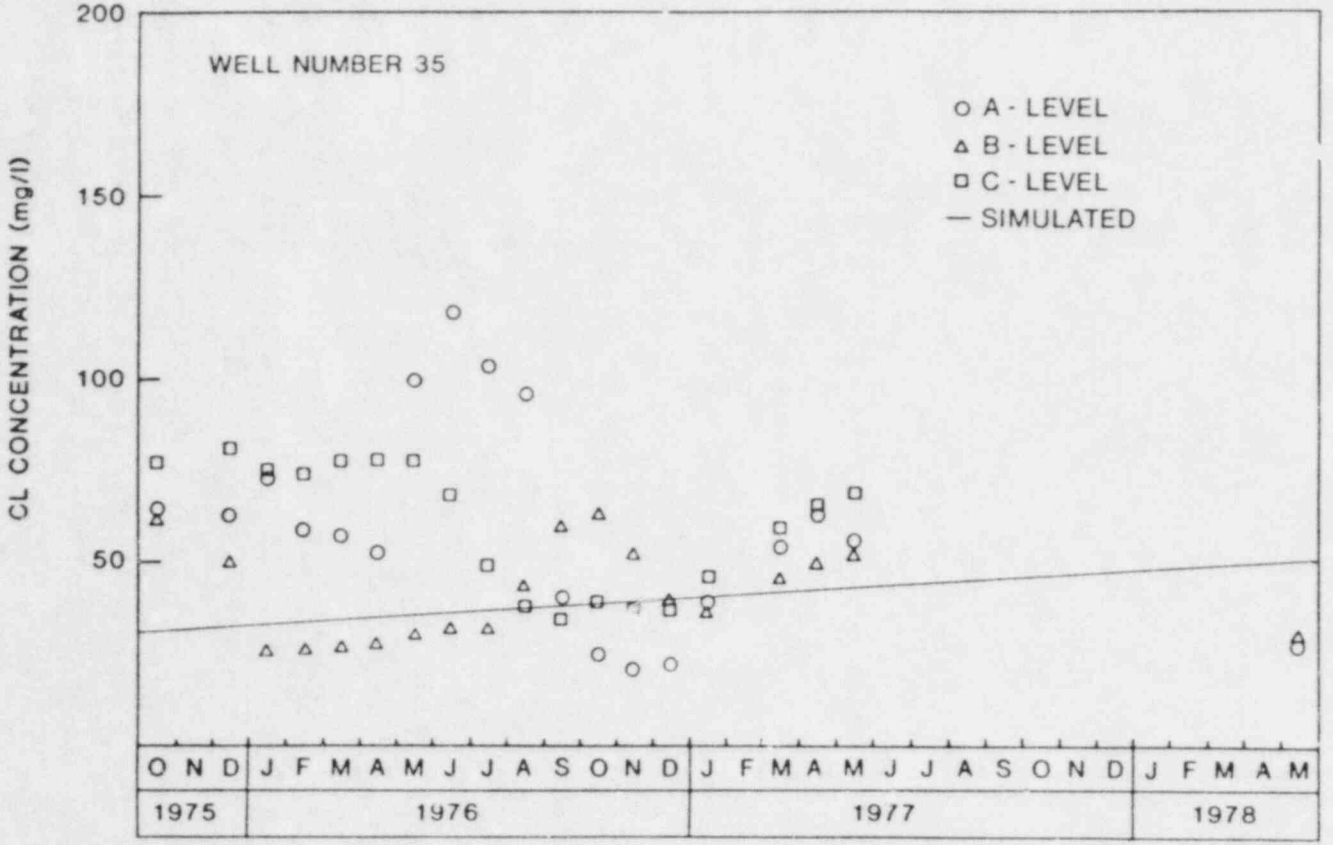

Figure 7-9. Observed and Simulated Chloride Concentration as a Function of Time for Well Number 35 (data from Cleary [1978]).

- The aquifer thickness is constant over this same region.
- Surface recharge is insignificant within the modeled region as compared to the total flow within the aquifer.
- The landfill is a line source.
- The landfill is the dominant source for chloride concentrations above background.
- Dilution due to recharge within the modeled region is insignificant.
- Contaminant dispersion may be characterized by two dispersivities, which are constant within the region modeled.
- Complete mixing over the thickness of the aquifer occurs within a few dispersion lengths of the source.

7.1.5 Numerical Simulation and Results

The input data for this problem include the three hydraulic parameters given in Table 7-1 (hydraulic conductivity, porosity and Darcy velocity). It also includes the direction of ground-water flow shown in Figure 7-2, i.e., the direction of the x-axis shown there. The output data consist of simulated isopleths for September, 1976, inferred values of longitudinal and transverse dispersivity, and an inferred source function to depict the leaching of chloride from the landfill. The date, September, 1976, was chosen so that the simulated result could be compared directly with the measured concentration distributions in Figure 7-6. Actually, any of the dates corresponding to measured isopleths in Figures 7-3 through 7-6 would have been equally satisfactory. Given the uncertainty in the well data at Level B, the results presented in these figures, which span the rather limited time period December, 1975 through December, 1976, are not significantly different.

A two-dimensional areal grid was chosen, which encompassed an area measuring 13,000 ft in length by 5,400 ft in width (Figure 7-6). The y-axis is aligned with the direction of ground-water flow, and the grid contains 53 (x-direction) by 24 (y-direction) blocks. Ranges of incremental values for Δx, Δy and Δt are given in Table 7-1. These values are consistent with criteria for the centered differencing schemes which were used.

Table 7-1. Flow and Transport Parameters for Problem 7.1.

Parameters	Symbol	Value	
		SI	English
Hydraulic conductivity	K	5.8×10^{-4} m/s	165 ft/d
Darcy velocity	u	1.2×10^{-6} m/s	.33 ft/d
Porosity	ϕ	.30	.30
System length (x-direction)	L_x	4206 m	13,800 ft
System width (y-direction)	L_y	1646 m	5,400 ft
Spatial increments	Δx	61-183 m	200-600 ft
	Δy	61-91 m	200-300 ft
Time increments	Δt	4.32×10^7 s	500 d
Spatial differencing	CIS*	---	---
Time differencing	CIT*	---	---

* CIS means centered-in-space, and CIT means centered-in-time.

The prescribed steady-state ground-water flow was established by the use of Dirichlet boundary conditions on the flow at $x = 0$ and $x = L_x$. For the contaminant, a row of source blocks was located along the $x = 0$ boundary. These sources were used both to maintain the observed background concentrations, as determined by Cleary [1978], and to simulate the landfill. The condition

$$\text{flux} = u(x=L_x)C \tag{7-1}$$

was used at the outer extremity of the region to characterize the migration of the chloride ion into the essentially semi-infinite domain of the aquifer. No-flow conditions were assumed for both $y = 0$ and $y = L_y$.

In performing the simulation, it was found that the shape of the plume was most sensitive to the staging of the source. To a much lesser extent, the plume was also sensitive to the values chosen for the dispersivities. The staging, which was obtained, is shown in Figures 7-10(a) and 7-10(b). Since dilution by rainfall was neglected and complete mixing within the aquifer was assumed, the source is given in units of concentration. Each source term is distributed in the spatial width variable y and is assumed to remain unchanged for a three-year time period. At the conclusion of such a period, the source term changes to another space-dependent source function. As shown, the movement of the various stages is generally from Pile 1 to Pile 2 to Pile 3 and then back to Pile 2. Actually, however, the source distributions typically contain components arising from more than one pile at a given time and reflect the actual usage of the landfill. Locations and times of usage of the various piles is generally consistent with historical records. However, a "trial-and-error" procedure was employed to determine the concentration magnitudes shown in Figure 7-10.

Dispersion was characterized by longitudinal and transverse coefficients

$$\alpha_L = 100 \text{ ft } (30.5 \text{ m}) \tag{7-2a}$$

$$\alpha_T = 15 \text{ ft } (4.6 \text{ m}) \tag{7-2b}$$

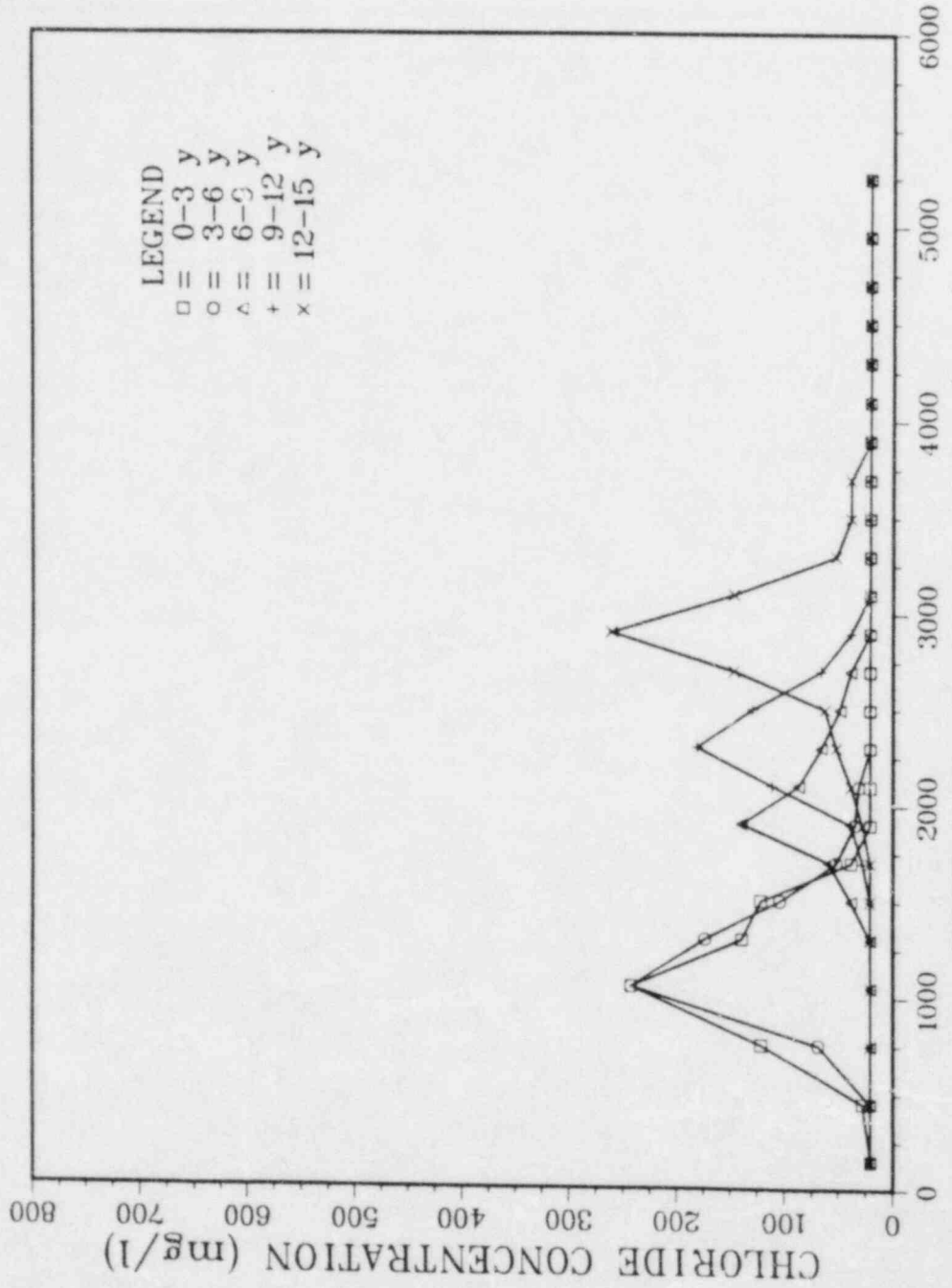

Figure 7-10a. Inferred Landfill Staging Through Year 15 (1962).

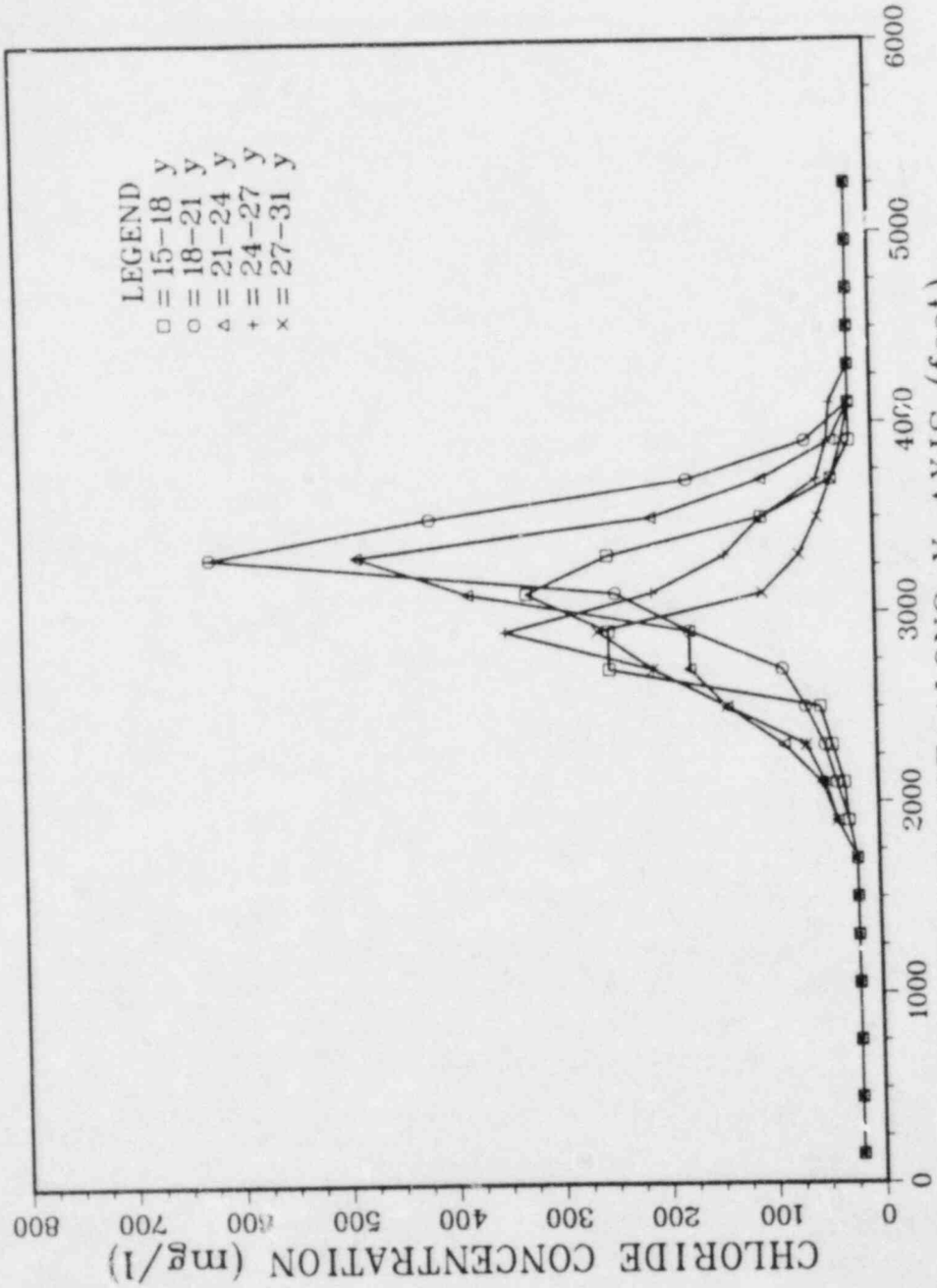

Figure 7-10b. Inferred Landfill Staging, Years 15 (1962) Through 31 (1978).

respectively. Gureghian et al [1981] reported values of 140 ft and 25 ft for these two quantities. Further, Kimmel and Braids [1980] reported a dispersion of 60 ft^2/day, which corresponds to a longitudinal dispersivity of 180 ft for this aquifer. Such discrepancies are, we feel, quite acceptable when one considers the relative insensitivity to these parameters in comparison to the source terms. Figure 7-5 gives both observed and simulated isopleths. As shown, the two compare quite favorably.

NOTATION

8.1 ROMAN SYMBOLS

A	constant drawdown function or cross sectional area normal to flow
b	aquifer thickness
b'	aquitard or confining layer thickness
c	total compressibility (rock and water)
c_p	specific heat of the fluid
c_{pm}	specific heat of the fluid and rock media
c_{pR}	specific heat of the rock (aquifer) formation
c'_{pm}	specific heat of the over/underburden rock and water
c'_{pR}	specific heat of the over/underburden rock
c_R	compressibility of the rock formation
c_W	compressibility of the fluid
$\tilde{C}_r$	time-dependent boundary concentration
$\tilde{C}_{ro}$	Bateman decay/production initial boundary concentration
C_r	concentration of radioactive (trace) components
D	retarded dispersion coefficient

D' hydraulic diffusivity of aquitard

D_m molecular diffusion

g acceleration of gravity

g_c units conversion factor equal to g for the English system and equal to unity for the SI system

$G(\tau)$ constant-drawdown dimensionless flow rate function

$H(u,\beta)$ Hantush function

I_r inventory of radionuclide component r

k permeability coefficient

k_{rs} product of branching ratio and daughter-parent mass fraction

k'_{rs} the factor k_{rs} divided by the retardation of species r

K hydraulic conductivity of aquifer or retardation factor

K' hydraulic conductivity of aquitard

K_m heat conductivity for fluid and rock

K'_m heat conductivity of fluid and rock for the over/underburden rock

L overall length of system

L_x length of system in x-direction

L_y length of system in y-direction

N_r generalized solution to transport equation

p pressure

p_o, p_l boundary pressure

P_e system Peclet number

Q pumping rate

r radius or radial distance

r_e external radius of simulated area

r_w radius of wellbore

R ratio of vertical permeability to horizontal permeability

s drawdown in aquifer or spatial coordinate

s_w specified drawdown at pumping well

S aquifer storativity

S_j Bateman coefficient $(k_{js} \lambda_s)$

S_s specific aquifer storativity

S'_s specific aquitard storativity

t time

T temperature, aquifer transmissivity or leach duration time

T_o initial temperature

T_l boundary temperature

T_I initial or injection temperature

T' temperature of fluid in over/underburden

u Darcy flux vector or dimensionless variable ($r^2S/4Tt$)

v retarded interstitial velocity

$W(u)$ well function

WI_o well index

x,y,z Cartesian coordinates

Y_{rj} Bateman coefficient $(e^{-\lambda_j t} - e^{-\lambda_r t})/(\lambda_r - \lambda_j)$

8.2 GREEK SYMBOLS

α dimensionless variable $[(K'_m \rho'_m c'_{pm})^{1/2} / (K_m \rho_m c_m)^{1/2}]$

α_ℓ geometrical allocation factor used for aquifer-influence functions

α_L longitudinal dispersivity

α_T transverse dispersivity

β dimensionless variable of Hantush leaky-aquifer function $[(r/4)(K'S'_s/TS)^{1/2}]$

γ dimensionless variable $(Q\rho c_p/4K_m)$

$\Gamma(\nu)$ Gamma function

Γ_H over/underburden heat coupling term

δ Dirac delta function

Δp drop in pressure from initial pressure

Δs special increment or incremental drawdown

Δt time increment

$\Delta\tau$ duration of one segment of thermal-energy-storage cycle

Δx_i spatial increment in x_i where $x_1 = x$, $x_2 = y$ and $x_3 = z$

θ dimensionless temperature, $(T-T_o)/(T_1-T_o)$, or convective/dispersive solution

λ decay constant of radionuclide

μ viscosity

ν dimensionless parameter ($Q\rho c_p/4\pi bK_m$)

ρ fluid density or dimensionless radial distance (r/r_w)

ρ_m combined density of aquifer formation and water

ρ'_m combined density of aquitard formation and water

ρ_R formation (aquifer) rock density

ρ'_R over/underburden rock density

τ radioactive half-life or dimensionless parameters [Tt/Sr_w^2 or $4K_m t/(\rho_m c_m b^2)$]

ϕ porosity of aquifer

ϕ' porosity of aquitard

χ dimensionless variable ($2x/b$)

ω dimensionless parameter ($2r/b$)

8.3 SUBSCRIPTS

A	aquifer
m	rock and water, i.e., medium
r	radioactive component
R	rock formation

REFERENCES

Avdonin, N.A., 1964. Some Formulas for Calculating the Temperature Field of a Stratum Subject of Thermal Injection, Neft' i Gaz, Vol. 7, No. 3, pp. 37-41.

Bear, J., 1979. Hydraulics of Groundwater, McGraw-Hill, New York, 567 pp.

Buscheck, T.A., Doughty, C., and Tsang, C.F., 1983. Prediction and Analysis of a Field Experiment on a Multi-layered Aquifer Thermal Energy Storage System with Strong Buoyancy Flow, Water Resour. Res., Vol. 19, No. 5, pp. 1307-1315.

Carter, R.D., and Tracy, C.W., 1960. An Improved Method for Calculating Water Influx, Trans. SPE of AIME, 219, 415-417, 1960.

Clark, S.P., Jr., ed, 1966. Handbook of Physical Constants.

Cleary, R.W., 1978. Final Report 208 Project, Nassau-Suffolk Regional Planning Board, Hauppauge, New York.

Coats, K.H., and Smith, B.D., 1964. Dead-End Pore Volume and Dispersion in Porous Media, Soc. Pet. Eng. J., Vol. 4, No. 1, p. 73.

Cohen, P., Franke, O.L., and Foxworthy, B.L., 1968. An Atlas of Long Island's Water Resources, New York State Water Resources Comm. Bull., 62, 117 pp.

Gureghian, A.B., Ward, D.S., and Cleary, R.W., 1981. A Finite Element Model for the Migration of Leachate from a Sanitary Landfill in Long Island, New York - Part II: Application, Water Res. Bull., Vol. 17, No. 1, pp. 62-66.

Hantush, M.S., 1960. Modification of the Theory of Leaky Aquifers, J. Geophys. Res., Vol. 65, pp. 3713-3725.

Hantush, M.S., 1961. Drawdown Around a Partially Penetrating Well, Am. Soc. Civil Eng. Proc., Vol 87, No. HY4, pp. 83-98.

Harada, M., Chambre, P.L., Foglia, M., Higashi, K., Iwamoto, F., Leung, D., Pigford, T.H., and Ting, D., 1980. Migration of Radionuclides through Sorbing Media Analytical Solutions - I, Lawrence Berkeley Laboratory Report LBL-10500.

INTRACOIN, 1983. International Nuclide Transport Code Intercomparison Study, Swedish Nuclear Power Inspectorate, Stockholm, Sweden.

Jacob, C.R., and Lohman, S.W., 1952. Non-steady Flow to a Well of Constant Drawdown in an Extensive Aquifer, Am. Geophys. Union Trans., Vol. 33, No. 4, pp. 559-569.

Kimmel, G.E., and Braids, O.E., 1975. Preliminary Findings of a Leachate Study on Two Landfills in Suffolk County, New York, J. Res. U.S. Geol. Survey, Vol. 3, No. 3, pp. 273-280.

Kimmel, G.E., and Braids, O.C., 1980. Leachate Plumes in Ground Water from Babylon and Islip Landfills, Long Island, New York, U.S. Geol. Survey, Prof. Paper P-1085, 38 pp.

Lester, D.H., Jansen, G., and Burkholder, H.C., 1975. Migration of Radionuclide Chains Through an Adsorbing Medium, AIChE Symp. Ser., Vol. 71, pp. 152-202.

Meyer, C.A., McClintock, R.B., Silvestri, G.J., and Spencer, R.C., 1968. 1967 ASME Stream Tables, 2nd Edition, The American Society of Mechanical Engineers, New York, 1968.

Molz, F.J., Warman, J.C., and Jones, T.E., 1978. Aquifer Storage of Heated Water, I, A Field Experiment, Ground Water, Vol. 16, pp. 234-241.

Molz, F.J., Parr, A.D., Andersen, P.F., Lucido, V.D., and Warman, J.C., 1979. Thermal Energy Storage in a Confined Aquifer: Experimental Results, Water Resour. Res., Vol. 15, No. 6, pp. 1509-1514.

Molz, F.J., Parr, A.D., Andersen, P.F., Lucido, V.D., and Warman, J.C., 1981. Thermal Energy Storage in a Confined Aquifer: Second Cycle, Water Resour. Res., Vol. 17, No. 3, pp. 641-645.

Molz, F.J., Melville, J.G., Parr, A.D., King, D.A., and Hopf, M.T., 1983. Aquifer Thermal Energy Storage: A Well Doublet Experiment at Increased Temperatures, Water Resour. Res., Vol. 19, No. 1, pp. 149-160.

Papadopulos, I.S., 1965. Nonsteady Flow to a Well in an Infinite Anisotropic Aquifer, Symp. Intern. Assoc. Sci. Hydrology, Dubrovinik.

Papadopulos, S.S., and Larson, S.P., 1978. Aquifer Storage of Heated Water, 2, Numerical Simulation of Field Results, Ground Water, Vol. 16, pp. 242-248.

Parr, A.D., Molz, F.J., and Melville, J.G., 1983a. Field Determination of Aquifer Thermal Energy Storage Parameters, Ground Water, Vol. 21, No. 1, pp. 22-35.

Parr, A.D., Melville, J.G., and Molz, F.J., 1983b. HP41C and TI59 Programs for Anisotropic Confined Aquifers, Ground Water, Vol. 21, No. 2, pp. 212-220.

Reed, J.E., 1980. Type Curves for Selected Problems of Flow to Wells in Confined Aquifers, Tech. of Water-Resour. Invest., U.S. Geol. Survey, Chpt. B3, Book 3, 106 pp.

Reeves, M., and Cranwell, R.M., 1981. User's Manual for the Sandia Waste-Isolation Flow and Transport Model (SWIFT) Release 4.81, SAND 81-2516, NUREG/CR-2324, Sandia National Laboratories, Albuquerque, NM.

Reeves, M., Johns, N.D., and Cranwell, R.M., 1984a. Theory and Implementation for SWIFT II, The Sandia Waste-Isolation Flow and Transport Model for Fractured Media, Release 3.83. To be published as a SAND-NUREG report, Sandia National Laboratories, Albuquerque, NM.

Reeves, M., Johns, N.D., and Cranwell, R.M., 1984b. Input Data Guide for SWIFT II, The Sandia Waste-Isolation Flow and Transport Model for Fractured Media, to be published as a SAND-NUREG report. Sandia National Laboratories, Albuquerque, NM.

Ross, B., Mercer, J.W., Thomas, S.D., and Lester, B.H., 1982. Benchmark Problems for Repository Siting Models, NUREG/CR-3097, U.S. Nuclear Regulatory Commission, 138 pp.

Silling, S.A., 1983. Final Technical Position on Documentation of Computer Codes for High-Level Waste Management, NUREG/CR-0856, U.S. Nuclear Regulatory Commission, 11 pp.

Sykes, J.F., Lantz, R.B., Pahwa, S.B., and Ward, D.S., 1982. Numerical Simulation of Thermal Energy Storage Experiment Conducted by Auburn University, Ground Water, Vol. 20, No. 5, pp. 569-576.

Theis, C.V., 1935. The Relation Between the Lowering of the Piezometric Surface and the Rate and Duration of Discharge of a Well Using Ground Water Storage, Am. Geophys. Union Trans., Vol. 16, pp. 519-524.

Tsang, C.F., Buscheck, T., and Doughty, C., 1981. Aquifer Thermal Energy Storage: A Numerical Simulation of Auburn University Field Experiments, Water Resour. Res., Vol. 17, No. 3, pp. 637-658.

NRC FORM 335 (16 83) — U.S. NUCLEAR REGULATORY COMMISSION

BIBLIOGRAPHIC DATA SHEET

1 REPORT NUMBER (Assigned by TIDC and Vol. No., if any)
NUREG/CR-3316
SAND83-1154

2 Leave blank

3 TITLE AND SUBTITLE
Verification and Field Comparison of the Sandia Waste-Isolation Flow and Transport Model (SWIFT)

4 RECIPIENT'S ACCESSION NUMBER

5 DATE REPORT COMPLETED
MONTH: February YEAR: 1984

6 AUTHOR(S)
David S. Ward, Mark Reeves and Leonard E. Duda

7 DATE REPORT ISSUED
MONTH: April YEAR: 1984

8 PERFORMING ORGANIZATION NAME AND MAILING ADDRESS (Include Zip Code)
Sandia National Laboratories
Waste Management Systems Division
Organization 6431
Albuquerque, NM 87185

9 PROJECT/TASK/WORK UNIT NUMBER

10 FIN NUMBER
A 1166

11 SPONSORING ORGANIZATION NAME AND MAILING ADDRESS (Include Zip Code)
Division of Waste Management
Office of Nuclear Material Safety and Safeguards
U.S. Nuclear Regulatory Commission
Washington, D.C. 20555

12a TYPE OF REPORT

12b PERIOD COVERED (Inclusive dates)
October, 1982 - February, 1984

13 SUPPLEMENTARY NOTES

14 ABSTRACT (200 words or less)

The SWIFT Model has been developed and maintained by Sandia National Laboratories. The Nuclear Regulatory Commission has sponsored this work under the high-level nuclear waste program. SWIFT is a fully-coupled, transient, three-dimensional model. It is implemented by a finite-difference code which solves the equations for flow and transport in geologic media and is used to evaluate repository-site performance. This document represents an important part of the quality-assurance records for the code. Here the process simulators for flow, heat and radionuclide transport are examined using two different types of tests. The analytical verifications test SWIFT calculations against analytical solutions, and the field comparisons test SWIFT calculations against field data. Both types of tests yield good agreement between the SWIFT computations and the comparative data.

15a KEY WORDS AND DOCUMENT ANALYSIS

15b DESCRIPTORS

16 AVAILABILITY STATEMENT
Unlimited

17 SECURITY CLASSIFICATION (This report)
Unclassified

18 NUMBER OF PAGES

19 SECURITY CLASSIFICATION (This page)
Unclassified

20 PRICE
$

UNITED STATES
NUCLEAR REGULATORY COMMISSION
WASHINGTON, D.C. 20555